

**Establishment and Maintenance of Pattern  
at the Ends of the Planarian Anterior-Posterior Axis**

by

Dayan J. Li

B.A., Molecular and Cellular Biology (2011)  
Harvard College, Cambridge, MA

SUBMITTED TO THE DEPARTMENT OF BIOLOGY IN PARTIAL  
FULFILLMENT OF THE  
REQUIREMENTS FOR THE DEGREE OF  
DOCTOR OF PHILOSOPHY  
AT THE  
MASSACHUSETTS INSTITUTE OF TECHNOLOGY

June 2017

© 2017 Dayan J. Li. All rights reserved.

The author hereby grants to MIT permission to reproduce and to distribute publicly  
paper and electronic copies of this thesis document in whole or in part in any  
medium now known or hereafter created.

**Signature redacted**

Signature of Author.....

.....  
Department of Biology  
May 19, 2017

**Signature redacted**

Certified By.....

.....  
Peter W. Reddien  
Professor of Biology  
Thesis Supervisor

**Signature redacted**

Accepted By.....

.....  
Amy E. Keating  
Professor of Biology  
Chair, Committee for Graduate Students



**ARCHIVES**



# Establishment and Maintenance of Pattern at the Ends of the Planarian Anterior-Posterior Axis

By

Dayan Li

Submitted to the Department of Biology on May 19, 2017  
in Partial Fulfillment of the Requirements for the Degree of Doctor of Philosophy in Biology

## ABSTRACT

How cellular and molecular processes are orchestrated to generate complex tissues and anatomical patterns is a longstanding question in biology. Planarians, flatworms capable of remarkable whole-body regeneration, are well suited for the study of patterning. They are adept at establishing pattern in new tissues during regeneration and maintaining pattern of existing tissues during homeostasis.

We focused our study of patterning along the planarian anterior-posterior (AP) axis spanning the head and the tail. Located at the ends of the AP axis are the anterior and posterior poles. As putative organizers, the anterior and posterior poles are regions defined by their expression of genes required for head and tail patterning, respectively. Using transplantation, we tested the organizing activity of the head tip region containing the anterior pole and demonstrated its ability to induce outgrowths containing a new AP axis and a midline. Furthermore, we studied the formation of the anterior pole during regeneration and determined that its location is set by three landmarks in pre-existing tissue – a polarized AP axis, the midline, and the dorsal-ventral median plane. By organizing regenerating tissue around a location determined by preexisting tissue, the anterior pole links existing positional cues to the establishment of new pattern.

To better understand pole function, we characterized the anterior and posterior pole transcriptomes by RNA sequencing. We identified several new genes highly expressed in the poles, including ones encoding transcription factors, cell surface receptors, and a secreted factor produced by both poles. Among them was *nr4A*, a nuclear receptor gene predominantly expressed in the body-wall muscle and found to regulate the expression of other muscle-enriched genes. Inhibition of *nr4A* during homeostasis resulted in both head and tail patterning defects characterized by a posterior shift of the anterior pole and an anterior shift of the posterior pole. This was accompanied by similar changes in the expression domains of head and tail patterning genes, and was followed by loss of muscle fibers at the head tip and the appearance of ectopic differentiated tissues normally restricted to the head and tail tip periphery. These results identified *nr4A* as a new planarian patterning gene that maintains head and tail identities, as well as anterior and posterior pole locations, at the ends of the planarian AP axis.

**Thesis Supervisor: Peter W. Reddien**  
**Title: Professor of Biology**



## ACKNOWLEDGMENTS

I would like to thank Peter for introducing me to the fascinating field of planarian regeneration. I began graduate school unsure about what topic to delve into, and after finishing a rotation in Peter's lab, my mind was set on studying such marvelous (and adorable-looking) organisms. Every time I walk out of a meeting with Peter, I learn something new, whether it is about science or the practice of science. Peter has taught me to approach science with rigor and has provided me the freedom and guidance I needed to develop as a scientist.

I am greatly indebted to fellow Reddien Lab members, who have generously helped me along the way. I owe special thanks to Mansi Srivastava, Lucila Scimone, and Omri Wurtzel, who have continuously provided their expertise and insightful critiques on my projects. Isaac and I collaborated on the pole transplantation experiment; working with him has been one of the highlights of my graduate experience. Irving, Lauren, and Kellie have been constant sources of technical help. My graduate program classmates, Amelie and Aneesha, have supported me throughout my stay in the lab. I owe much of my progress to them, and all of the Reddien Lab members who have made my graduate studies such an enjoyable and formative experience.

To my friends outside of the laboratory, it would be a dissertation in itself to describe all we have experienced together during these past four years. I would like to acknowledge my Paul and Daisy Soros Fellowship classmates in Boston and my MD-PhD program classmates who have cheered me on and taught me so incredibly much. My BG friends, certainly the social highlight of my graduate years, have provided me a haven to just enjoy life and be myself. I consider all of them my extended family, and deeply appreciate all the times they have been there for me.

Lastly and most importantly, my loved ones, Mom, Dad, John, and Yong, have been incredible sources of comfort, happiness, and inspiration throughout all these years. John has been such a caring younger brother, and a buddy I have been able to share unforgettable moments with. Yong has been my other half - his love, support, and humor have been my sustenance throughout, and I could not have made it this far without him. Finally, it is impossible to express how much I am grateful for my parents. Mom and Dad first instilled in me a curiosity about the world, and have sacrificed immensely to give me the opportunity to succeed. I owe all my success to them.

I dedicate this thesis to my grandmother Luo Yueying. Her love, kindness, courage, and energy knew no bounds, and she will always be my role model. I miss her dearly.



## TABLE OF CONTENTS

<b>CHAPTER 1: Introduction</b> .....	9
Overview of Planarian Regeneration .....	11
Mechanisms of Planarian Regeneration.....	16
Patterning in Planarian Regeneration.....	22
References.....	51
<b>CHAPTER 2: Landmarks in existing tissue at wounds are utilized to generate pattern in regenerating tissue</b> .....	63
Abstract .....	65
Introduction.....	66
Results and Discussion .....	67
Conclusions.....	100
Tables.....	101
Materials and Methods.....	102
Acknowledgements.....	108
References.....	109
<b>CHAPTER 3: Nuclear receptor NR4A patterns the ends of the planarian anterior-posterior axis</b> .....	113
Abstract .....	115
Introduction.....	116
Results.....	119
Discussion.....	166
Tables.....	172
Materials and Methods.....	191
References.....	196
<b>CHAPTER 4: Conclusions and Future Directions</b> .....	201
The Organizing Activity of the Planarian Poles .....	203
Planarian Pole Transcriptome and Function .....	206
The Role of <i>nr4A</i> in Patterning.....	209
Summary .....	211
References.....	212



# **CHAPTER 1**

## **Introduction**



## **Overview of Planarian Regeneration**

### **Primer on animal regeneration**

Across the animal kingdom, regeneration, known as the ability to replace or repair body parts, is a remarkable biological feat shared by many organisms. Regeneration is a fundamental process for survival, as it allows animals to recover from a multitude of injuries. Even in the absence of injuries, regenerative processes are needed to replace aging cells during homeostasis.

Among the animals that possess regenerative capacity are those as diverse as cnidarians, arthropods, mollusks, annelids, platyhelminthes, and vertebrates (Alvarado and Tsonis, 2006; Tanaka and Reddien, 2011). Not all regenerative animals are made equal in their regenerative potential, which roughly negatively correlates with increasingly body complexity (Poss, 2010). Organisms with simpler body plans, such as hydra and flatworms, can engage in whole-body regeneration from just small fragments. Higher-order animals like zebrafish and newts are able to regenerate whole organs like the heart, the spinal cord, and the appendages. Humans cannot fully regenerate as many organs, but we still retain our capacity to regenerate the skin, the gut epithelium, and liver, for example (Baddour et al., 2012).

Whatever the regeneration potential, common cellular and molecular mechanisms exist across species to enable the process. The replacement of lost cells can be achieved through asymmetric division of resident stem cells that generate more of themselves and progeny that will differentiate into the specialized tissue types (Weissman et al., 2001). Regeneration can also occur via dedifferentiation or transdifferentiation of other differentiated cells surrounding the injury (Jopling et al., 2011). In addition to the cellular source of regeneration, many

evolutionarily conserved signaling pathways, like the Wnt, Fgf, Bmp, and hedgehog pathways, influence the identity and organization of the new tissue (Alvarado and Tsonis, 2006).

Because different organisms use similar cellular and molecular toolkits to carry out their regeneration, using experimentally tractable animals to study regeneration can lead to important and widely applicable insights into this fascinating and still mysterious phenomenon. In one extreme case, knowledge of the signals involved in planarian regeneration can lead to the re-activation of head regrowth in a regeneration-deficient planarian species (Liu et al., 2013; Sikes and Newmark, 2013).

### **The planarian as a regenerative model organism**

Capable of whole-body regeneration, planarians are free-living freshwater flatworms that have been used as animal models for regeneration for more than a hundred years (Morgan, 1900). Evolutionarily, they belong to the superphylum Lophotrochozoa, which includes the segmented annelids and the molluscs (Fig. 1C). Together with the sister clade of Ecdysozoans, which include *Drosophila* and *C. elegans*, Lophotrochozoans comprise the Protostomes, one-half of the branch of Bilaterians, the other half being Deuterostomes (Adoutte et al., 2000; Philippe et al., 2009) (Fig. 1C). A commonly used species of planarians is *Schmidtea mediterranea*, which exists as a sexually reproducing strain of cross-fertilizing hermaphrodites and as an asexual strain that has lost its reproductive organs following a chromosomal translocation (Sánchez Alvarado et al., 2002). The asexual strain reproduces via fission of tail fragments, therefore generating a clonal line of animals with uniform genetic background that aids genetic experimentation (Sánchez Alvarado et al., 2002).

**Figure 1. Planarian anatomy**

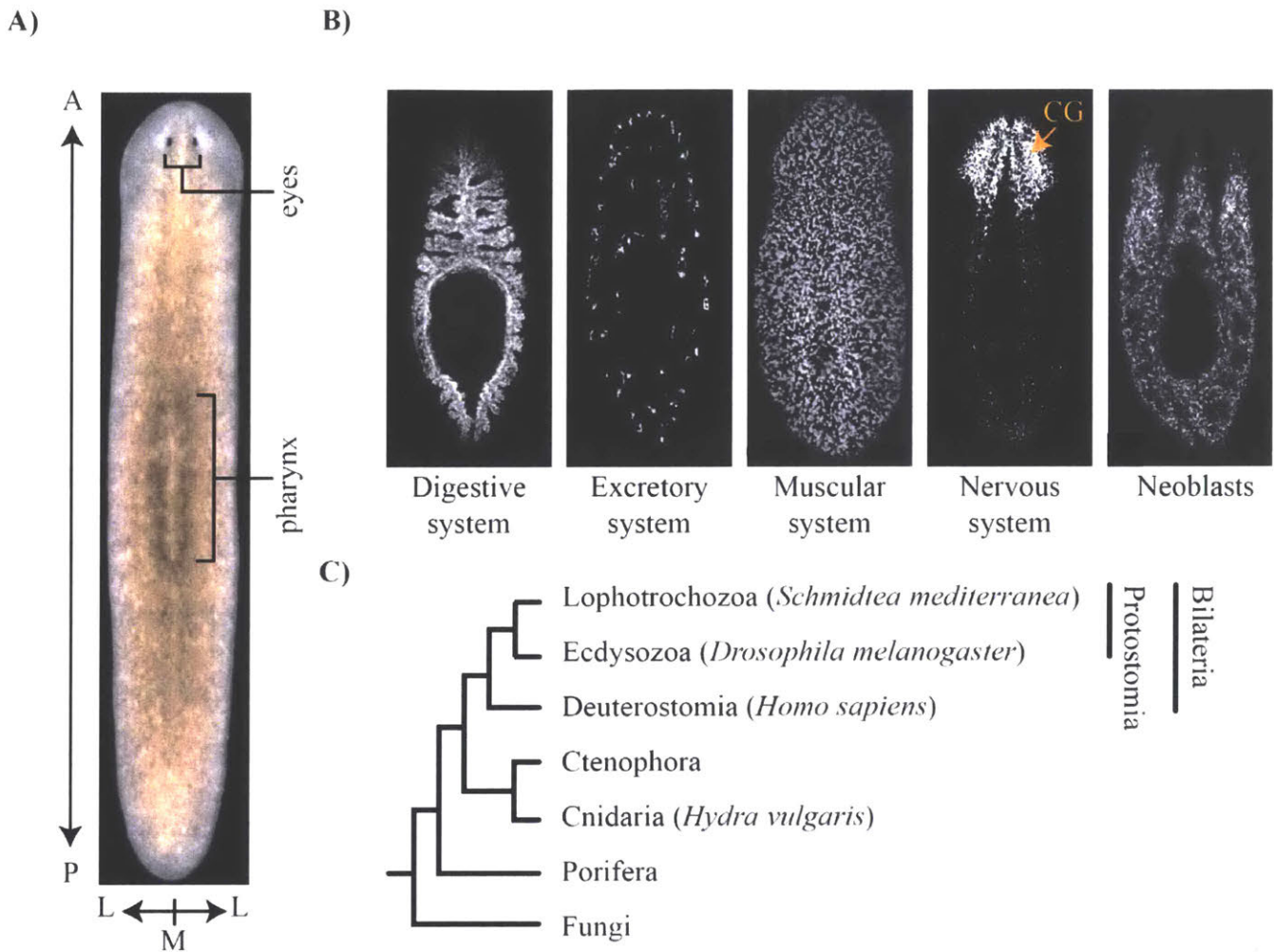


**Figure 1. Planarian anatomy.** (A) Dorsal view of a live planarian worm, with its anterior(A)-posterior(P) axis oriented vertically and medial(M)-lateral(L) axis oriented horizontally. (B) Fluorescence *in situ* hybridization with RNA probes of genes expressed in the digestive system (*methionine adenosyltransferase*), excretory system (*carbonic anhydrase*), muscular system (*collagen*), nervous system (*choline acetyltransferase*), and neoblasts (*smedwi-1*). CG indicates cephalic ganglion. (C) Phylogenetic relationship between the planarian *Schmidtea mediterranea*, a Lophotrochozoan, and other organisms. Commonly known representative organisms are named in parentheses. Branch lengths are not drawn to scale.

The planarian body plan is organized along an anterior-posterior (AP) axis spanning from head to tail, a ventral-dorsal (DV) axis, and a medial-lateral (ML) axis (Fig. 1A). Despite the simplicity of its body plan, planarians possess many specialized tissue types (Hyman, 1951) (Fig. 1B). Their central nervous system consists of two anterior cephalic lobes connected to ventral nerve cords that span along the AP axis. Neurons present throughout the body make up the planarian peripheral nervous system. Also connected to the nervous system is a pair of photoreceptors located dorsally in the head responsible for mediating the planarian phototactic behavior. In the midbody, planarians possess a muscular pharynx that protrudes through the mouth opening on the ventral surface for food ingestion. The pharynx is connected to the intestinal tract composed of three major branches, one anterior and two posterior, that pervade the animal. Scattered throughout the body is an extensive network of protonephridia that compose the planarian excretory system. On their surface, planarians are lined by a layer of epithelium that contains ventral ciliated cells responsible for their gliding movement. Beneath the epithelium lies the body wall muscle consisted of a mesh of longitudinal, circular, and diagonal fibers. Finally, though planarians lack a coelom, they contain mesenchymal tissue that fills in the space between the intestinal tract and the musculature. This tissue, known as the parenchyma, contains many different cell types including the cycling cells called neoblasts, which serve as the source of all new cells in the planarian body and underlie the planarian regenerative potential.

Planarians are masters of regeneration. Over the course of a week, they can regenerate entire bodies from very small fragments and wound geometries (Morgan, 1898). Each of the regenerated pieces will also give rise to full bodies after serial amputations, indicating that planarians have almost unlimited regenerative potential. Two processes are at play during

planarian regeneration – epimorphosis and morphallaxis (Morgan, 1898; Reddien and Sánchez Alvarado, 2004). In epimorphosis, an unpigmented outgrowth of newly generated cells called the blastema emerges from the wound site and eventually develops into specialized missing tissues. In morphallaxis, existing differentiated tissues are reorganized to re-establish proper proportions in the animal. Both epimorphosis and morphallaxis are essential processes during regeneration, as the former is involved the production of new cells and the latter is required to restore proper tissue scales.

Although planarians have been studied for over a century, only in the past decade have we gained genetic and molecular insights into the mechanisms of regeneration, including the heterogeneity and potential of neoblasts, and the signals involved in directing the proper tissue formation. This is in large part due to the sequencing of the planarian genome (Robb et al., 2015), the development of RNA interference (RNAi) to study gene function (Newmark et al., 2003; Sánchez Alvarado and Newmark, 1999), RNA *in situ* hybridization protocols to localize gene expression (Pearson et al., 2009), and most recently single-cell RNA sequencing that enabled studies of transcriptional responses at single-cell resolution (Wurtzel et al., 2015).

## Mechanisms of Planarian Regeneration

### Neoblasts as the source of all new cells

Unlike in other regenerative organisms (e.g. newts) where transdifferentiation and dedifferentiation of terminally differentiated cells play prominent roles in replacing lost parts, in planarians, resident stem cells – the neoblasts – are responsible for the animal's regenerative potential. Neoblasts are described as small (5-8  $\mu\text{m}$  in diameter), round cells with high nuclear-to-cytoplasm ratio present in the planarian parenchyma (Wolff, 1948). Recent RNA sequencing studies have found that many of the genes specifically expressed in neoblasts have conserved roles in stem cell maintenance, including *smedwi-1* and *smedwi-2*, which encode PIWI proteins found in germ cells in other organisms (Eisenhoffer et al., 2008; Galloni, 2012; Labbé et al., 2012; Önal et al., 2012; Palakodeti et al., 2008; Reddien et al., 2005b; Resch et al., 2012; van Wolfswinkel et al., 2014; Wagner et al., 2012).

Neoblasts comprise, as estimated by morphology, 25-30% of all cells in the planarian body, and are the only sources of dividing cells (Baguñà et al., 1989) (Baguñà, 1976; Baguñà et al., 1989). When gamma irradiation is applied to kill all dividing cells, planarians lose their regenerative ability and ultimately die, suggesting that neoblasts are the sole source of new cells during regeneration and homeostasis (Bardeen and Baetjer, 1904). In addition, when irradiated animals are injected with cells enriched with neoblasts via size fractionation, they are able to survive and recover their regenerative abilities (Baguñà et al., 1989). When injections were performed with cell fractions enriched with differentiated cells, no irradiation rescue was observed (Baguñà et al., 1989).

Another line of evidence showing that neoblasts are the source of new cells comes from cell labeling experiments using Bromodeoxyuridine (BrdU), which is incorporated into the DNA specifically during the S phase of the cell cycle. After planarians were fed with food containing BrdU, the first and only cells to incorporate BrdU were the neoblasts (Newmark and Sánchez Alvarado, 2000). This is followed by the detection of BrdU in non-neoblasts, likely neoblast progeny of differentiating and differentiated cells, 35 hours after first labeling (Newmark and Sánchez Alvarado, 2000). These neoblast descendants were observed both in the blastema and in differentiated tissues, indicating that they contribute new cells during regeneration and tissue turnover (Newmark and Sánchez Alvarado, 2000).

Experimental evidence thus far however, could not resolve the potency of the neoblasts. Were they pluripotent stem cells capable of differentiating into every other tissue type or did they comprise of a mix of lineage-restricted stem cell types? A convincing answer for this question was provided by the injection of a single neoblast into a lethally irradiated host (Wagner et al., 2011). Some of the injected worms were able to survive irradiation and recover regenerative capacity, demonstrating that at least a subset of neoblasts are pluripotent stem cells capable of self-renewal and differentiation into all the diverse cells in the planarian (Wagner et al., 2011).

Our understanding of the neoblast population was further refined by studies revealing the heterogeneity within the cycling cell population. RNA sequencing of neoblasts revealed that they expressed many transcription factors associated with differentiated tissues like the pharynx, the gut, and the muscle (Scimone et al., 2014a). These transcription factors labeled non-overlapping neoblasts and in many cases were required for the generation of their associated tissue types (Scimone et al., 2014a). Additionally, neoblast gene expression profiling at the single-cell level

revealed that neoblasts comprise two major functionally distinct classes (van Wolfswinkel et al., 2014). One is the zeta-neoblasts, characterized in part by their expression of the transcription factor gene *zfp-1*, and the other is the sigma-neoblasts, defined by their high expression of *sox-P1* and *sox-P2*. While the zeta-class is a more lineage-restricted class of neoblasts that gives rise to epidermal cells, the sigma-neoblasts are a collectively pluripotent class of cells capable of giving rise to all lineages, including zeta-class. Together, this evidence points to a model whereby the neoblast compartment is comprised of diverse groups of cells expressing class- and lineage-specific transcription factors that make neoblasts competent to differentiate into cells of their respective tissue types in both regeneration and homeostasis (Reddien, 2013). Whether a naïve neoblast population with low expression of tissue-specific transcription factor gives rise to specialized neoblasts committed to specific lineages or whether specialized neoblasts can switch lineage competencies is still an open question currently being investigated.

### **Phases of planarian regeneration**

Distinct cellular and molecular events characterize different phases in planarian regeneration. Response to injury begins with the migration of dorsal and ventral epidermal cells towards the wound site to cover and protect the wound surface (Baguña et al., 1994). This epidermal response, occurring within 30 minutes of the injury, is accompanied by the contraction of local musculature to help bring the dorsal and ventral epidermis together (Chandebois, 1980).

The rapid mechanical response to injury is followed by changes in cell proliferation, apoptosis, and gene expression that define the regeneration steps into an early wound-response phase that occurs regardless of the injury type, and a late regeneration phase specific to injuries

that necessitate tissue replacement and patterning.

### **Proliferative and apoptotic responses**

In planarians, increases in mitotic activity of neoblasts are observed after wounding. The mitotic response differs in its dynamics and location depending on whether the injury results in loss of tissue. Neoblasts undergoing cell division can be visualized and quantified *in situ* by immunofluorescence of phosphorylated histone H3 (H3P), which marks cells during the mitotic phase of the cell cycle (Henzel et al., 1997; Newmark and Sánchez Alvarado, 2000). Quantification of mitotic density across different amputated planarians fragments revealed that there are two bursts of mitosis following wounding (Wenemoser and Reddien, 2010). The first occurred at 6 hours post amputation (hpa), followed by decreasing mitotic activity until 18 hpa. Afterwards, mitotic activity increased and peaked at 48 hpa and was sustained for days after. Notably, dividing neoblasts during the first 6 hour peak were observed throughout the entire animal, whereas mitosis at 48 hours accumulated at the wound sites, likely due to cell migration (Guedelhofer and Sánchez Alvarado, 2012). Moreover, the localized increase in the number of mitotic cells during the second peak was only observed at wounds that resulted in tissue loss. Animals that received needle pokes or incisions not resulting in tissue removal only exhibited the body-wide increase in mitosis at 6 hpa. The first phase of mitosis is thought to be part of a general response to mechanical injury while the second phase of mitosis is a local response to the cellular renewal requirements of missing tissue.

Similarly, the amount and location of cell death in animal fragments behave in a biphasic manner (Pellettieri et al., 2010). The visualization of apoptotic cells in planarians can be

accomplished via the TUNEL (terminal deoxynucleotidyl transferase-mediated dUTP nick end labeling) assay. In amputated fragments, there is an increase in the number of apoptotic cells near the wound site at 4 hpa. This is followed by an increase in apoptotic cell numbers across the entire fragment at three days post amputation, followed by a gradual decrease to baseline. Whereas the rapid localized apoptotic burst is thought to be a direct response to the injury, the second body-wide increase in apoptosis is thought to result from extensive tissue remodeling that occurs during regeneration. Supporting this hypothesis, the second wave of apoptosis was more pronounced in tissue fragments lacking more complex structures such as the head and a pharynx (versus fragments regenerating only the tail) and scaled up with the amount of tissue amputated. Together, the proliferative and apoptotic responses after injury help define two important phases of planarian regeneration, one that occurs as the animals mount an early response to tissue damage and a later one that occurs as the injured fragments undergo patterning.

### **Transcriptional responses**

Changes in transcriptional programs also come in phases. A microarray-based transcriptional screen for wound-induced genes at different time points after animal amputation (30 minutes to 12 hours) determined that a subset of genes were upregulated within 30 minutes of wounding (Wenemoser et al., 2012). Many of these, including *jun-1*, *fos-1*, and *egr11*, encode homologs of immediate early genes, such as transcription and signaling factors. A late wave of wound-induced genes, upregulated between 3 and 12 hours following wounding, included subepidermally expressed genes that encode patterning factors like *wnt1*, *nlg1*, *inhibin-1*, and *folliculin*. Many of the genes identified in this screen were induced by different injury types,

including those that did and did not result in tissue loss. This suggests that a common transcriptional program is activated upon injury and serves as a generic response to wounds in preparation for the diverse cellular requirements that may be required depending on the injury context.

Single-cell RNA sequencing of wound sites at different time points after injury corroborated this observation (Wurtzel et al., 2015). Regardless of the nature of the injury, a common set of genes was upregulated during the early 4 and 12 hour time period of injury response, including many identified from the microarray study. Moreover, a large proportion of the generic wound-response genes were expressed in one of three cell types – neoblasts, epidermis, or muscle. When transcriptional responses were followed long-term in tail pieces that regenerated head and in incisions that did not require regeneration, many genes diverged in their expression. These genes include those encoding tissue-patterning factors, genes associated with specialized neoblasts, and markers of differentiated anterior tissues. Additionally, these divergent gene expression programs could be grouped into two temporal phases, an earlier phase (34-39 hpa) that included genes enriched in specialized neoblasts and patterning genes expressed in the head, and a later phase (at around 72 hpa) that included genes enriched in differentiated cell types in the head. Together, this data delineates the progression of the transcriptional landscape during regeneration, starting with a generic wound response program (0-24 hpa), followed by the expression of injury-specific patterning factors and specialized neoblast genes (~30 hpa), and culminating in the expression of differentiated tissue markers (~ 70 hpa).

## **Patterning in Planarian Regeneration**

### **Patterning**

During the period following the early cellular and molecular responses to wounding, planarians are faced with the challenge of regenerating exactly what is lost. Given the multitude of injury types that result in numerous wound geometries, varying amounts of tissue loss, and different identities of lost tissue, the generation of proper form in the new tissue and its integration with existing tissues are complex challenges that must be overcome for successful regeneration. This process is referred to as patterning, and involves carefully coordinated cell-to-cell communication to ensure that correct cell numbers, identities, and locations are established to faithfully replicate and maintain tissue architecture and organization.

### **Patterning along the AP axis**

In planarians, the establishment and maintenance of pattern have been most extensively studied along the AP axis. Experiments studying regeneration along the AP axis date back to more than 100 years ago, when TH Morgan observed the formation of a head from both the anterior and posterior wounds of thin transverse slices (Morgan, 1898; 1900). An explanation for this result invoked the presence of gradient of a molecule – a morphogen - that influenced the identity of surrounding tissues in a concentration-dependent manner (Morgan, 1905). Furthermore, although planarians amputated at any location along its AP axis can regenerate a head, the rate of head regeneration decreased at more posterior amputation planes (Sivickis, 1931). These early

experimental observations in planarian regeneration along the AP axis preceded and helped inform later hypotheses regarding the development of form and pattern, including Lewis Wolpert's positional information theory (Wolpert, 1969) and the existence of an organizing center as the source of morphogens (Lewis et al., 1977; Meinhardt, 1978; Slack, 1987). While multiple attempts have been made to isolate morphogens in planarians (Adell et al., 2010), it was not until the last decade, when RNAi methods were developed in these organisms, that the signals influencing planarian head and tail regeneration were identified.

Several Wnt signaling pathway components have been found to regulate planarian head and tail regeneration, revealing that Wnt signaling to be major regulator of AP identity during planarian regeneration and homeostasis. Specifically, Wnt signaling is required to establish and maintain tail identity while inhibition of Wnt signaling is required for head identity. *β-catenin-1*, encoding the downstream transcription factor of Wnt signaling, was identified in planarians as a gene crucial in AP polarity (Gurley et al., 2008; Iglesias et al., 2008; Petersen and Reddien, 2008). In animals with amputated tails, inhibition of *β-catenin-1* resulted in the regeneration of an ectopic head in the place of a tail, phenocopying the two-headed worm phenotype observed by TH Morgan (Gurley et al., 2008; Petersen and Reddien, 2008). The ectopic head contained a pair of photoreceptors, two cephalic ganglia, and intestinal branching pattern seen in normal heads. Heads also regenerated from lateral incisions made on the sides of the *β-catenin-1* animal (Gurley et al., 2008; Petersen and Reddien, 2008). Strikingly, in uninjured animals, long-term inhibition of *β-catenin-1* resulted in multiple head-like structures appearing along the sides (dorsal-ventral boundary) of the animal, suggesting that Wnt signaling is important in inducing and maintaining posterior identity during tissue regeneration and homeostasis. Conversely, RNAi of *APC*, a negative regulator of Wnt signaling, resulted in two-tailed animals with the

regeneration of an ectopic tail at the anterior amputation site (Gurley et al., 2008). In homeostasis, APC RNAi resulted in the appearance of tail buds along the dorsal-ventral boundary of the animal (Gurley et al., 2008). These experiments showed that Wnt signaling is both necessary and sufficient to promote posterior planarian identity. Still other genes encoding Wnt pathway components, like *evi/wntless*, which is necessary for Wnt secretion (Adell et al., 2009), and more recently *teashirt* (Owen et al., 2015; Reuter et al., 2015), a transcriptional target of Wnt signaling, have been identified as functionally important in Wnt-mediated specification of posterior identity, as RNAi of either *evi/wntless* and *teashirt* led to the double-headed phenotype observed in  *$\beta$ -catenin-1* RNAi.

Given that  *$\beta$ -catenin-1* is broadly expressed throughout the body of the animal, but anterior and posterior identities have different Wnt signaling requirements, there is likely differential regulation of the  *$\beta$ -catenin-1* activity across the AP axis. Consistent with this, genes encoding Wnt ligands, such *wnt1*, *wnt11-1*, *wnt11-2*, and *wntP-2*, and a Wnt receptor *frizzled-4* are expressed regionally in the tails (Gurley et al., 2010; Petersen and Reddien, 2009) (Fig. 2A). All of them except for *wnt1*, which is expressed linearly in a few cells at the midline of the tail tip, have graded expression domains from posterior to anterior (Gurley et al., 2010; Petersen and Reddien, 2009) (Fig. 2A). Conversely, genes encoding Wnt pathway inhibitors, such as *sFRP-1*, *sFRP-2*, and *notum* are expressed in graded anterior domains (Gurley et al., 2010) (Fig. 2A). In addition, *wntA* is expressed in the posterior region of the cephalic lobes while *notum*, besides being expressed in a small cluster at the head tip, is also expressed a small number of neural cells in the anterior commissure of the brain (Gurley et al., 2010; Hill and Petersen, 2015; Petersen and Reddien, 2011) (Fig. 2A).

Varying extents of defects in head and tail regeneration observed in the RNAi of many of these upstream Wnt signaling components highlight the dual roles Wnt signaling plays in regulating AP polarity (i.e. the decision to make a head or a tail) versus head and tail patterning during regeneration (Stückemann et al., 2017). While inhibition of *wnt1* resulted in ectopic head regeneration phenotypes seen in *β-catenin-1* RNAi (Adell et al., 2009; Petersen and Reddien, 2009), inhibition of *wnt11-2* and *wntP-2* expression did not lead to defects in regeneration polarity, but rather in tail patterning defects (Adell et al., 2009; Lander and Petersen, 2016; Scimone et al., 2016). During posterior regeneration, *wnt11-2* RNAi animals developed stunted tails that showed midline defects, such as fused intestinal branches and ventral nerve cords (Adell et al., 2009). Similarly, while *wntP-2* RNAi enhanced the *wnt1* RNAi regeneration polarity phenotype, RNAi of *wntP-2* alone had no effect on regeneration polarity (Lander and Petersen, 2016; Petersen and Reddien, 2009; Scimone et al., 2016). Rather, long-term inhibition of *wntP-2* resulted in the appearance of ectopic posterior mouths and pharynges, defects associated with tissue turnover during homeostasis (Lander and Petersen, 2016; Scimone et al., 2016).

**Figure 2. Planarian PCGs and model for muscle-mediated patterning**

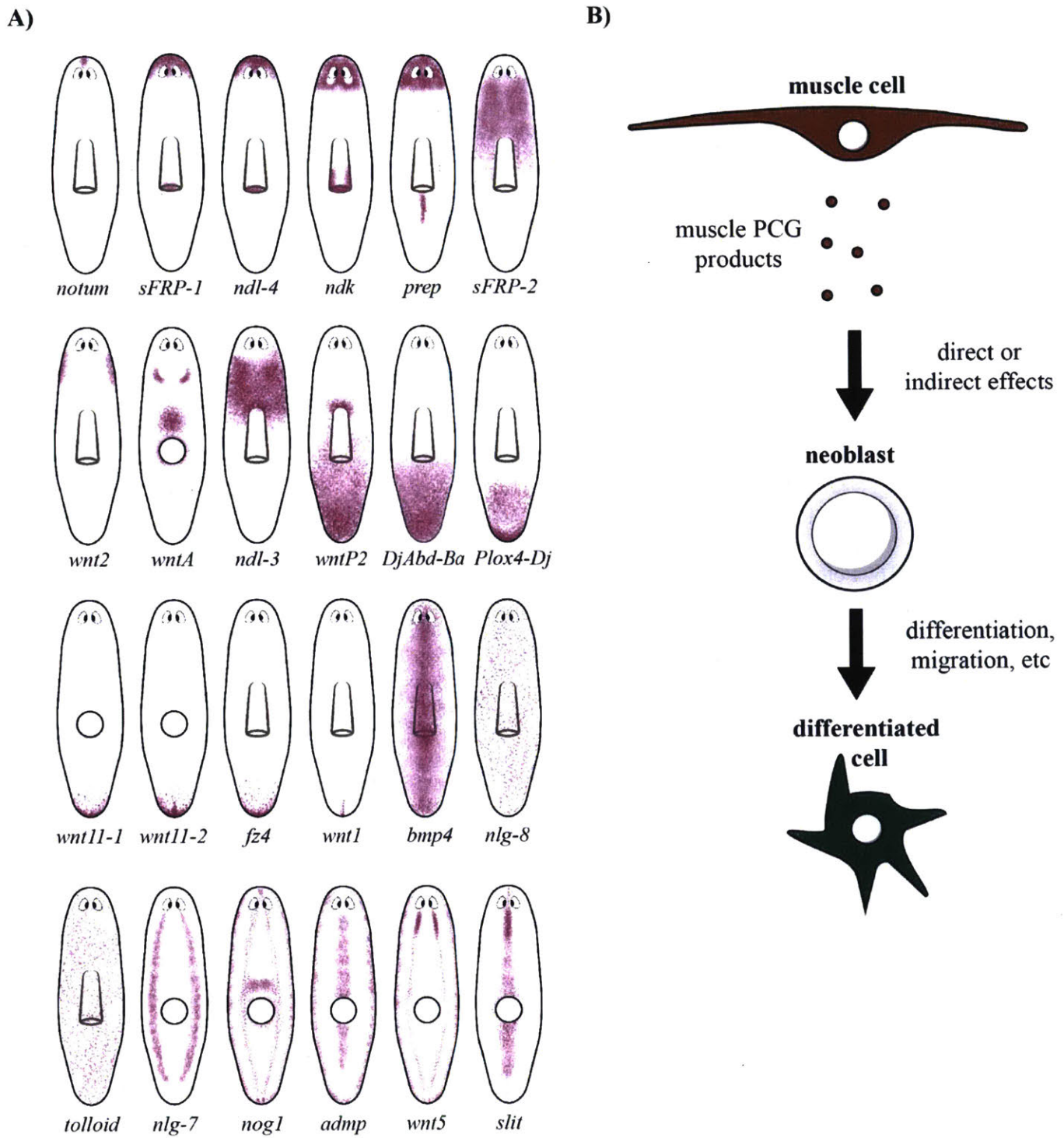


**Figure 2. Planarian PCGs and model for muscle-mediated patterning.** (A) Expression patterns of various planarian positional control genes (PCGs) in domains along the AP (vertical), ML (horizontal), and DV (in-out of the page) axes. Animal figures in dorsal view show the pharyngeal tube in the midbody; animal figures in ventral view show the circular mouth in the midbody. Figure is adapted from Reddien (2011). (B) Muscle signaling model in which muscle cells express PCGs, and produce PCG products (secreted morphogens or other signaling proteins) that influence, directly or indirectly, the behavior of neoblasts, which include differentiation into specific cell types and/or migration into appropriate locations. Whether muscle cells directly communicate with neoblasts has not been established.

In the head, *notum* appears to play roles in both regeneration polarity and head patterning. RNAi of *notum* in animals leads to the regeneration of a tail in the place of a head at the anterior-facing wounds, phenocopying the effects of *APC* RNAi (Petersen and Reddien, 2011). Unlike *APC* RNAi, however, *notum* RNAi in uninjured worms did not result in the formation of ectopic tail buds at the DV boundary. Instead, it led to the formation of ectopic anterior eyes and a reduction in brain size, effects that were suppressed by RNAi of *wntA* expressed in the posterior brain (Hill and Petersen, 2015). Furthermore, perturbation of *notum* expression at the tip of the head via RNAi of various transcription factors that regulate its head tip expression resulted in head patterning, not regeneration polarity defects. The patterning roles of *notum* and *wnt1* at the head and tail tips, respectively, will be discussed in detail in a later section. Similar to the effects of *wntA* RNAi, RNAi of *fz5/8-4* expressed in a restricted domain in the head also results in head patterning defects involving posterior brain expansion and posterior ectopic eyes (Lander and Petersen, 2016; Scimone et al., 2016). The range of polarity and head and tail patterning defects observed in the RNAi of Wnt signaling pathway components may be attributable to the degree of Wnt signaling inhibition, with strong inhibition affecting polarity and weaker inhibition leading to patterning defects. This is consistent with the observation that RNAi of the downstream Wnt pathway effector  *$\beta$ -catenin-1* results in polarity phenotypes that are more penetrant than inhibiting *wnt1*, one of the many upstream Wnt pathway ligands (Gurley et al., 2008; Petersen and Reddien, 2008; 2009). Furthermore, *APC(RNAi)*, which leads to ectopic tail regeneration, can also result in a range of head patterning phenotypes including cyclopia and stunted heads when administered at diluted dosages (Gurley et al., 2008).

Although Wnt signaling is a major regulator of polarity and patterning along the AP axis, other molecules also play important roles. Planarian Hedgehog signaling regulates regeneration

polarity by regulating Wnt signaling. Inhibition of *ptc*, a Hh pathway inhibitor, resulted in ectopic tail regeneration from anterior-facing wounds (Rink et al., 2009; Yazawa et al., 2009). Conversely, inhibition of pathway activators *hh* and *gli* caused tail regeneration defects ranging from reduced or absent tail tissue to ectopic heads (Rink et al., 2009; Yazawa et al., 2009). The effects of Hh signaling on regeneration were attributed to its regulation of Wnt signaling, specifically on its effects on the expression of *wnt1*. During regeneration, *wnt1* expression reduced in *hh(RNAi)* and increased in *ptc(RNAi)* (Rink et al., 2009; Yazawa et al., 2009). Furthermore, *wnt1(RNAi)* suppressed the *ptc(RNAi)* phenotype at anterior wounds and enhanced *hh(RNAi)* phenotype at posterior wounds, leading to the ectopic regeneration of heads (Rink et al., 2009; Yazawa et al., 2009).

In addition to major signaling pathways, biophysical properties of cells have also been implicated in regeneration polarity. Pharmacological block of gap junctions and triple RNAi of gap junction components *innexin-5*, *-12*, and *-13* resulted in the regeneration of heads from posterior-facing wounds (Nogi and Levin, 2005). Exposure of praziquantel, an antiparasitic drug, increased intracellular calcium levels and also led to the formation of ectopic posterior heads (Nogi et al., 2009). The increase in intracellular calcium levels at anterior blastemas was dependent on H<sup>+</sup>, K<sup>+</sup>-ATPase-mediated membrane depolarization, and inhibiting membrane depolarization blocked head regeneration (Beane et al., 2011). How changes in the biophysical properties of cells lead to regeneration polarity is still unclear, and more studies are needed to understand what effects ion flow and membrane depolarization have on transcriptional programs that regulate regeneration.

Another signaling pathway important in tissue patterning along the AP axis is the FGF signaling pathway. RNAi of *nou-darake* (*ndk*), a putative FGF antagonist gene specifically

expressed in the head (Fig. 2A), led to a dramatic posterior expansion of brain tissues and posterior ectopic eyes, causing a hypercephalization phenotype (Cebrià et al., 2002). Conversely, inhibition of *ndl-3*, an FGF receptor-like gene enriched in the prepharyngeal region (Fig. 2A), resulted in the ectopic formation of posterior mouths and pharynges. Both *ndk* and *ndl-3* cooperate with Wnt signaling components *fz5/8-4* and *wntP-2*, respectively, to maintain proper tissue patterning along the AP axis during homeostasis (Lander and Petersen, 2016; Scimone et al., 2016).

Several transcription factors have been described to pattern planarian heads. *pbx* and *prep* are TALE class homeobox transcription factor genes that are expressed broadly throughout the worm and enriched in the head, respectively. RNAi of *pbx* and *prep* does not affect head-versus-tail regeneration polarity, but causes head patterning abnormalities like the absence or fusion of the eyes and disruption of genes regionally expressed in the head (and tail for *pbx(RNAi)*). In addition to *pbx* and *prep*, several planarian homologs to the HOX gene cluster of transcription factors are expressed in graded domains across the AP axis. Although HOX genes are notable for AP axial fate specification in developing embryos (McGinnis and Krumlauf, 1992; Wellik, 2009), no functional roles of planarian HOX gene homologs have yet been reported (Currie et al., 2016).

### **Patterning along the DV axis**

Patterning in planarians also depends on the asymmetric specification of tissues along the DV axis. The central nervous system (CNS), consisting of two anterior cephalic lobes each connected to a nerve cord that extends into the tail, is located ventrally. In contrast, planarian

photoreceptors develop at the dorsal surface of the head and project axons ventrally into the brain. Furthermore, the planarian epidermis also exhibits DV asymmetry, as the ventral epidermis contains the majority of ciliated cells that are important for normal locomotion. Along the lateral edges of the animal, where the dorsal and ventral surfaces meet, lies the DV boundary, which is marked by the expression of several markers, including the epidermal genes *laminB* (Kato et al., 1999) and NB.22.1e (Eisenhoffer et al., 2008).

The development of DV axial identity in many metazoans is governed by the activity of the Bone morphogenic protein (Bmp) signaling pathway (De Robertis and Kuroda, 2004; Meinhardt, 2015). In planarians, Bmp signaling also plays a crucial role in DV patterning during regeneration and homeostasis. Specifically, Bmp signaling promotes dorsal and inhibits ventral pattern. The first planarian *bmp* homolog was isolated from *Dugesia japonica* (Orii et al., 1998). Its expression along a midline stripe on the dorsal side of the animal suggested that it may play a role in DV or midline patterning (Orii et al., 1998). Subsequent studies have identified planarian homologs to other components of the Bmp pathway, including *bmp2/4/decapentaplegic* and *admp* (encoding Bmp pathway ligands), *smad1* and *smad4-1* (encoding Bmp pathway transcription factors), and *tolloid* (encoding an extracellular Bmp pathway antagonist) (Gaviño and Reddien, 2011; Molina et al., 2007; Orii and Watanabe, 2007; Reddien et al., 2007). RNAi of *bmp4*, *smad1*, *smad4-1*, and *tolloid* resulted in expansion of ventral identity to the dorsal region of the animals, including decreased expression of dorsal markers, ectopic dorsal expression of ventral markers, and dorsal duplication of the brain, the nerve cords, and of the DV boundary (Molina et al., 2007; Orii and Watanabe, 2007; Reddien et al., 2007). Additionally, inhibiting Bmp signaling resulted in the ectopic appearance of ciliated epidermis on the dorsal surface, allowing animals to swim on their “backs” (Reddien et al., 2007). Many of these

phenotypes were observed in regenerating and uninjured animals, demonstrating that Bmp signaling is important in both establishing new DV pattern and maintaining DV pattern during tissue turnover. Interestingly, whereas *bmp4* was expressed in the dorsal midline, *admp* was expressed in the ventral midline, suggesting that their opposing expression domains along the DV axis define the DV poles seen in the Bmp/Admp signaling centers during metazoan embryogenesis (Gaviño and Reddien, 2011; Molina et al., 2007). *admp(RNAi)* enhanced the ventralizing phenotype of *bmp4(RNAi)*, suggesting that *admp* acts together with *bmp4* to establish dorsal pattern in planarians (Molina et al., 2007). In addition, several planarian *noggin* genes, which act as canonical Bmp pathway antagonists, have been identified (Molina et al., 2011; 2009). Simultaneous inhibition of planarian *nog1* and *nog2* resulted in dorsalized phenotypes including ectopic ventral expression of a dorsal marker and anteroventral outgrowths that occasionally developed eyes (Molina et al., 2011). Notably, *nlg-8*, a planarian *noggin*-like gene (with an insertion in the *noggin* domain-encoding region), was expressed broadly on the dorsal side (Molina et al., 2009; 2011). RNAi of *nlg-8* recapitulated the neural phenotypes seen in *bmp4(RNAi)*, demonstrating that unlike *nog1* and *nog2*, *nlg-8* acts to promote Bmp signaling in planarians (Molina et al., 2011).

### **Patterning along the ML axis**

There is evidence indicating that Bmp signaling also plays a role in patterning the planarian medial-lateral axis. First of all, *bmp4* and *admp* are expressed at the midline on the dorsal and ventral surfaces, respectively (Gaviño and Reddien, 2011; Molina et al., 2007; Orii and Watanabe, 2007) (Fig. 2A). In a sagittally amputated piece that does not contain the existing

midline, new *bmp4* expression is observed near the lateral wound side, suggesting that such expression may help set the new midline of the regenerating thin slice (Orii and Watanabe, 2007). RNAi of *bmp4*, *admp*, *smad*, and *tolloid* results in lateral regeneration defects, including the absence of expression of DV boundary markers and small or absent lateral blastemas (Gaviño and Reddien, 2011; Molina et al., 2007; Orii and Watanabe, 2007; Reddien et al., 2007). In transversely amputated animals, disruption of Bmp signaling yielded indented anterior and posterior blastemas (Gaviño and Reddien, 2011; Molina et al., 2007; Reddien et al., 2007). In these animals, the midline crossover of axons from the photoreceptors is aberrant or missing (Gaviño and Reddien, 2011; Molina et al., 2007; Reddien et al., 2007). After long-term inhibition of *bmp4* and *smad*, some animals also develop ectopic photoreceptors medial to the original photoreceptors (Reddien et al., 2007). The role of Bmp signaling in patterning the planarian ML axis is consistent with its role in ML patterning in other contexts, such as development of the heart and viscera in zebrafish (Monteiro et al., 2008), morphogenesis of the mouse telencephalon (Chizhikov and Millen, 2005), and axon guidance (Charron and Tessier-Lavigne, 2005).

In addition to the Bmp pathway, *wnt5* and *slit* were found to reciprocally pattern the ML axis during regeneration and homeostasis by restricting the expansion of medial and lateral tissues, respectively. *slit* encodes a protein from a well conserved family of axon guidance proteins important for nervous system development. In both *Drosophila* and vertebrates, *slit* mutants present with collapse of commissural and longitudinal axonal tracts at the midline (Rothberg et al., 1990) (Kidd et al., 1999) (Long et al., 2004). In zebrafish development, Wnt5 mediates the midline convergence of primordia for unpaired organs like the pancreas, liver, and the heart (Matsui et al., 2005). In planarians, *wnt5* is expressed lateral to the ventral nerve cords, including on the DV boundary, whereas *slit* is expressed in a midline stripe medial to the nerve

cords (Cebrià et al., 2007; Gurley et al., 2010) (Fig. 2A). In both regenerating and intact animals, RNAi of *wnt5* resulted in the lateralization of midline tissues, including the thickening of the cephalic lobes and ventral nerve cords, development of lateral ectopic eyes, and development of lateral ectopic pharynges (Gurley et al., 2010). In addition, ventral *slit* expression domain in *wnt5(RNAi)* animals laterally expanded beyond the ventral nerve cords and into the body periphery (Gurley et al., 2010). RNAi of *slit*, on the other hand, resulted in the collapse of the midline involving the fusion of the cephalic lobes, ectopic medial eyes, and ectopic *wnt5* expression across the midline (Cebrià et al., 2007).

### **Planarian muscle as the source of patterning information**

The identification of the multitude of regionalized factors important in positional identity across the AP, DV, and ML axes has shed light into the mechanisms of patterning during regeneration and homeostasis. These domains of gene expression must be stably maintained during tissue turnover and must also dynamically change after injury in order to faithfully inform pattern formation and maintenance. Clues to how this is accomplished came from observations of patterning gene expression in irradiated animals. In a non-irradiated amputated tail, the initial broad *wntP-2* expression reflects the old AP axial positioning of the preexisting tissue before amputation (Gurley et al., 2010; Petersen and Reddien, 2009). However, as the tail fragment regeneration progresses, *wntP-2* expression is gradually restricted to a more posterior domain as the AP axis is re-scaled to the new dimensions of the regenerate (Petersen and Reddien, 2009). In animals irradiated before tail amputation, such *wntP-2* expression domain still scaled normally in the tail pieces, indicating that the dynamic change in *wntP-2* expression was not dependent on

neoblasts, and instead occurred in differentiated cells (Petersen and Reddien, 2009). Similarly, in DV patterning, new *bmp4* expression on thin lateral regenerates from sagittal amputations was still observed after irradiation (Reddien et al., 2007). Neoblast-independent induction of expression of a *noggin-like* gene was also observed in *Dugesia japonica* (Ogawa et al., 2002). Furthermore, transplantation experiments in which grafts from donor worms were placed into recipient worms in reversed DV polarity resulted in regeneration of outgrowths due to positional conflict between the grafts and the host tissue (Kato et al., 1999). In parallel experiments in which either the grafts or the hosts were irradiated, such outgrowths still formed and exhibited newly established DV axes and anterior and posterior characteristics as observed in outgrowths from non-irradiated transplantation experiments (Kato et al., 2001). These results suggest that differentiated cells are the source of positional cues that induce morphogenesis.

A systematic characterization of the expression characteristics of the known regionally expressed genes implicated in patterning showed that nearly all of the genes examined were expressed predominantly in a subepidermal layer of differentiated cells (Witchley et al., 2013). Furthermore, there was a high degree of overlap in expression among the regionalized genes, suggesting that they are expressed in the same cell population (Witchley et al., 2013). Co-expression analysis of the expression of regionalized genes with markers for various differentiated tissues identified muscle cells as the cells that predominantly express almost every previously reported planarian patterning gene (Witchley et al., 2013). This finding further demonstrated that the body-wall muscle is the source of positional information that guides patterning during regeneration and homeostasis.

## The planarian body-wall muscle

The planarian body-wall muscle consists of a compact 7-12  $\mu\text{m}$  thick net of subepidermal muscle fibers (Cebrià et al., 1997; Cebrià, 2016). The body-wall musculature of *Schmidtea mediterranea* is composed of four layers – circular, longitudinal, diagonal, and longitudinal fibers from the outermost to the innermost layer (Cebrià et al., 1997; Cebrià, 2016). Along the DV boundary, there are also DV fibers that run the DV axis (Cebrià et al., 1997; Cebrià, 2016). Planarian muscle cells are mononucleated cells that range from 150-200  $\mu\text{m}$  in length and 5-10  $\mu\text{m}$  in width (Baguña and Romero, 1981; MacRae, 1963). Within them, their myofilaments are arranged in irregularly distributed dense bodies that are occasionally interspersed with structures known as Z bars (Hori, 1983; Lanzavecchia, 1977; MacRae, 1963; 1965; Morita, 1965; Reuter, 1977; Rieger et al., 1991). Recent development of multiple antibodies highlighting structural components of muscle fibers have enabled the visualization of the planarian muscle at exquisite detail (Cebrià et al., 1997; Ross et al., 2015).

Planarian muscle cells are transcriptionally characterized by their expression of *collagen*, *troponin*, and *tropomyosin* (Witchley et al., 2013). In addition, a planarian *myoD* homolog is expressed in the body-wall muscle in *Schmidtea mediterranea* (Cebrià et al., 1997) (Reddien et al., 2005a). A member of a conserved family of bHLH transcription factor genes, *myoD* promotes the commitment and differentiation of the skeletal muscle lineage in many other metazoans (Buckingham and Rigby, 2014; Davis et al., 1987; Weintraub et al., 1991). In addition to being expressed in planarian body-wall muscle, *myoD* is also expressed in neoblasts, likely playing a role in neoblast differentiation into muscle cells (Scimone et al., 2014a). RNAi of *myoD* during regeneration results in pointed blastemas and heads, a phenotype attributed to

defects in body-wall musculature (Reddien et al., 2005a). Differentiated myocytes marked by an antibody against myosin heavy chain are seen by one day after injury in the preexisting tissue abutting the amputation site (Cebrià et al., 1997). As regeneration progresses, myocytes at different stages of differentiation appear within the blastema (Cebrià et al., 1997). A few muscle fibers were also observed crossing the boundary between the preexisting tissue and the regenerating blastema (Cebrià et al., 1997). Although it is uncertain whether these muscle fibers are old fibers that have extended into the regenerating zone or new fibers that have joined fibers from the existing tissue, the integration of fibers from new and old tissue is consistent with the idea that the preexisting tissue, and especially the planarian body-wall muscle, plays an instructive role during regeneration.

### **Muscle positional information model**

The identification of muscle cells as a widespread and region-specific source of patterning molecules, combined with the large pool of neoblasts capable of responding to signals via proliferation, migration, and gene expression, gave rise to a new model explaining a broad mechanism of planarian regeneration (Fig. 2B). Present throughout the animal body, muscle cells respond to different types of injuries by changing their expression of patterning genes to accommodate axis perturbations from tissue loss. Newly established and rescaled expression domains of patterning molecules from muscle cells then promote, directly or indirectly, the specification and/or migration of neoblasts into the appropriate replacement tissues (Witchley et al., 2013) (Fig. 2B). In uninjured animals, the constitutive expression of patterning genes at specific domains along the animal axes continuously maintains neoblast-dependent renewal of

specialized tissues during tissue turnover (Reddien, 2011). Through this process, the muscle and neoblast compartments make up a robust and flexible system that can reliably and flexibly respond to a diverse set of injuries (Reddien, 2011; Witchley et al., 2013). A compelling demonstration of this system lies in the specification of dorsal and ventral epidermal cell identities. Bmp pathway genes like *bmp4* are one of the patterning genes expressed in the body-wall muscle. RNAi of *bmp4*, which results in a ventralization phenotype, leads to the encroachment of ventral epidermis cell types and ventral markers onto dorsal epidermis (Wurtzel et al., 2017). Lethal irradiation prior to *bmp4* RNAi suppressed the epidermal ventralization phenotype, suggesting that neoblasts are the cells that responded to Bmp signaling perturbation and generated the epidermal phenotype (Wurtzel et al., 2017). Consistent with this hypothesis, epidermal progenitors expressing a ventral epidermal marker were observed next to ectopic ventral epidermis (Wurtzel et al., 2017). This indicated that aberrant Bmp signaling caused improper specification and/or migration of neoblasts and their progenitors. To date, these results provide the strongest evidence supporting the role of muscle-specific patterning gene expression in determining the behavior of neoblasts and the fate of differentiated tissues.

### **Planarian anterior and posterior poles**

The model in which muscle cells express regional gradients of patterning genes, many encoding secreted signaling proteins, invokes the concepts of morphogen gradients and organizing centers. The existence of local tissues (the organizers) producing diffusible factors (the morphogens) that influence the fates of surrounding cells in a concentration-dependent manner has been shown many times over in several embryological contexts, including in amphibians (the Spemann-

Mangold organizer) (Spemann and Mangold, 1924), chicks (Waddington, 1933), mice (Beddington, 1994), and zebrafish (Shih and Fraser, 1996). In these cases, organizers help pattern surrounding tissues for example, by modulating the levels of signaling of the Wnt pathway and the Bmp pathway across the AP and DV axes, respectively.

Regenerative organisms have also been shown to use organizers as patterning centers during tissue regeneration. In hydra, cnidarians capable of whole-body regeneration, transplantations of oral or aboral tips onto the side of the animal resulted in the induction of ectopic axes (Browne, 1909; Kadu et al., 2012; Wolpert et al., 1971). Many of the signals responsible for such inductive effects were later identified as Wnt ligands at the oral end (Lengfeld et al., 2009; Nakamura et al., 2011), suggesting that a gradient of Wnt signaling exists to pattern the oral-aboral axis. In zebrafish, capable of regenerating their fins, the non-proliferative distal end of the fin blastema was found to act as an organizer by using Wnt signaling to direct the proliferation and differentiation of cells in the proximal blastema (Wehner et al., 2014).

In planarians, the head and tail tips have been subjects of intense interest due to their roles as organizers at the ends of the AP axis. Clues to the organizing properties of the head date back to the first systematic planarian transplantation study conducted by Felix Santos (Santos, 1931). Using the *Planaria dorotocephala* and *Planaria maculata* species, Santos transplanted portions of the head that included the photoreceptors and the cephalic ganglia onto various regions along the AP axis of recipients. Many of the grafts successfully gave rise to ectopic head outgrowths containing properly organized eyes and brain tissue. Some grafts in the posterior regions of the hosts even induced the formation of ectopic pharynges of the reverse polarity. It was not until the advent of RNAi in planarians that the inductive capacity of these head pieces

was attributed to the graded activity of signaling pathways like the Wnt pathway.

Wnt/ $\beta$ -catenin signaling is both necessary and sufficient to promote posterior identity. Studies on the planarian Wnt pathway components have identified many genes with regionalized expression in the head and the tail. Of those genes, *notum* expression in the head and *wnt1* expression in the tail have gained increased scrutiny. *notum* encodes a secreted Wnt antagonist that in *Drosophila* has shown to act as a deacylase by removing an essential palmitoleate moiety from Wnt proteins (Kakugawa et al., 2015). *wnt1* encodes a secreted Wnt ligand that has been shown to regulate anterior-posterior patterning in many organisms by signaling through the canonical Wnt/ $\beta$ -catenin pathway (Yamaguchi, 2001). In planarians, *notum* is expressed in a small cluster of cells at the midline of the tip of the head (Petersen and Reddien, 2011) (Fig. 3). *wnt1*, on the other hand is expressed in a longitudinal line of few cells at the midline of the tip of the tail (Gurley et al., 2010; Petersen and Reddien, 2008; 2009) (Fig. 3). Owing to their locations at the extreme ends of the AP axis, *notum* and *wnt1* expression domains at the head and tail tips have been denoted, respectively, as the anterior and posterior poles of the planarian (Adell et al., 2009; Gurley et al., 2010; Petersen and Reddien, 2009; 2011; Reddien, 2011). Like many other mRGs, both *notum* and *wnt1* are predominantly expressed in the body-wall muscle, with about 80% of *notum*<sup>+</sup> cells at the anterior pole and about 95% of *wnt1*<sup>+</sup> cells at the posterior pole expressing the muscle marker *troponin* in uninjured animals (Witchley et al., 2013). In regeneration, the dynamics of *notum* and *wnt1* expression bear striking similarities. Both have two phases of expression defined not only by expression dynamics, but also by expressing cell type, expression pattern, and function during regeneration (Fig. 3).

*notum* expression is first observed at anterior-facing wounds at 6 hpa in scattered cells

along the wound edge (Petersen and Reddien, 2011). Strongest at 18 hpa and decreasing by 24 hpa, *notum* expression during this period defines the wound-induced phase (Petersen and Reddien, 2011). During this phase, *notum* expression is almost exclusively in muscle (98% co-expression with collagen at 16 hpa) (Witchley et al., 2013), and as expected, is irradiation-insensitive (Chen et al., 2013; Scimone et al., 2014b). *notum* is the earliest known wound-induced gene to be asymmetrically expressed between anterior and posterior-facing wounds (Wurtzel et al., 2015), and this characteristic implicates *notum* in regeneration polarity. Indeed, RNAi of *notum* in regeneration results in the formation of tails at anterior-facing wounds. The second phase of *notum* expression during regeneration is observed by 48 hpa, when *notum* begins to be highly expressed in a cluster of cells along the midline at the tip of the anterior blastema. This expression pattern is consolidated by 72 hpa and persists thereafter, including in fully regenerated worms. At this stage, cells that express *notum* are newly produced cells, and as expected, this clustered *notum* expression is observed in neoblasts and is eliminated by irradiation (Scimone et al., 2014b). It is this latter radiation-sensitive *notum* expression that defines the anterior pole and regulates head patterning (Fig. 3). The timing of the pole phase of *notum* expression coincides with the upregulation of many other patterning genes (Wenemoser et al., 2012; Wurtzel et al., 2015). RNAi of *notum* during regeneration results in ectopic tail formation at anterior-facing wounds seen in APC RNAi experiments where regeneration polarity is affected (Gurley et al., 2008; Petersen and Reddien, 2008; 2011). However, RNAi of *notum* in uninjured animals, which decouples the role of *notum* in head patterning from its role in regeneration polarity, results in head patterning defects such as ectopic eyes and reduced brain size and not does lead to ectopic tails that we see in *APC* homeostasis RNAi (Hill and Petersen, 2015; Petersen and Reddien, 2008).

Figure 3. Planarian anterior and posterior pole formation

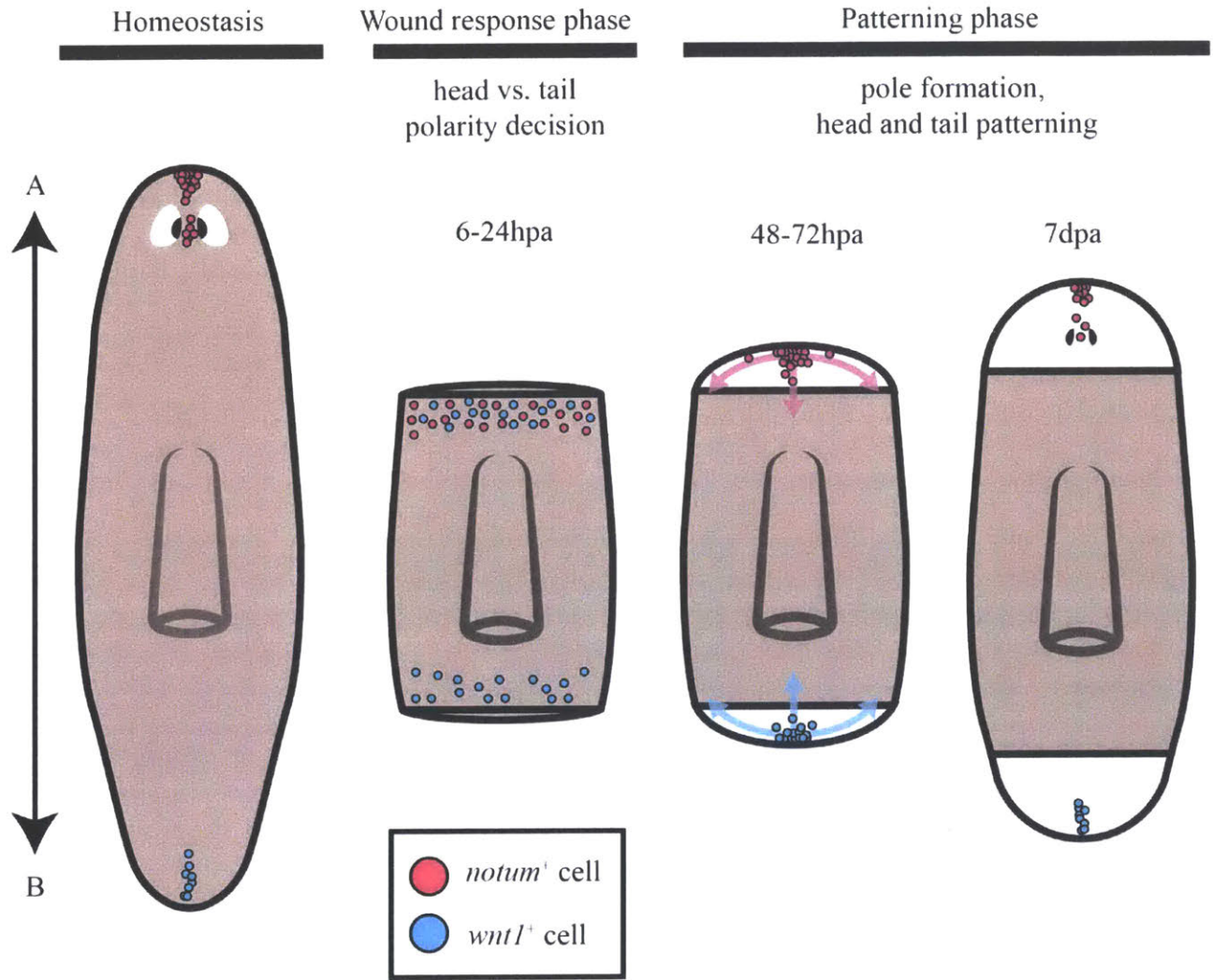


**Figure 3. Planarian anterior and posterior pole formation.** In homeostasis, the planarian anterior and posterior poles are located along the midline of the head and tail tips, respectively, with *notum*<sup>+</sup> anterior pole cells aggregated in a cluster and *wnt1*<sup>+</sup> posterior pole cells organized in a line. *notum*<sup>+</sup> cells in between the eyes are neural cells at the anterior brain commissure and are not part of the pole. During the wound response phase (6-24 hpa), before the formation of the poles, *notum* and *wnt1* are expressed in muscle cells near the wounds. Polarized expression of *notum* at the anterior-facing wound leads to the decision to regenerate a head, while unopposed Wnt signaling at posterior-facing wound leads to the decision to regenerate a tail. During the patterning phase, anterior (*notum*<sup>+</sup>) and posterior (*wnt1*<sup>+</sup>) pole cells are specified along the midline at the tip of the anterior and posterior blastemas, respectively (48-72hpa). During this time, the poles organize the blastema along AP and ML axes. By 7 days post amputation (dpa), properly patterned heads and tails are formed, and the posterior pole domain becomes linearized. Figure is adapted from Owlarn et al. (2016) and Scimone et al. (2014b).

*wnt1*, on the other hand, is first expressed in cells scattered at both anterior- and posterior-facing wound edges starting at 16 hpa (Petersen and Reddien, 2009) (Fig. 3). Similar to wound-induced *notum* expression, wound-induced *wnt1* expression wanes between 24 to 48 hpa, is concentrated in muscle cells, and is irradiation-insensitive (Petersen and Reddien, 2009; Witchley et al., 2013). By 48 hpa, *wnt1* is expressed in a cluster of cells along the midline at the tip of the posterior blastema only (Petersen and Reddien, 2009) (Fig. 3). This pattern, reminiscent of *notum* expression in the regenerating anterior pole, defines the posterior pole phase of *wnt1* expression, which occurs in new cells and is eliminated by irradiation (Petersen and Reddien, 2009). RNAi of *wnt1* resulted in ectopic head formation at posterior-facing wounds, indicating that it plays a role in regeneration polarity (Adell et al., 2009; Petersen and Reddien, 2009). In sagittal amputations running along the AP axis, wound-induced *wnt1* is expressed along the entire AP wound edge (Petersen and Reddien, 2009). When *wnt1(RNAi)* animals were sagittally amputated, they formed extra photoreceptors and expanded anterior marker expression in the regenerated head portions, indicating that wound-induced *wnt1* also plays a role in preventing anteriorization during patterning after sagittal amputations (Petersen and Reddien, 2009). However, the effect of long-range signaling from posterior pole-expressed *wnt1* cannot be ruled out. So far, a homeostatic *wnt1(RNAi)* phenotype has not been observed.

Besides *notum* and *wnt1*, the anterior and posterior poles are defined by the expression of many of other genes. Anterior pole cells also express *follistatin (fst)* (Gaviño et al., 2013; Roberts-Galbraith and Newmark, 2013), a gene encoding a secreted inhibitor of the TGF- $\beta$  signaling pathway. While *fst* expression is concentrated in the anterior pole in uninjured animals, it is also present in cells scattered throughout the body (Gaviño et al., 2013; Roberts-Galbraith

and Newmark, 2013). *fst* is a wound-induced gene with strong expression at both anterior- and posterior-facing wounds by 6 hpa (Gaviño et al., 2013). RNAi of *fst* results in small or absent blastemas after injuries resulting in missing tissue, including in head amputations, indicating that *fst* is broadly required for regeneration (Gaviño et al., 2013). *fst(RNAi)* animals with small anterior blastemas fail to regenerate the anterior pole and cephalic ganglia, expressed reduced levels of the head mRGs *sFRP-1* and *ndk*, but do not express posterior markers, indicating a role for *fst* in anterior patterning but not regeneration polarity (Roberts-Galbraith and Newmark, 2013).

Besides genes encoding secreted factors, cells at the anterior pole also express transcription factor genes *foxD* and *zic-1*, which are important for anterior pole cell specification (Scimone et al., 2014b; Vásquez-Doorman and Petersen, 2014; Vogg et al., 2014). *foxD* belongs to a conserved family of genes encoding winged-helix transcription factors that play roles in cell proliferation, growth, and differentiation (Benayoun et al., 2011). Members of the *Fox* gene family are expressed in the anterior region of embryos of several species, including *Drosophila*, amphioxus, and *Xenopus*, and in *Drosophila* are required in head and midline patterning (Cadigan et al., 1994; Dirksen and Jamrich, 1992; Grossniklaus et al., 1992; Häcker et al., 1995; Weigel et al., 1989; Yu et al., 2003). In planarians, *foxD* has a wound-induced expression phase at the ventral midline 6 hpa, and is also expressed at the anterior pole in regeneration and in uninjured animals (Scimone et al., 2014b). RNAi of *foxD* resulted in defects in head regeneration, including absence of the anterior pole, cyclopia, small anterior blastemas, and medial collapse of cephalic ganglia (Scimone et al., 2014b). Tail regeneration and the posterior pole were spared in *foxD(RNAi)* animals, showing that *foxD* specifically regulated patterning in the head (Scimone et al., 2014b). None of the *foxD(RNAi)* animals developed ectopic posterior

identities in the anterior blastema, indicating that *foxD* does not regulate regeneration polarity, consistent with its anterior pole expression (Scimone et al., 2014b). Furthermore, *foxD* RNAi did not affect wound-induced expression of *notum*, again showing that the *foxD*(RNAi) head patterning phenotype is attributable to disrupting the patterning phase of *notum* expression (Scimone et al., 2014b). Finally, in the regenerating anterior poles at 72 hpa, *foxD* is expressed in neoblasts (Scimone et al., 2014b). This, together with the absence of the anterior pole in *foxD* RNAi, suggests that *foxD* is required for anterior pole specification.

Similarly, *zic-1*, encoding a zinc finger protein, is required for anterior pole formation (Vásquez-Doorman and Petersen, 2014; Vogg et al., 2014). *zic-1* is first expressed at both anterior- and posterior-facing wounds at 18hpa, but later during regeneration is enriched only at the anterior blastema in anterior pole cells (Vásquez-Doorman and Petersen, 2014). *zic-1* and *foxD* regulate each other's expression and also the expression of *notum* and *fst* (Vogg et al., 2014). *zic-1* RNAi phenocopies *foxD* RNAi, resulting in head regeneration defects such as cyclopia, medial collapse of cephalic ganglia, small anterior blastemas, and reduced or absent expression of head mRGs (Vásquez-Doorman and Petersen, 2014; Vogg et al., 2014). Like *foxD* RNAi, *zic-1* did not result in regeneration polarity defects, had no effect in wound-induced *notum* expression, and was expressed in neoblasts at the regenerating anterior pole (Vásquez-Doorman and Petersen, 2014; Vogg et al., 2014). Together, these results showed that *foxD* and *zic-1* act together to specify anterior pole cells and regulate head patterning during regeneration. Although *foxD* and *zic-1* are also required for *notum*, *fst*, and each other's expression during homeostasis, no homeostatic patterning defects have been reported for *foxD* and *zic-1* RNAi (Vásquez-Doorman and Petersen, 2014; Vogg et al., 2014). This suggests that while *foxD* and *zic-1* are required to newly specify anterior pole cells during regeneration, once the pole is

formed, the anterior pole is dispensable for the maintenance of head patterning. Testing this hypothesis requires more analysis of the homeostasis phenotype using head mRGs.

Anterior pole formation and patterning depends on two other transcription factors, *pitx* and *islet*. *pitx* encodes a member of the family of paired class homeobox/pituitary homeobox transcription factors involved in the terminal differentiation of progenitors and maintenance of their cell-type-specific functions (Flames and Hobert, 2011; Hobert, 2008; 2011). *islet1* encodes a LIM-homeobox gene that controls proliferation, survival, and migration of progenitor cells or multipotent stem cells in the organogenesis of multiple organisms (Ahlgren et al., 1997; Cai et al., 2003; Takuma et al., 1998; Thor and Thomas, 1997). Both planarian *pitx* and *islet* are co-expressed in cells at the anterior pole region during regeneration, although their co-expression with other pole markers remains to be tested (Currie and Pearson, 2013; März et al., 2013). *pitx* and *islet* regulate each other's expression and RNAi of either *pitx* or *islet* results in cyclopia, a midline defect seen in many anterior-pole deficient phenotypes (Currie and Pearson, 2013; März et al., 2013). Consistent with this, *pitx* and *islet* RNAi both result in the loss of midline marker *slit* in regenerating blastemas (Currie and Pearson, 2013; März et al., 2013).

The midline collapse phenotype (e.g. reduced midline marker expression, cyclopia, cephalic lobe fusion) often seen in the disruption of anterior pole genes revealed that the anterior pole patterns the head not only along the AP axis but also along the ML axis. The location of the anterior pole at the midline of the head tip is suspect for this role, and the formation of the pole at that location is hypothesized to nucleate new midline formation at the regenerating blastema. How the anterior pole is first established at the midline, however, is unclear. The wound-induced expression of *foxD* at the ventral midline of old tissue at wound edges may play a role in the setting the midline for the blastema. This intriguing potential role of *foxD* in using preexisting

tissue to inform the regeneration of midline remains to be tested.

*pitx* and *islet* are notable because they are also expressed in *wnt1*<sup>+</sup> posterior pole cells in the regenerating blastema (Currie and Pearson, 2013; Hayashi et al., 2011; März et al., 2013). Additionally, *islet* is expressed in neoblast progeny expressing *wnt1* (Hayashi et al., 2011), suggesting that it may play a role in the specification of posterior pole cells. Consistent with this, *islet* and *pitx* are required for posterior pole regeneration (Currie and Pearson, 2013; Hayashi et al., 2011; März et al., 2013). However, they are dispensable for wound-induced *wnt1* expression, suggesting that both *pitx* and *islet* mediate the patterning, but not the polarity-determining phase of regeneration (Currie and Pearson, 2013; Hayashi et al., 2011; März et al., 2013). Indeed, *pitx* and *islet(RNAi)* animals exhibit tail patterning defects during regeneration, such as stunted tails with decreased or absent expression of posterior mRGs (Currie and Pearson, 2013; Hayashi et al., 2011; März et al., 2013). Besides causing posterior patterning defects, *pitx* and *islet* RNAi also causes midline collapse in the regenerating tail, including fused ventral nerve cords, fused posterior intestinal branches, and reduced *slit* expression (Currie and Pearson, 2013; Hayashi et al., 2011; März et al., 2013). These simultaneous defects in ML and AP patterning observed in posterior (and anterior) pole perturbations show that the planarian poles play crucial roles as organizers of new ML and AP axes.

Another gene required for the formation of both anterior and posterior poles is *pbx*, which encodes for a TALE-class homeodomain transcription factor that acts together with Hox proteins in many organisms to regulate AP patterning (Pöpperl et al., 2000; Rauskolb et al., 1993; Takács-Vellai et al., 2007; Vlachakis et al., 2000). In planarians, *pbx* expression is not enriched at the poles, but is present throughout the body including in neoblasts and differentiated tissues like the CNS and the pharynx (Chen et al., 2013). RNAi of *pbx* eliminates *notum* and *wnt1*

expression in regenerating poles but spares their wound-induced expression, indicating that *pbx* functions specifically during the patterning phase of regeneration (Chen et al., 2013). In addition, *pbx* is also required for pole maintenance, as long-term *pbx* RNAi in uninjured animals results in decreased numbers of *notum*<sup>+</sup> and *wnt1*<sup>+</sup> cells at the head and tail tips, respectively (Chen et al., 2013). These pole defects in regeneration and homeostasis were accompanied by both head and tail patterning defects, including smaller blastemas, absent eye regeneration, impaired eye maintenance, and lack of new expression or improper maintenance of expression of multiple head and tail mRGs (Chen et al., 2013). Intriguingly, *pbx* RNAi prevented some broadly expressed mRGs like *ndl-3*, *wnt2*, and *wntP-2* from scaling away from the regenerating anterior or posterior blastemas (Chen et al., 2013). Similarly, long-term homeostasis *pbx* RNAi resulted in the anterior encroachment of the more posterior head mRG *wnt2* (Chen et al., 2013). Given that the poles are located at the anterior and posterior tips of the animals, these results are consistent with a possible role of the poles in instructing head and tail tip identity by restricting and rescaling mRG expression pattern during regeneration and homeostasis.

Although functional studies of the anterior and posterior poles have demonstrated their role in head and tail patterning, many questions remain unresolved. Given the requirement of the poles in both AP and ML patterning, are the patterning roles along the two axes distinct functions mediated by distinct molecules? In-depth understanding of the complex roles the poles play in patterning requires a more detailed characterization of the pole transcriptomes, which may reveal additional pole factors that mediate patterning. Furthermore, because many pole genes (e.g. *notum*, *wnt1*, *foxD*, and *fst*) exhibit wound-induced expression, it is unclear whether the patterning defects observed in RNAi during regeneration are a result of perturbing the pole or of perturbing their non-pole wound-induced expression. Directly testing the inductive properties

of the poles, therefore, requires carefully controlled transplantation experiments that have historically served as the basis for the identification of organizers.

## References

- Adell, T., Cebrià, F., Saló, E., Kay, R.R., Thompson, C.R.L., and Strutt, D. (2010). Gradients in planarian regeneration and homeostasis. *Cold Spring Harbor Perspectives in Biology* 2, a000505.
- Adell, T., Saló, E., Boutros, M., and Bartscherer, K. (2009). Smed-Evi/Wntless is required for  $\beta$ -catenin-dependent and -independent processes during planarian regeneration. *Development* 136, 905–910.
- Adoutte, A., Balavoine, G., Lartillot, N., Lespinet, O., Prud'homme, B., and de Rosa, R. (2000). The new animal phylogeny: reliability and implications. *Proc Natl Acad Sci U S A* 97, 4453–4456.
- Ahlgren, U., Pfaff, S.L., Jessell, T.M., Edlund, T., and Edlund, H. (1997). Independent requirement for ISL1 in formation of pancreatic mesenchyme and islet cells. *Nature* 385, 257–260.
- Alvarado, A.S., and Tsonis, P.A. (2006). Bridging the regeneration gap: genetic insights from diverse animal models. *Nat. Rev. Genet.* 7, 873–884.
- Baddour, J.A., Sousounis, K., and Tsonis, P.A. (2012). Organ repair and regeneration: an overview. *Birth Defects Res. C Embryo Today* 96, 1–29.
- Baguñà, J., and Romero, R. (1981). Quantitative analysis of cell types during growth, degrowth and regeneration in the planarians *Dugesia mediterranea* and *Dugesia tigrina*. *Hydrobiologia*.
- Baguñà, J. (1976). Mitosis in the intact and regenerating planarian *Dugesia mediterranea* n.sp. II. Mitotic studies during regeneration, and a possible mechanism of blastema formation. *J. Exp. Zool.* 195, 65–79.
- Baguñà, J., Saló, E., and Auladell, C. (1989). Regeneration and pattern formation in planarians. III . Evidence that neoblasts are totipotent stem cells and the source of blastema cells. *Development* 86, 77–86.
- Baguñà, J., Saló, E., Romero, R., Garcia-fernàndez, J., and Bueno, D. (1994). Regeneration and pattern formation in planarians: cells, molecules and genes. *Zoological Science* 11, 781–795.
- Bardeen, C.R., and Baetjer, F.H. (1904). The inhibitive action of the Roentgen rays on regeneration in planarians. *The Journal of Experimental Zoology* 1, 191–195.
- Beane, W.S., Morokuma, J., Adams, D.S., and Levin, M. (2011). A Chemical Genetics Approach Reveals H,K-ATPase-Mediated Membrane Voltages Required for Planarian Head Regeneration. *Chemistry & Biology* 18, 77–89.
- Beddington, R.S. (1994). Induction of a second neural axis by the mouse node. *Development (Cambridge, England)* 120, 613–620.

- Benayoun, B.A., Caburet, S., and Veitia, R.A. (2011). Forkhead transcription factors: key players in health and disease. *Trends in Genetics* 27, 224–232.
- Browne, E.N. (1909). The production of new hydranths in hydra by the insertion of small grafts. *J. Exp. Zool.* 7, 1–23.
- Buckingham, M., and Rigby, P.W.J. (2014). Gene regulatory networks and transcriptional mechanisms that control myogenesis. *Developmental Cell* 28, 225–238.
- Cadigan, K.M., Grossniklaus, U., and Gehring, W.J. (1994). Localized expression of sloppy paired protein maintains the polarity of *Drosophila* parasegments. *Genes & Development* 8, 899–913.
- Cai, C.-L., Liang, X., Shi, Y., Chu, P.-H., Pfaff, S.L., Chen, J., and Evans, S. (2003). Isl1 identifies a cardiac progenitor population that proliferates prior to differentiation and contributes a majority of cells to the heart. *Developmental Cell* 5, 877–889.
- Cebrià, F., Vispo, M., NEWMARK, P., Bueno, D., and Romero, R. (1997). Myocyte differentiation and body wall muscle regeneration in the planarian *Girardia tigrina*. *Dev Genes Evol* 207, 306–316.
- Cebrià, F. (2016). Planarian Body-Wall Muscle: Regeneration and Function beyond a Simple Skeletal Support. *Frontiers in Cell and Developmental Biology* 4, 433–10.
- Cebrià, F., Guo, T., Jopek, J., and Newmark, P.A. (2007). Regeneration and maintenance of the planarian midline is regulated by a *islet/i* orthologue. *Developmental Biology* 307, 394–406.
- Cebrià, F., Kobayashi, C., Umesono, Y., Nakazawa, M., Mineta, K., Ikeo, K., Gojobori, T., Itoh, M., Taira, M., Sánchez Alvarado, A., et al. (2002). FGFR-related gene *nou-darake* restricts brain tissues to the head region of planarians. *Nature* 419, 620–624.
- Chandebois, R. (1980). The dynamics of wound closure and its role in the programming of planarian regeneration. II—Distalization. *Development, Growth & Differentiation* 22, 693–704.
- Charron, F., and Tessier-Lavigne, M. (2005). Novel brain wiring functions for classical morphogens: a role as graded positional cues in axon guidance. *Development (Cambridge, England)* 132, 2251–2262.
- Chen, C.-C.G., Wang, I.E., and Reddien, P.W. (2013). *ipbx/i* is required for pole and eye regeneration in planarians. *Development (Cambridge, England)* 729, 719–729.
- Chizhikov, V.V., and Millen, K.J. (2005). Roof plate-dependent patterning of the vertebrate dorsal central nervous system. *Developmental ...* 277, 287–295.
- Currie, K.W., and Pearson, B.J. (2013). Transcription factors *lhx1/5-1* and *pitx* are required for the maintenance and regeneration of serotonergic neurons in planarians. *Development* 140, 3577–3588.

- Currie, K.W., Brown, D.D.R., Zhu, S., Xu, C., Voisin, V., Bader, G.D., and Pearson, B.J. (2016). HOX gene complement and expression in the planarian *Schmidtea mediterranea*. *EvoDevo* 1–11.
- Davis, R.L., Weintraub, H., and Lassar, A.B. (1987). Expression of a single transfected cDNA converts fibroblasts to myoblasts. *Cell* 51, 987–1000.
- De Robertis, E.M., and Kuroda, H. (2004). Dorsal-Ventral Patterning and Neural Induction in *Xenopus*/i Embryos. *Annu. Rev. Cell Dev. Biol.* 20, 285–308.
- Dirksen, M.L., and Jamrich, M. (1992). A novel, activin-inducible, blastopore lip-specific gene of *Xenopus laevis* contains a fork head DNA-binding domain. *Genes & Development* 6, 599–608.
- Eisenhoffer, G.T., Kang, H., and Sánchez Alvarado, A. (2008). Molecular analysis of stem cells and their descendants during cell turnover and regeneration in the planarian *Schmidtea mediterranea*/i. *Cell Stem Cell* 3, 327–339.
- Flames, N., and Hobert, O. (2011). Transcriptional control of the terminal fate of monoaminergic neurons. *Annu. Rev. Neurosci.* 34, 153–184.
- Galloni, M. (2012). Global irradiation effects, stem cell genes and rare transcripts in the planarian transcriptome. *Int. J. Dev. Biol.* 56, 103–116.
- Gaviño, M.A., and Reddien, P.W. (2011). A Bmp/Admp Regulatory Circuit Controls Maintenance and Regeneration of Dorsal-Ventral Polarity in Planarians. *Current Biology : CB* 21, 294–299.
- Gaviño, M.A., Wenemoser, D., Wang, I.E., and Reddien, P.W. (2013). Tissue absence initiates regeneration through Follistatin-mediated inhibition of Activin signaling. *Elife* 2, e00247.
- Grossniklaus, U., Pearson, R.K., and Gehring, W.J. (1992). The *Drosophila* sloppy paired locus encodes two proteins involved in segmentation that show homology to mammalian transcription factors. *Genes & Development* 6, 1030–1051.
- Guedelhofer, O.C., and Sánchez Alvarado, A. (2012). Amputation induces stem cell mobilization to sites of injury during planarian regeneration. *Development (Cambridge, England)* 139, 3510–3520.
- Gurley, K.A., Elliott, S.A., Simakov, O., Schmidt, H.A., Holstein, T.W., and Sánchez Alvarado, A. (2010). Expression of secreted Wnt pathway components reveals unexpected complexity of the planarian amputation response. *Developmental Biology* 347, 24–39.
- Gurley, K.A., Rink, J.C., and Sánchez Alvarado, A. (2008).  $\beta$ -Catenin Defines Head Versus Tail Identity During Planarian Regeneration and Homeostasis. *Science* 319, 323–327.
- Hayashi, T., Motoishi, M., Yazawa, S., Itomi, K., Tanegashima, C., Nishimura, O., Agata, K., and Tarui, H. (2011). A LIM-homeobox gene is required for differentiation of Wnt-expressing cells at the posterior end of the planarian body. *Development* 138, 3679–3688.

- Häcker, U., Kaufmann, E., Hartmann, C., Jürgens, G., Knöchel, W., and Jäckle, H. (1995). The *Drosophila* fork head domain protein crocodile is required for the establishment of head structures. *The EMBO Journal* *14*, 5306–5317.
- Henzel, M.J., Wei, Y., Mancini, M.A., Van Hooser, A., Ranalli, T., Brinkley, B.R., Bazett-Jones, D.P., and Allis, C.D. (1997). Mitosis-specific phosphorylation of histone H3 initiates primarily within pericentromeric heterochromatin during G2 and spreads in an ordered fashion coincident with mitotic chromosome condensation. *Chromosoma* *106*, 348–360.
- Hill, E.M., and Petersen, C.P. (2015). Wnt/Notum spatial feedback inhibition controls neoblast differentiation to regulate reversible growth of the planarian brain. *Development (Cambridge, England)* *142*, 4217–4229.
- Hobert, O. (2008). Regulatory logic of neuronal diversity: terminal selector genes and selector motifs. *Proc. Natl. Acad. Sci. U.S.A.* *105*, 20067–20071.
- Hobert, O. (2011). Regulation of terminal differentiation programs in the nervous system. *Annu. Rev. Cell Dev. Biol.* *27*, 681–696.
- Hori, I. (1983). Differentiation of myoblasts in the regenerating planarian *Dugesia japonica*. *Cell Differentiation* *12*, 155–163.
- Hyman, L.H. (1951). *The Invertebrates: Platyhelminthes And Rhynchocoela: The Acoelomate Bilateria (Volume-2)*.
- Iglesias, M., Gomez-Skarmeta, J.L., Salo, E., and Adell, T. (2008). Silencing of *Smed-catenin1* generates radial-like hypercephalized planarians. *Development* *135*, 1215–1221.
- Jopling, C., Boue, S., and Izpisua Belmonte, J.C. (2011). Dedifferentiation, transdifferentiation and reprogramming: three routes to regeneration. *Nature Publishing Group* *12*, 79–89.
- Kadu, V., S, S.G., and Ghaskadbi, S. (2012). Induction of secondary axis in hydra revisited: New insights into pattern formation. *Int J Mol Cell Med* *1*, 11–20.
- Kakugawa, S., Langton, P.F., Zebisch, M., Howell, S.A., Chang, T.-H., Liu, Y., Feizi, T., Bineva, G., O'Reilly, N., Snijders, A.P., et al. (2015). Notum deacylates Wnt proteins to suppress signalling activity. *Nature* *519*, 187–192.
- Kato, K., Orii, H., Watanabe, K., and Agata, K. (1999). The role of dorsoventral interaction in the onset of planarian regeneration. *Development* *126*, 1031–1040.
- Kato, K., Orii, H., Watanabe, K., and Agata, K. (2001). Dorsal and Ventral Positional Cues Required for the Onset of Planarian Regeneration May Reside in Differentiated Cells. *Developmental Biology* *233*, 109–121.
- Kidd, T., Bland, K.S., and Goodman, C.S. (1999). Slit is the midline repellent for the robo receptor in *Drosophila*. *Cell* *96*, 785–794.

- Labbé, R.M., Irimia, M., Currie, K.W., Lin, A., Zhu, S.J., Brown, D.D.R., Ross, E.J., Voisin, V., Bader, G.D., Blencowe, B.J., et al. (2012). A Comparative Transcriptomic Analysis Reveals Conserved Features of Stem Cell Pluripotency in Planarians and Mammals. *Stem Cells (Dayton, Ohio)* 30, 1734–1745.
- Lander, R., and Petersen, C. (2016). Wnt, Ptk7, and FGFR1 expression gradients control trunk positional identity in planarian regeneration. *Elife* 5, 1689–1699.
- Lanzavecchia, G. (1977). Morphological Modulations in Helical Muscles (Aschelminthes and Annelida). (Elsevier), pp. 133–186.
- Lengfeld, T., Watanabe, H., Simakov, O., Lindgens, D., Gee, L., Law, L., Schmidt, H.A., Özbek, S., Bode, H., and Holstein, T.W. (2009). Multiple Wnts are involved in Hydra organizer formation and regeneration. *Developmental Biology* 330, 186–199.
- Lewis, J., Slack, J.M.W., and Wolpert, L. (1977). Thresholds in development. *Journal of Theoretical Biology* 65, 579–590.
- Liu, S.Y., Selck, C., Friedrich, B., Lutz, R., Vila-Farré, M., Dahl, A., Brandl, H., Lakshmanaperumal, N., Henry, I., and Rink, J.C. (2013). Reactivating head regrowth in a regeneration-deficient planarian species. *Nature* 500, 81–84.
- Long, H., Sabatier, C., Ma, L., Plump, A., Yuan, W., Ornitz, D.M., Tamada, A., Murakami, F., Goodman, C.S., and Tessier-Lavigne, M. (2004). Conserved roles for Slit and Robo proteins in midline commissural axon guidance. *Neuron* 42, 213–223.
- MacRae, E.K. (1963). Observations on the fine structure of pharyngeal muscle in the planarian *dugesia tigrina*. *The Journal of Cell Biology* 18, 651–662.
- MacRae, E.K. (1965). The fine structure of muscle in a marine turbellarian. *Zeitschrift Für Zellforschung Und Mikroskopische Anatomie* 68, 348–362.
- Matsui, T., Raya, A., Kawakami, Y., Collol-Massot, C., Capdevila, J., Rodríguez-Esteban, C., and Izpisua Belmonte, J.C. (2005). Noncanonical Wnt signaling regulates midline convergence of organ primordia during zebrafish development. *Genes & Development* 19, 164–175.
- März, M., Seebeck, F., and Bartscherer, K. (2013). A Pitx transcription factor controls the establishment and maintenance of the serotonergic lineage in planarians. *Development* 140, 4499–4509.
- McGinnis, W., and Krumlauf, R. (1992). Homeobox genes and axial patterning. *Cell* 68, 283–302.
- Meinhardt, H. (1978). Space-dependent cell determination under the control of a morphogen gradient. *Journal of Theoretical Biology* 74, 307–321.
- Meinhardt, H. (2015). Dorsoventral patterning by the Chordin-BMP pathway: a unified model from a pattern-formation perspective for *Drosophila*, vertebrates, sea urchins and *Nematostella*.

Developmental Biology 405, 137–148.

Molina, M.D., Neto, A., Maeso, I., Gómez-Skarmeta, J.L., Cebrià, F., Go, L., and Saló, E. (2011). Noggin and noggin-like genes control dorsoventral axis regeneration in planarians. *Current Biology* : CB 21, 300–305.

Molina, M.D., Saló, E., and Cebrià, F. (2007). The BMP pathway is essential for re-specification and maintenance of the dorsoventral axis in regenerating and intact planarians. *Developmental Biology* 311, 79–94.

Molina, M.D., Saló, E., and Cebrià, F. (2009). Expression pattern of the expanded noggin gene family in the planarian *iSchmidtea mediterranea/i*. *Gene Expr. Patterns* 9, 246–253.

Monteiro, R., van Dinter, M., Bakkers, J., Wilkinson, R., Patient, R., Dijke, ten, P., and Mummery, C. (2008). Two novel type II receptors mediate BMP signalling and are required to establish left-right asymmetry in zebrafish. *Developmental Biology* 315, 55–71.

Morgan, T.H. (1898). Experimental studies of the regeneration of *Planaria maculata*. *Archiv Für Entwicklungsmechanik Der Organismen* 7, 364–397.

Morgan, T.H. (1900). Regeneration in Planarians. *Archiv Fur Entwicklungsmechanik Der Organismen* 10, 58–119.

Morgan, T.H. (1905). “Polarity” considered as a phenomenon of gradation of materials. *J. Exp. Zool.* 2, 495–506.

Morita, M. (1965). Electron microscopic studies on planaria: I. Fine structure of muscle fiber in the head of the planarian *Dugesia dorotocephala*. *Journal of Ultrastructure Research*.

Nakamura, Y., Tsiairis, C.D., Özbek, S., and Holstein, T.W. (2011). Autoregulatory and repressive inputs localize Hydra Wnt3 to the head organizer. *Proc. Natl. Acad. Sci. U.S.A.* 108, 9137–9142.

Newmark, P.A., and Sánchez Alvarado, A. (2000). Bromodeoxyuridine Specifically Labels the Regenerative Stem Cells of Planarians. *Developmental Biology* 220, 142–153.

Newmark, P.A., Reddien, P.W., Cebrià, F., and Sánchez Alvarado, A. (2003). Ingestion of bacterially expressed double-stranded RNA inhibits gene expression in planarians. *Proc Natl Acad Sci U S A* 100 *Suppl*, 11861–11865.

Nogi, T., and Levin, M. (2005). Characterization of innexin gene expression and functional roles of gap-junctional communication in planarian regeneration. *Developmental Biology* 287, 314–335.

Nogi, T., Zhang, D., Chan, J.D., and Marchant, J.S. (2009). A novel biological activity of praziquantel requiring voltage-operated Ca<sup>2+</sup> channel beta subunits: subversion of flatworm regenerative polarity. *PLOS Neglected Tropical Diseases* 3, e464.

- Ogawa, K., Ishihara, S., Saito, Y., Mineta, K., Nakazawa, M., Ikeo, K., Gojobori, T., Watanabe, K., and Agata, K. (2002). Induction of a noggin-Like Gene by Ectopic DV Interaction during Planarian Regeneration. *Developmental Biology* 250, 59–70.
- Orii, H., and Watanabe, K. (2007). Bone morphogenetic protein is required for dorso-ventral patterning in the planarian *Dugesia japonica*. *Development, Growth & Differentiation* 49, 345–349.
- Orii, H., Kato, K., Agata, K., and Watanabe, K. (1998). Molecular Cloning of Bone Morphogenetic Protein (BMP) Gene from the Planarian *Dugesia japonica*. *Zoological Science* 15, 871–877.
- Owen, J.H., Wagner, D.E., Chen, C.-C., Petersen, C.P., and Reddien, P.W. (2015). *teashirt* is required for head-versus-tail regeneration polarity in planarians. *Development* 142, 1062–1072.
- Önal, P., Grün, D., Adamidi, C., Rybak, A., Solana, J., Mastrobuoni, G., Wang, Y., Rahn, H.-P., Chen, W., Kempa, S., et al. (2012). Gene expression of pluripotency determinants is conserved between mammalian and planarian stem cells. *The EMBO Journal* 31, 2755–2769.
- Palakodeti, D., Smielewska, M., Lu, Y.-C., Yeo, G.W., and Graveley, B.R. (2008). The PIWI proteins SMEDWI-2 and SMEDWI-3 are required for stem cell function and piRNA expression in planarians. *RNA (New York, N.Y.)* 14, 1174–1186.
- Pearson, B.J., Eisenhoffer, G.T., Gurley, K.A., Rink, J.C., Miller, D.E., and Sánchez Alvarado, A. (2009). Formaldehyde-based whole-mount in situ hybridization method for planarians. *Dev. Dyn.* 238, 443–450.
- Pellettieri, J., Fitzgerald, P., Watanabe, S., Mancuso, J., Green, D.R., Sánchez Alvarado, A., and Sánchez, A. (2010). Cell death and tissue remodeling in planarian regeneration. *Developmental Biology* 338, 76–85.
- Petersen, C.P., and Reddien, P.W. (2008). *Smed-βcatenin-1* is required for anteroposterior blastema polarity in planarian regeneration. *Science* 319, 327–330.
- Petersen, C.P., and Reddien, P.W. (2009). A wound-induced Wnt expression program controls planarian regeneration polarity. *Proc. Natl. Acad. Sci. U.S.A.* 106, 17061–17066.
- Petersen, C.P., and Reddien, P.W. (2011). Polarized *notum* activation at wounds inhibits Wnt function to promote planarian head regeneration. *Science* 332, 852–855.
- Philippe, H., Derelle, R., Lopez, P., Pick, K., Borchiellini, C., Boury-Esnault, N., Vacelet, J., Renard, E., Houliston, E., Quéinnec, E., et al. (2009). Phylogenomics revives traditional views on deep animal relationships. *Current Biology : CB* 19, 706–712.
- Poss, K.D. (2010). Advances in understanding tissue regenerative capacity and mechanisms in animals. *Nat. Rev. Genet.* 11, 710–722.
- Pöpperl, H., Rikhof, H., Chang, H., Haffter, P., Kimmel, C.B., and Moens, C.B. (2000). *lazarus*

- is a novel pbx gene that globally mediates hox gene function in zebrafish. *Mol. Cell* 6, 255–267.
- Rauskolb, C., Peifer, M., and Wieschaus, E. (1993). extradenticle, a regulator of homeotic gene activity, is a homolog of the homeobox-containing human proto-oncogene pbx1. *Cell* 74, 1101–1112.
- Reddien, P.W. (2013). Specialized progenitors and regeneration. *Development* 140, 951–957.
- Reddien, P.W. (2011). Constitutive gene expression and the specification of tissue identity in adult planarian biology. *Trends in Genetics* 27, 277–285.
- Reddien, P.W., and Sánchez Alvarado, A. (2004). Fundamentals of Planarian Regeneration. *Annu. Rev. Cell Dev. Biol.* 20, 725–757.
- Reddien, P.W., Bermange, A.L., Kicza, A.M., and Sánchez Alvarado, A. (2007). BMP signaling regulates the dorsal planarian midline and is needed for asymmetric regeneration. *Development* 134, 4043–4051.
- Reddien, P.W., Bermange, A.L., Murfitt, K.J., Jennings, J.R., Sánchez Alvarado, A., and Alvarado, A.S. (2005a). Identification of genes needed for regeneration, stem cell function, and tissue homeostasis by systematic gene perturbation in planaria. *Developmental Cell* 8, 635–649.
- Reddien, P.W., Oviedo, N.J., Jennings, J.R., Jenkin, J.C., and Sánchez Alvarado, A. (2005b). SMEDWI-2 is a PIWI-like protein that regulates planarian stem cells. *Science* 310, 1327–1330.
- Resch, A.M., Palakodeti, D., Lu, Y.-C., Horowitz, M., and Graveley, B.R. (2012). Transcriptome Analysis Reveals Strain-Specific and Conserved Stemness Genes in *Schmidtea mediterranea*. *PLoS ONE* 7, e34447.
- Reuter, H., Mrz, M., Vogg, M.C., Eccles, D., Gr fol-Bold, L., Wehner, D., Owlarn, S., Adell, T., Weidinger, G., and Bartscherer, K. (2015). beta-Catenin-Dependent Control Of Positional Information Along The AP body axis in planarians involves a teashirt family member. *Cell Reports* 10, 253–265.
- Reuter, M. (1977). Ultrastructure of the Stylet Protractor Muscle in *Gyratrix hermaphroditus* (Turbellaria, Rhabdocoela). *Acta Zoologica* 58, 179–184.
- Rieger, R.M., Tyler, S., Smith, J., III, and Rieger, G.E. (1991). *Platyhelminthes: Turbellaria. A Microscopic Anatomy of Invertebrates, Vol. 3: Platyhelminthes and Nemertinea* (New York: Wiley-Liss).
- Rink, J.J.C., Gurley, K.A.K., Elliott, S.A., Sánchez Alvarado, A., and Alvarado, A.S. (2009). Planarian Hh signaling regulates regeneration polarity and links Hh pathway evolution to cilia. *Science* 326, 1406–1410.
- Robb, S.M.C., Gotting, K., Ross, E., and Sánchez Alvarado, A. (2015). SmedGD 2.0: The *Schmidtea mediterranea* genome database. *Genesis* 00, n/a–n/a.

Roberts-Galbraith, R.H.R., and Newmark, P.A.P. (2013). Follistatin antagonizes Activin signaling and acts with Notum to direct planarian head regeneration. *Proc Natl Acad Sci U S A* *110*, 1363–1368.

Ross, K.G., Omuro, K.C., Taylor, M.R., Munday, R.K., Hubert, A., King, R.S., and Zayas, R.M. (2015). Novel monoclonal antibodies to study tissue regeneration in planarians. *BMC Developmental Biology* *15*, 2.

Rothberg, J.M., Jacobs, J.R., Goodman, C.S., and Artavanis-Tsakonas, S. (1990). slit: an extracellular protein necessary for development of midline glia and commissural axon pathways contains both EGF and LRR domains. *Genes & Development* *4*, 2169–2187.

Santos, F.V. (1931). Studies on transplantation in planaria. *Physiological Zoology*.

Sánchez Alvarado, A., and Newmark, P.A. (1999). Double-stranded RNA specifically disrupts gene expression during planarian regeneration. *Proc. Natl. Acad. Sci. U.S.a.* *96*, 5049–5054.

Sánchez Alvarado, A., Newmark, P.A., Robb, S.M., and Juste, R. (2002). The Schmidtea mediterranea database as a molecular resource for studying platyhelminthes, stem cells and regeneration. *Development (Cambridge, England)* *129*, 5659–5665.

Scimone, M.L., Cote, L.E., Rogers, T., and Reddien, P.W. (2016). Two FGFR-L-Wnt circuits organize the planarian anteroposterior axis. *Elife* *5*, 905.

Scimone, M.L., Kravarik, K.M., Lapan, S.W., and Reddien, P.W. (2014a). Neoblast specialization in regeneration of the planarian *iSchmidtea mediterranea/i*. *Stem Cell Reports* *3*, 339–352.

Scimone, M.L., Lapan, S.W., and Reddien, P.W. (2014b). A forkhead transcription factor is wound-induced at the planarian midline and required for anterior pole regeneration. *PLoS Genet* *10*, e1003999.

Shih, J., and Fraser, S.E. (1996). Characterizing the zebrafish organizer: microsurgical analysis at the early-shield stage. *Development (Cambridge, England)* *122*, 1313–1322.

Sikes, J.M., and Newmark, P.A. (2013). Restoration of anterior regeneration in a planarian with limited regenerative ability. *Nature* *500*, 77–80.

Sivickis, P.B. (1931). A quantitative study of regeneration along the main axis of the triclad body (*Arch Zool Ital*).

Slack, J.M.W. (1987). Morphogenetic gradients — past and present. *Trends in Biochemical Sciences* *12*, 200–204.

Spemann, H., and Mangold, H. (1924). Über Induktion von Embryonalanlagen durch Implantation artfremder Organisatoren. *Archiv Fur Entwicklungsmechanik Der Organismen* *100*, 599–638.

Stückemann, T., Cleland, J.P., Werner, S., Vu, H.T.-K., Bayersdorf, R., Liu, S.-Y., Friedrich, B., Jülicher, F., and Rink, J.C. (2017). Antagonistic Self-Organizing Patterning Systems Control Maintenance and Regeneration of the Anteroposterior Axis in Planarians. *Developmental Cell* 40, 248–263.e4.

Takács-Vellai, K., Vellai, T., Chen, E.B., Zhang, Y., Guerry, F., Stern, M.J., and Müller, F. (2007). Transcriptional control of Notch signaling by a HOX and a PBX/EXD protein during vulval development in *C. elegans*. *Developmental ...* 302, 661–669.

Takuma, N., Sheng, H.Z., Furuta, Y., Ward, J.M., Sharma, K., Hogan, B.L., Pfaff, S.L., Westphal, H., Kimura, S., and Mahon, K.A. (1998). Formation of Rathke's pouch requires dual induction from the diencephalon. *Development (Cambridge, England)* 125, 4835–4840.

Tanaka, E.M., and Reddien, P.W. (2011). The cellular basis for animal regeneration. *Developmental Cell* 21, 172–185.

Thor, S., and Thomas, J.B. (1997). The *Drosophila* islet gene governs axon pathfinding and neurotransmitter identity. *Neuron* 18, 397–409.

van Wolfswinkel, J.C., Wagner, D.E., and Reddien, P.W. (2014). Single-Cell Analysis Reveals Functionally Distinct Classes within the Planarian Stem Cell Compartment. *Stem Cell* 1–14.

Vásquez-Doorman, C., and Petersen, C.P. (2014). *zic-1* Expression in Planarian neoblasts after injury controls anterior pole regeneration. *PLoS Genet* 10, e1004452.

Vlachakis, N., Ellstrom, D.R., and Sagerström, C.G. (2000). A novel pbx family member expressed during early zebrafish embryogenesis forms trimeric complexes with Meis3 and Hoxb1b. *Developmental Dynamics : an Official Publication of the American Association of Anatomists* 217, 109–119.

Vogg, M.C., Owlarn, S., Pérez Rico, Y.A., Xie, J., Suzuki, Y., Gentile, L., Wu, W., and Bartscherer, K. (2014). Stem cell-dependent formation of a functional anterior regeneration pole in planarians requires Zic and Forkhead transcription factors. *Developmental Biology* 390, 136–148.

Waddington, C.H. (1933). Induction by the Primitive Streak and its Derivatives in the Chick. *Journal of Experimental Biology* 10, 38–46.

Wagner, D.E., Ho, J.J., and Reddien, P.W. (2012). Genetic Regulators of a Pluripotent Adult Stem Cell System in Planarians Identified by RNAi and Clonal Analysis. *Stem Cell* 10, 299–311.

Wagner, D.E., Wang, I.E., and Reddien, P.W. (2011). Clonogenic neoblasts are pluripotent adult stem cells that underlie planarian regeneration. *Science* 332, 811–816.

Wehner, D., Cizelsky, W., Vasudevaro, M.D., Özhan, G., Haase, C., Kagermeier-Schenk, B., Röder, A., Dorsky, R.I., Moro, E., Argenton, F., et al. (2014). Wnt/ $\beta$ -catenin signaling defines organizing centers that orchestrate growth and differentiation of the regenerating zebrafish caudal fin. *CellReports* 6, 467–481.

Weigel, D., Jürgens, G., Küttner, F., Seifert, E., and Jäckle, H. (1989). The homeotic gene fork head encodes a nuclear protein and is expressed in the terminal regions of the *Drosophila* embryo. *Cell* 57, 645–658.

Weintraub, H., Davis, R., Tapscott, S., Thayer, M., Krause, M., Benezra, R., Blackwell, T.K., Turner, D., Rupp, R., and Hollenberg, S. (1991). The myoD gene family: nodal point during specification of the muscle cell lineage. *Science (New York, N.Y.)* 251, 761–766.

Weissman, I.L., Anderson, D.J., and Gage, F. (2001). Stem and progenitor cells: origins, phenotypes, lineage commitments, and transdifferentiations. *Annu. Rev. Cell Dev. Biol.* 17, 387–403.

Wellik, D.M. (2009). Hox genes and vertebrate axial pattern. *Current Topics in Developmental Biology* 88, 257–278.

Wenemoser, D., and Reddien, P.W. (2010). Planarian regeneration involves distinct stem cell responses to wounds and tissue absence. *Developmental Biology* 344, 979–991.

Wenemoser, D., Lapan, S.W., Wilkinson, A.W., Bell, G.W., and Reddien, P.W. (2012). A molecular wound response program associated with regeneration initiation in planarians. *Genes & Development* 26, 988–1002.

Witchley, J.N., Mayer, M., Wagner, D.E., Owen, J.H., and Reddien, P.W. (2013). Muscle Cells Provide Instructions for Planarian Regeneration. *Cell Reports* 4, 1–9.

Wolff, E. (1948). Sur la migration des cellules de régénération chez les planaires. *Rev. Suisse Zool.*

Wolpert, L. (1969). Positional information and the spatial pattern of cellular differentiation. *Journal of Theoretical Biology* 25, 1–47.

Wolpert, L., Hicklin, J., and Hornbruch, A. (1971). Positional information and pattern regulation in regeneration of hydra. *Symposia of the Society Experimental Biology* 25, 391–415.

Wurtzel, O., Cote, L.E., Poirier, A., Satija, R., Regev, A., and Reddien, P.W. (2015). A Generic and Cell-Type-Specific Wound Response Precedes Regeneration in Planarians. *Developmental Cell* 35, 632–645.

Wurtzel, O., Oderberg, I.M., and Reddien, P.W. (2017). Planarian Epidermal Stem Cells Respond to Positional Cues to Promote Cell-Type Diversity. *Developmental Cell* 40, 491–504.e495.

Yamaguchi, T.P. (2001). Heads or tails: Wnts and anterior-posterior patterning. *Current Biology* : CB 11, R713–R724.

Yazawa, S., Umesono, Y., Hayashi, T., Tarui, H., and Agata, K. (2009). Planarian Hedgehog/Patched establishes anterior-posterior polarity by regulating Wnt signaling. *Proc. Natl. Acad. Sci. U.S.A.* 106, 22329–22334.

Yu, J.-K., Holland, N.D., and Holland, L.Z. (2003). *AmphiFoxQ2*, a novel winged helix/forkhead gene, exclusively marks the anterior end of the amphioxus embryo. *Archiv Für Entwicklungsmechanik Der Organismen* 213, 102–105.

## **CHAPTER 2**

### **Landmarks in existing tissue at wounds are utilized to generate pattern in regenerating tissue**

**Isaac M. Oderberg, Dayan J. Li, M. Lucila Scimone, Michael A. Gaviño,  
and Peter W. Reddien**

Experiments shown in Figures 1A-C and Figure S1 were performed by IMO and DJL.

Experiments shown in Figures 1D-F, Figures 2-4, and Figures S2-S4 were performed by IMO.

All authors contributed to the design of experiments or editing of the manuscript.

Published as:

Oderberg, I.M., Li, D.J., Scimone, M.L., Gaviño, M.A., and Reddien, P.W. (2017). Landmarks in Existing Tissue at Wounds Are Utilized to Generate Pattern in Regenerating Tissue. *Current Biology* 1–24.



## **Abstract**

Regeneration in many organisms involves the formation of a blastema, which differentiates and organizes into the appropriate missing tissues. How blastema pattern is generated and integrated with pre-existing tissues is a central question in the field of regeneration. Planarians are free-living flatworms capable of rapidly regenerating from small body fragments (Reddien and Sánchez Alvarado, 2004). A cell cluster at the anterior tip of planarian head blastemas (the anterior pole) is required for establishment of anterior-posterior (AP) and midline blastema pattern (Scimone et al., 2014; Vásquez-Doorman and Petersen, 2014; Vogg et al., 2014). Transplantation of the head tip into tails induced host tissues to grow patterned head-like outgrowths containing a midline. Given the important patterning role of the anterior pole, understanding how it becomes localized during regeneration would help explain how wounds establish pattern in new tissue. Anterior pole progenitors were specified at the pre-existing midline of regenerating fragments, even when this location deviated from the medial-lateral (ML) median plane of the wound face. Anterior pole progenitors were specified broadly on the dorsal-ventral (DV) axis, and subsequently formed a cluster at the DV boundary of the animal. We propose that three landmarks of pre-existing tissue at wounds set the location of anterior pole formation – a polarized AP axis, the pre-existing midline, and the dorsal-ventral median plane. Subsequently, blastema pattern is organized around the anterior pole. This process, utilizing positional information in existing tissue at unpredictably shaped wounds, can influence patterning of new tissue in a manner that facilitates integration with pre-existing tissue in regeneration.

## Introduction

Pattern formation during animal development can be initiated by symmetry-breaking mechanisms including asymmetric maternal factors in oocytes and the location of sperm entry (Driever and Nüsslein-Volhard, 1988) {DeRobertis2000} . Similar to development, animal regeneration requires mechanisms to establish tissue pattern, in tissue outgrowths called blastemas. However, tissue pattern establishment in blastemas must occur in the absence of embryonic pattern-initiating processes. Furthermore, regeneration has the additional challenge of integrating new tissue with existing tissue in the context of unpredictable injuries. An elegant solution to this challenge would be if pattern-initiating processes relied on cues present at the wound face. Planarians are a classic regenerative model system and are capable of regenerating from a large array of injuries, making them well suited to address the origins of pattern in blastemas. Planarian regeneration involves both blastema formation and the remodeling of pre-existing tissue (Reddien and Sánchez Alvarado, 2004), and requires proliferative cells (neoblasts) that include pluripotent stem cells (Wagner et al., 2011).

Planarian head regeneration involves the formation of a cluster of specialized muscle cells at the anterior head tip called the anterior pole (Scimone et al., 2014). The anterior pole expresses *notum* (Petersen and Reddien, 2011) , *follistatin* (Gaviño et al., 2013; Roberts-Galbraith and Newmark, 2013), and the transcription factors *foxD* (Scimone et al., 2014) and *zic-1* . *foxD* and *zic-1* (Vásquez-Doorman and Petersen, 2014; Vogg et al., 2014) are required for anterior pole formation through the specialization of neoblasts into anterior pole progenitors. *foxD* or *zic-1* RNAi blocks pole regeneration and results in aberrant AP and ML patterning gene

expression and absent or medially collapsed differentiated head tissues. These findings indicate a requirement for the anterior pole in AP and ML blastema patterning (Scimone et al., 2014; Vásquez-Doorman and Petersen, 2014; Vogg et al., 2014). The planarian anterior pole has some similarities to other discrete regions of cells in developing embryos, such as the amphibian Spemann-Mangold organizer, that regulate patterning of neighboring tissue (Scimone et al., 2014; Spemann and Mangold, 1924; Vásquez-Doorman and Petersen, 2014). Therefore, the position of the regenerated anterior pole is likely critical to proper patterning, but how this positioning is controlled is poorly understood.

## **Results and Discussion**

### **Tissue fragments containing the anterior pole can induce patterned outgrowths in host tissue following transplantation**

Transplantation was used to test the inductive capacities of the planarian head tip, which contains the anterior pole ("pole fragments") (Figure 1A, Figure S1A-G). Donor animals were lethally irradiated to ablate all neoblasts (Dubois, 1949); any resultant outgrowth involving new cells would therefore be produced by host tissues in response to the transplant. As a control, we also transplanted equally sized head tip regions that were offset from the midline and lacking the anterior pole ("flank fragments"). Juxtaposition of different body regions causes outgrowths in planarians (Chandebois, 1985; Santos, 1931; 1929; Sugino, 1937; Kato et al., 1999) , and accordingly, both pole and flank transplants generated outgrowths (Figure 1A).

Out of 86 “pole fragment” transplantations, 22 animals exhibited outgrowths, 18 of which possessed two eyes and were mobile (Figure 1A). Out of 66 “flank fragment” transplantations, 29 animals exhibited outgrowths, only six of which possessed eyes; the rest were immobile tissue spikes (Figure 1A). To assess patterning in these outgrowths, we performed fluorescent *in situ* hybridization (FISH) with RNA probes for *foxD/notum* (anterior pole), *sFRP-1* (anterior head tip), *slit* (midline), *ndl-2* (pre-pharyngeal region), *opsin* (photoreceptor neurons), and *laminB* (DV boundary). Pole transplant outgrowths with eyes (n = 8/8) and without eyes (n=3/4) displayed AP patterning and a midline (Figure 1B, S1H). These outgrowths displayed entirely dorsal identity and little dorsal-ventral boundary (n=4/4) (Figure S1I). Flank transplant outgrowths with eyes also had AP patterning and a midline (n = 6/6), whereas the spike outgrowths expressed only *ndl-2* and no other anterior or midline markers (n = 8/8) (Figure 1B, S1H). Transplanted flank regions thus had less efficient, but not absent, potential to induce head pattern. Together with prior RNAi experiments that ablated the anterior pole, these data indicate an important role for cells at the anterior head tip in organizing head pattern. This motivated study of pole formation mechanisms to understand the logic by which head blastema pattern is formed and integrated with the pattern of pre-existing tissue.



**Figure 1**

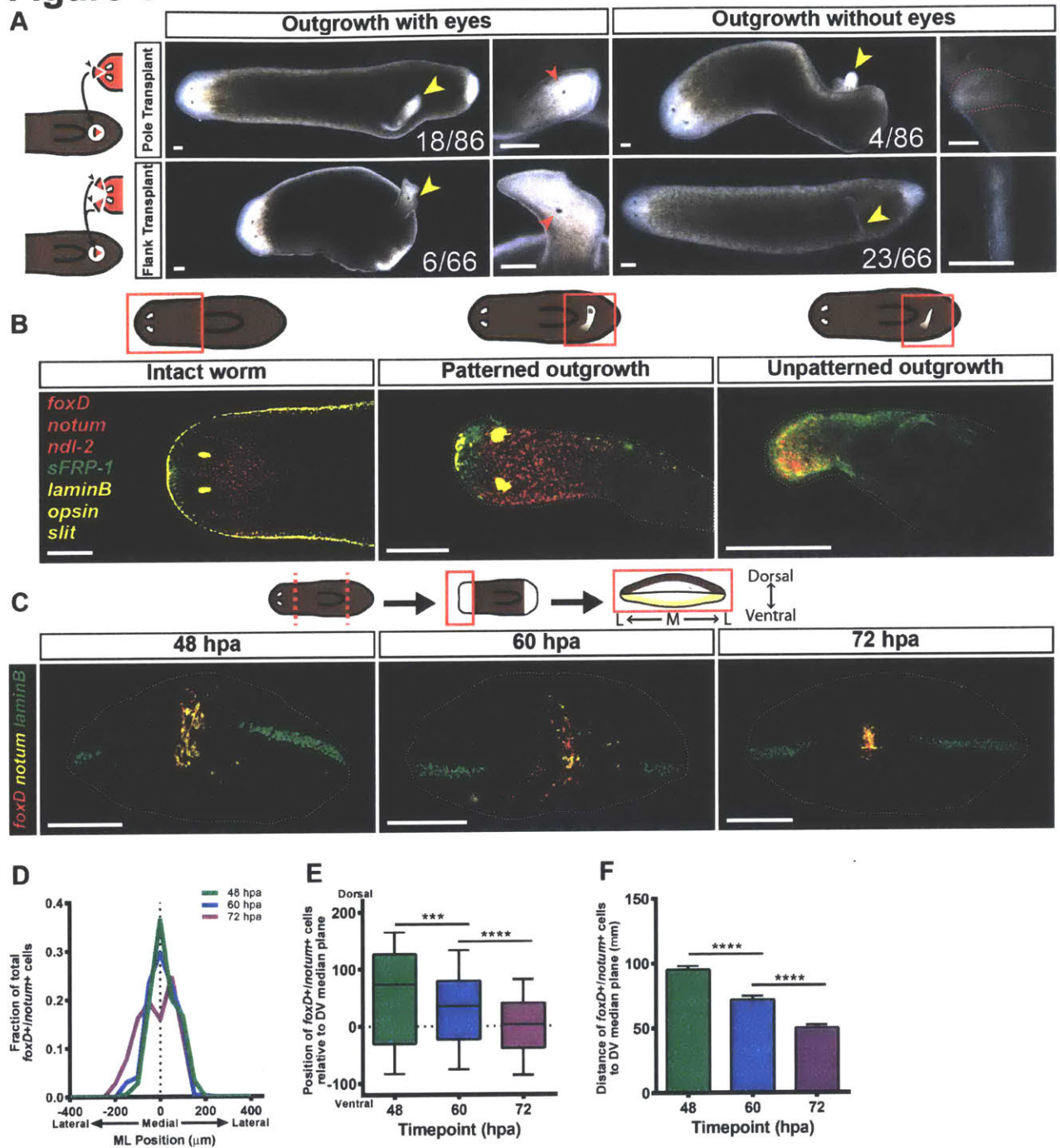


**Figure 1. Anterior pole progenitors are specified medially and in a broad DV domain. (A)** Live images of animals 14 days after pole or flank transplantation. Yellow arrowheads mark the site of an outgrowth. Red arrowheads mark an ectopic eye. **(B)** Triple FISH for *foxD/notum/ndl-2*, *sFRP-1*, and *slit/laminB/opsin* at 14 days following transplantation. Merged images are displayed. For single-channel images see Figure S1H. For **(A-B)** dorsal view, anterior is to the left. Scale bars, 200uL **(C)** Triple FISH for *foxD*, *notum* and *laminB* at 48, 60, and 72 hpa. Medial *foxD+/notum+* cells coalesce to the DV median plane with time. Maximal intensity projections shown. *en face* view of anterior blastema, dorsal is up. Scale bars, 200uL **(D)** The distribution of the positions of *foxD+/notum+* cells on the ML axis is centered roughly around the ML median plane of the fragment (dotted line). 48 hpa, n=18 worms; 60 hpa, n=24 worms; 72 hpa, n=18 worms. **(E)** The distribution of the positions of *foxD+/notum+* cells on the DV axis becomes tighter and closer to the DV median plane over time. Data were compared with a Mann-Whitney test. 48 vs 60 hpa, \*\*\*p=0.0003, n>289 cells; 60 vs 72 hpa, \*\*\*\*p<0.0001, n>289 cells. **(F)** The distance between *foxD+/notum+* cells and the DV median plane grows smaller over time. Data were compared using a Student's t-test. 48 vs 60 hpa, \*\*\*\*p<0.0001, n>289 cells; 60 vs 72 hpa, \*\*\*\*p<0.0001, n>289 cells. See also Figure S1 and Figure S2.

# Figure S1

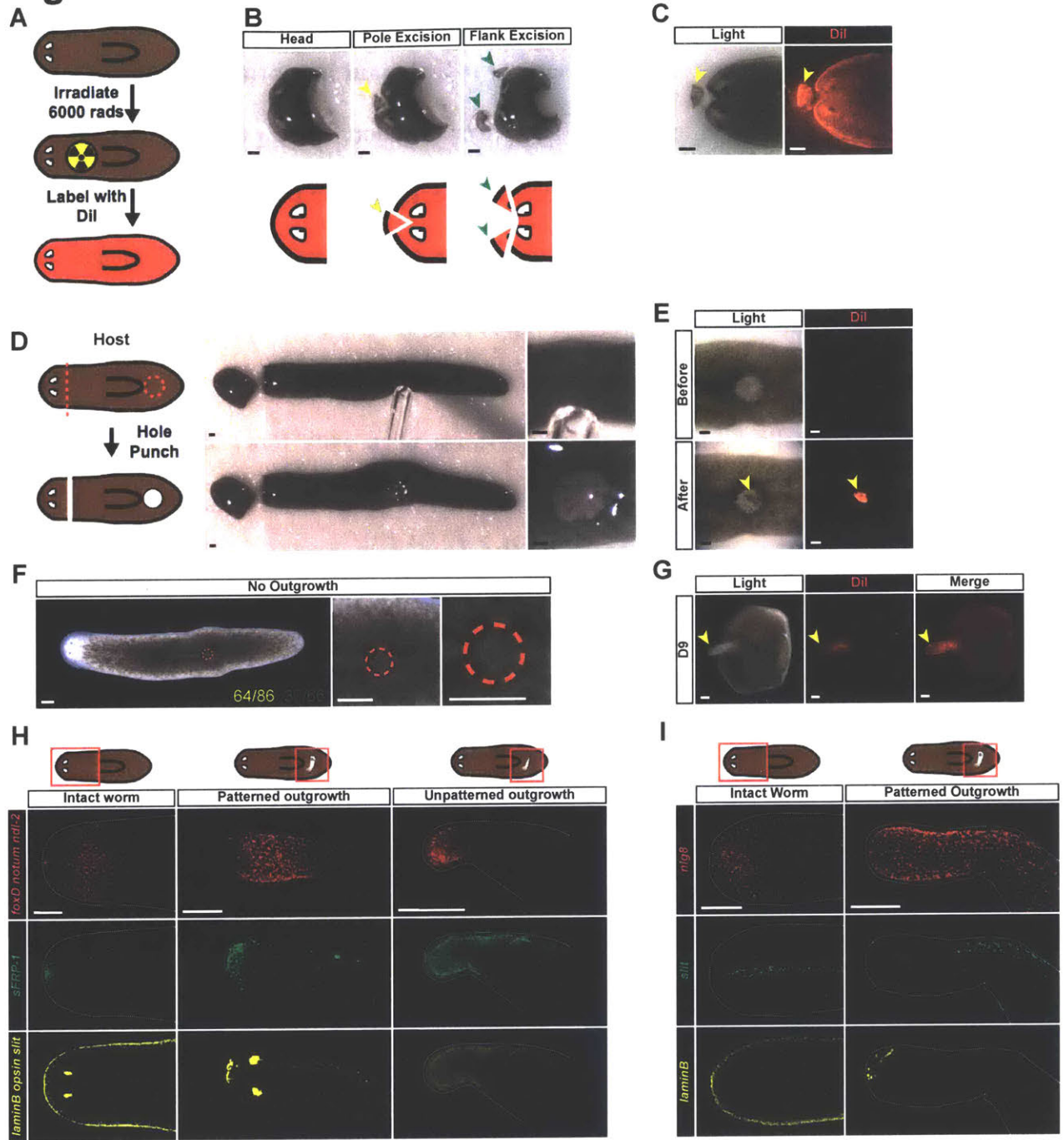


**Figure S1. Pole transplantation procedure and outcomes. Related to Figure 1.**

(A) Donors were lethally irradiated (6000 rads) 24 hours prior to transplantation. Animals were incubated in a 1:500 dilution of DiI (2  $\mu$ L) in planaria H<sub>2</sub>O overnight. (B) The donors' heads were amputated. From a single donor, a pole piece was excised, and transplanted, and then two flank pieces were excised, and transplanted. (C) The donor heads and pole fragments were positive for DiI signal. (D) Hosts were placed on a filter paper over ice, and a glass capillary was used to create a "hole punch" wound in the host. (E) The pole fragment or flank fragment was transplanted into the "hole punch" wound, and the animals was placed in a recovery chamber. (F) A majority of transplantations resulted in no outgrowth. n=64/86 pole transplants and n=37/66 flank transplants resulted in no outgrowth. A red dotted circle marks the site of failed outgrowth. (G) Outgrowths were positive for DiI signal, indicating that the outgrowths contained donor tissue. (B-G) Dorsal view, anterior is to the left. Scale bars, 200  $\mu$ L. (H) Triple FISH for *foxD/notum/ndl-2*, *sFRP-1*, and *slit/laminB/opsin* at 14 days following transplantation. Single-channel images are displayed. For merged images see Figure 1B. (I) Triple FISH for *nlg8*, *slit*, and *laminB* at 14 days following transplantation. Single-channel images are displayed. Pole transplant outgrowths have entirely dorsal identity (n=4/4). (H-I) Maximal intensity projections shown. Dorsal view, anterior is to the left. Scale bars, 200  $\mu$ L.

## **Anterior pole progenitors are specified medially and in a broad DV domain**

To understand pole positioning during regeneration, we first characterized anterior pole progenitor specification. Anterior pole progenitors are specified by expression of transcription factors such as *foxD* and *zic-1* and appear medially at anterior-facing wounds (Scimone et al., 2014; Vásquez-Doorman and Petersen, 2014; Vogg et al., 2014). The distribution of pole progenitors along the DV axis is poorly understood, so we imaged and quantified anterior pole progenitor specification in blastemas viewed *en face* (head-on) (Figure 1C, Figure S2A).

Pole progenitors were detected with *foxD* and *notum* expression. Because *notum* is also expressed in the brain (Hill and Petersen, 2015; Petersen and Reddien, 2011), we examined only *foxD/notum* double-positive cells, which were present by 48 hours post amputation (hpa). These cells were centered at the ML median plane (midpoint between the right and left wound sides) from 48 hpa to 72 hpa (Figures 1C-D). The position of pole progenitors was quantified relative to the DV median plane (the midpoint between the dorsal and ventral sides) estimated using *laminB* expression (which marks the dorsal-ventral boundary (Tazaki et al., 2002)). *foxD+/notum+* cells were initially dispersed on the DV axis (Figure 1C, Figure 1E). The distributions of these progenitors grew narrower and closer to the DV median plane with time, accumulating in a cluster by 72 hpa (Figure 1C, Figure 1E). Similarly, the average distance of anterior pole progenitors to the DV median plane grew smaller with time (Figure 1F). *zic-1+/notum+* cells and *follistatin+/notum+* cells displayed similar dynamics (Figures S2B-H).

We hypothesized that the *foxD+/notum+* cells include early stage anterior pole progenitors, which are the result of neoblast specialization. Irradiation depletes neoblasts (Figure S2J) and, consistent with previous reports (Scimone et al., 2014; Vásquez-Doorman and Petersen, 2014), blocked formation of anterior pole progenitors and the pole (Figures S2K). To

support the idea that the *foxD+/notum+* cells observed were the result of neoblast specialization, animals were labeled with RNA probes to *foxD* and *smedwi-1*, which is a marker for neoblasts (Reddien, 2005). *foxD+/smedwi-1+* cells were present from 24 to 72 hpa (Figure 2A) and were biased medially (Figure 2B), similar to *foxD+/notum+* cells. However, the distributions of *foxD+/smedwi-1+* cells along the DV axis did not become significantly narrower over time (Figure 2C) and the distance between the *foxD+/smedwi-1+* cells and the DV median plane did not become smaller over time (Figure S2I). These results suggest that anterior pole progenitors are specialized from neoblasts at the ML median plane, but broadly along the DV axis, only accumulating at the DV median plane as post-mitotic progenitors.

**Figure 2**

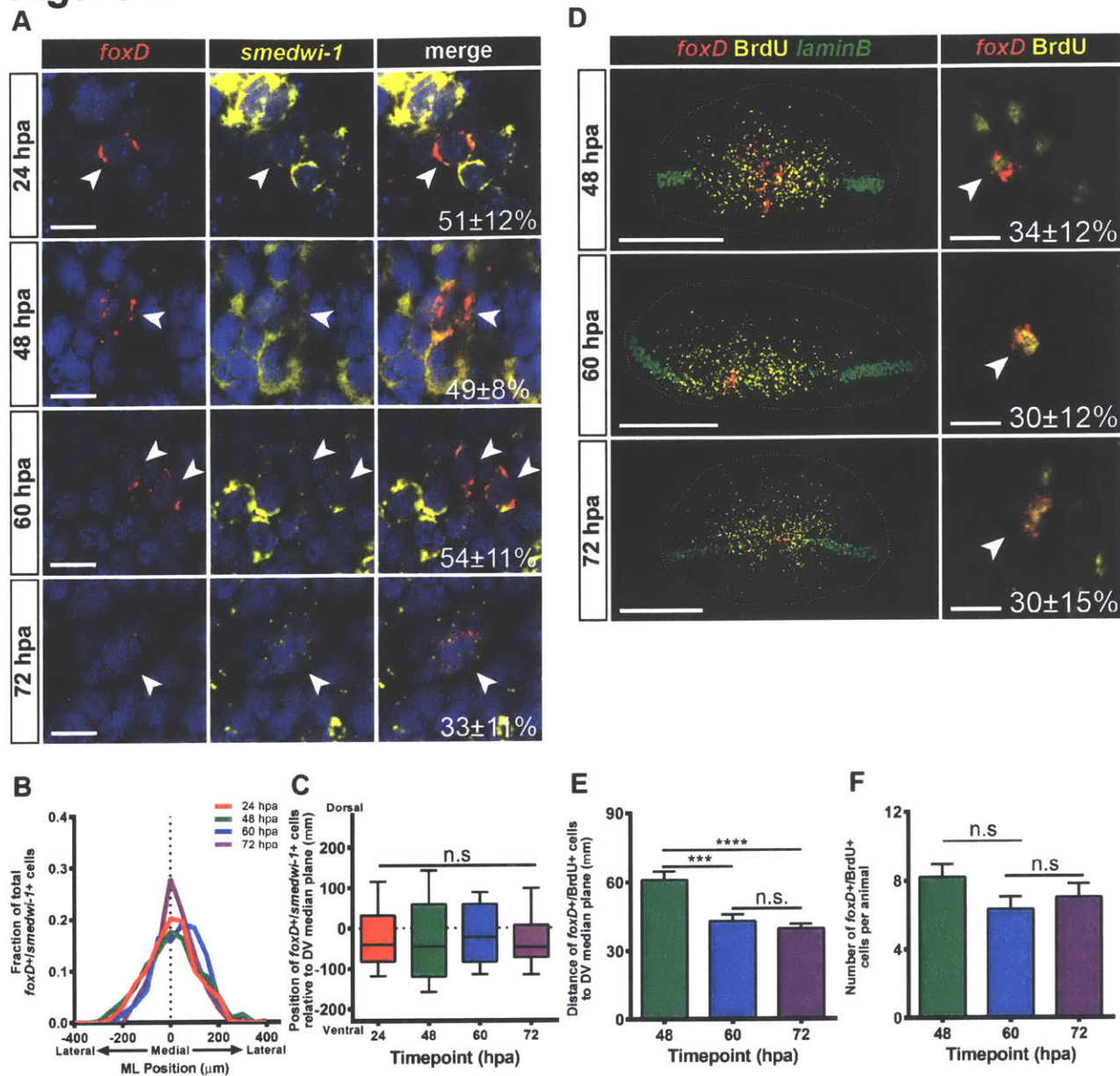
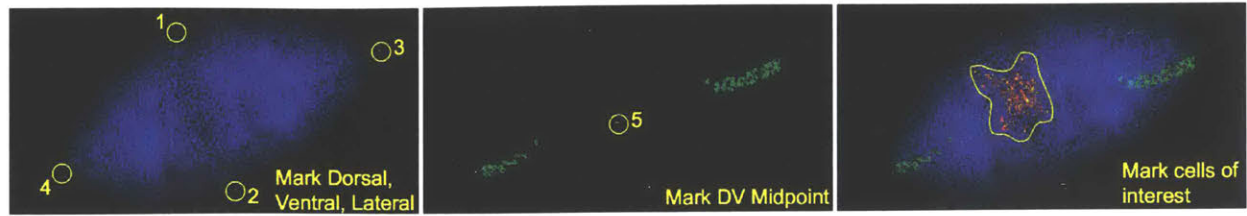


**Figure 2. Anterior pole progenitors are specified medially and in a broad DV domain.**

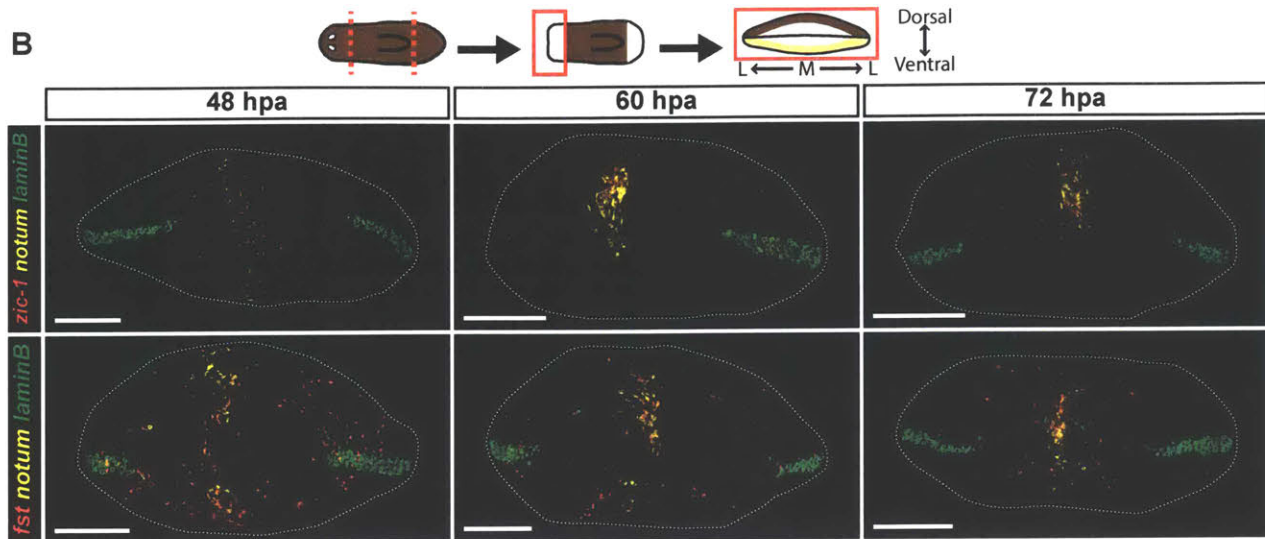
(A) Double FISH for *foxD* and *smadwi-1* at 24, 48, 60, and 72 hpa. Nuclear signal (DAPI) is shown in blue. A proportion of *foxD*<sup>+</sup> cells were also *smadwi-1*<sup>+</sup> at all timepoints examined (24 hpa, 51±21%, n = 810 cells; 48 hpa, 49±8%, n = 763 cells; 60 hpa, 54±11%, n = 211 cells; 72 hpa, 33±11%, n = 242 cells). (B) The distribution of the positions of *foxD*<sup>+</sup>/*smadwi-1*<sup>+</sup> cells on the ML axis is centered roughly around the ML median plane of the fragment (dotted line). 24 hpa, n=29 worms; 48 hpa, n=19 worms; 60 hpa, n=8 worms; 72 hpa, n=8 worms. (C) *foxD*<sup>+</sup>/*smadwi-1*<sup>+</sup> cells are spread along the DV axis. DV median plane, dotted line. Data compared by Kruskal-Wallis test. n.s. n>75 cells. (D) Double FISH for *foxD* and *laminB*, and immunolabeling for BrdU at 48, 60, and 72 hpa. Left panel: *foxD*<sup>+</sup>/BrdU<sup>+</sup> cells are scattered along the DV axis, and coalesce to a cluster with time. Right panel: White arrowhead indicates *foxD*<sup>+</sup>/BrdU<sup>+</sup> cell. Percent of *foxD*<sup>+</sup> cells which were BrdU<sup>+</sup>, lower right. (E) The distance between *foxD*<sup>+</sup>/BrdU<sup>+</sup> cells and the DV median plane is smaller at 60 and 72 hpa than it is at 48 hpa. Data were compared by Student's t-test. 48 hpa vs 60 hpa, \*\*\*p=0.0007, n>114 cells; 48 hpa vs 72 hpa, \*\*\*\*p<0.0001, n>189 cells; 60 hpa vs 72 hpa, n.s., n>114 cells. (F) The number of *foxD*<sup>+</sup>/BrdU<sup>+</sup> cells per animal is similar at all timepoints examined. Data were compared by Student's t-test. 48 hpa vs 60 hpa, n.s., n>18 animals; 60 hpa vs 72 hpa, n.s., n>18 animals. All images are an *en face* view of anterior blastema, dorsal is up. Left panels of (D), maximal intensity projections shown. Scale bars, 200uL. For (A) and right panels of (D) single confocal slices shown. Scale bars, 10 mm. For (E-F) data are represented as mean ± SEM. See also Figure S2.

# Figure S2

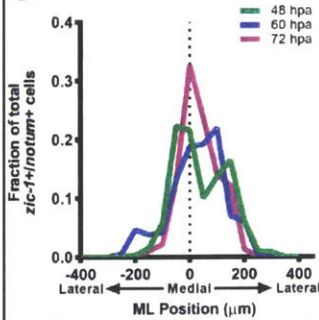
A



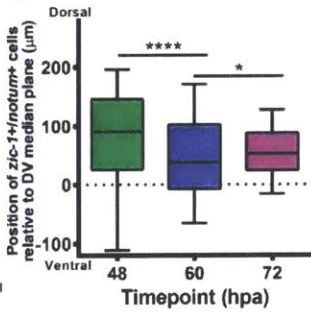
B



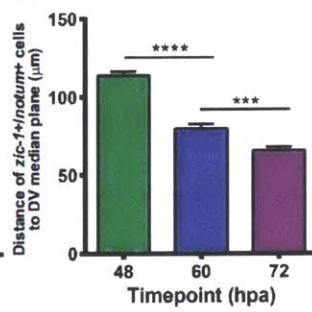
C



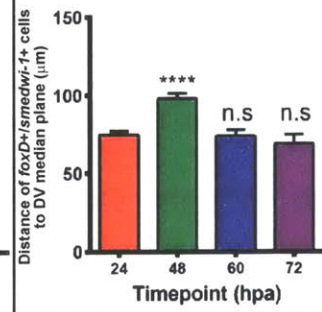
D



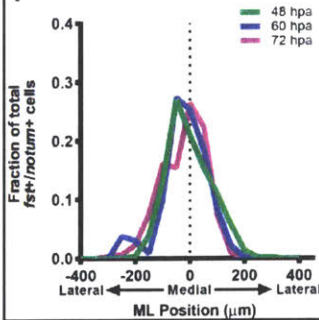
E



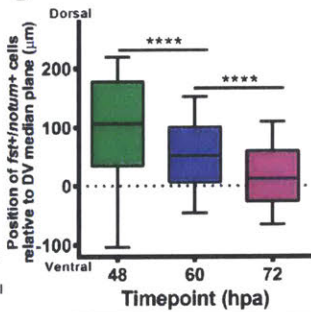
I



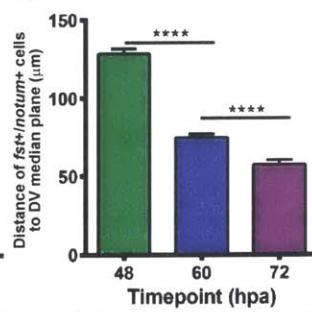
F



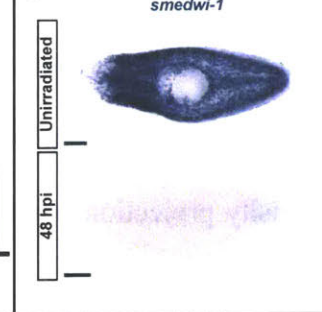
G



H



J



K

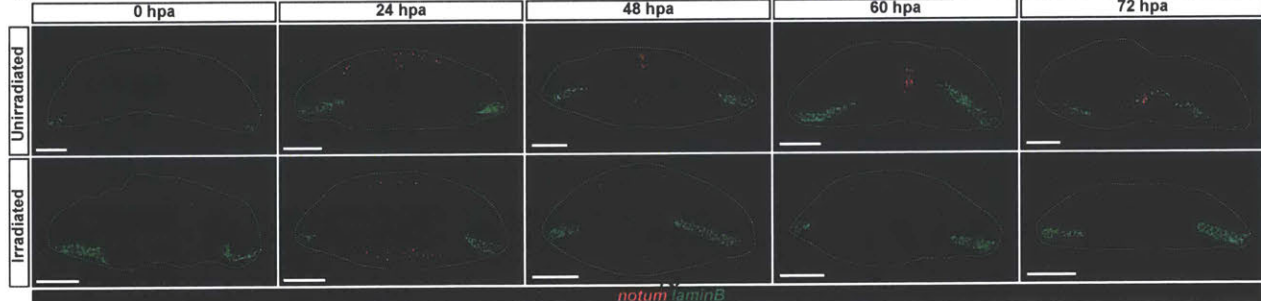


**Figure S2. Anterior pole progenitors are specified medially and in a broad DV domain.**

**Related to Figure 1 and Figure 2.**

(A) During image quantification, multiple attributes of each image were marked in the following order. The locations of the dorsal-most point, ventral-most point, and the two lateral-most points were marked. The location of the estimated DV median plane was marked using *laminB* signal as a guide. The positions of the cells of interest were marked. (B) Triple FISH for *zic-1* or *follistatin*, and *notum* and *laminB* at 48, 60, and 72 hpa. *zic-1+/notum+* and *follistatin+/notum+* cells appear around 48 hpa at the ML median plane of the anterior-facing wound, and accumulate over time near the DV median plane. (C) The distribution of the positions of *zic-1+/notum+* cells on the ML axis is centered on the ML median plane of the fragment (dotted line). 48 hpa, n=16 worms; 60 hpa, n=15 worms; 72 hpa, n=14 worms. (D) The distribution of the positions of *zic-1+/notum+* cells on the DV axis becomes tighter over time. Data were compared by a Mann-Whitney test. 48 vs 60 hpa, \*\*\*\*p<0.0001, n>473 cells; 60 vs 72 hpa, \*p=0.0283, n>364 cells. (E) The distance between *zic-1+/notum+* cells and the DV median plane grows smaller over time. Data were compared using a Student's t-test. 48 vs 60 hpa, \*\*\*\*p<0.0001, n>473 cells; 60 vs 72 hpa, \*\*\*p=0.0002, n>364 cells. (F) The distribution of the positions of *follistatin+/notum+* cells on the ML axis is centered roughly around the ML median plane of the fragment (dotted line). 48 hpa, n=16 worms; 60 hpa, n=16 worms; 72 hpa, n=12 worms. (G) The distribution of the positions of *follistatin+/notum+* cells on the DV axis becomes tighter and closer to the DV median plane over time. Data were compared with a Mann-Whitney test. 48 vs 60 hpa, \*\*\*\*p<0.0001, n>479 cells; 60 vs 72 hpa, \*\*\*\*p<0.0001, n>298 cells. (H) The distance between *follistatin+/notum+* cells and the DV median plane grows smaller over time. Data were compared using a Student's t-test. 48 vs 60 hpa, \*\*\*\*p<0.0001, n>479 cells; 60 vs 72 hpa,

\*\*\*\* $p < 0.0001$ ,  $n > 298$  cells. **(I)** The distance between *foxD*<sup>+</sup>/*smedwi-1*<sup>+</sup> cells and the DV median plane at 60 and 72 hpa is comparable to the distance at 24 hpa. At 48 hpa this distance is increased. Data are represented as mean  $\pm$  SEM and analyzed using a Student's t-test. 48 hour, 60 hour, and 72 hour timepoints were compared to 24 hpa. 48 hpa \*\*\*\* $p < 0.0001$ ,  $n > 311$  cells, 60 hpa n.s.,  $n > 114$  cells, 72 hpa n.s.,  $n > 75$  cells. **(J)** Colorimetric *in situ* hybridization for the expression of the gene *smedwi-1*, which marks neoblasts. 48 hours post irradiation (hpi), animals were completely depleted of neoblasts. **(K)** Double FISH for *notum* and *laminB* at 0, 24, 48, 60, and 72 hpa following lethal irradiation (6000 rads). At 0 hpa, anterior pole expression of *notum* has been completely eliminated by transverse amputation. At 24 hpa, wound-induced *notum* expression still occurs in animals that have been lethally irradiated. From 48 to 72 hpa, anterior pole progenitors do not appear and no anterior pole is formed in animals which have been lethally irradiated. For FISH images in **(B)** and **(K)** *en face* view of the anterior blastema, dorsal is up. Scale bars, 200  $\mu$ L **(J)**, ventral view, anterior is to the left. Scale bars, 200  $\mu$ L. For **(D)** and **(G)**, reference point is the DV median plane, which is estimated using *laminB* expression (dotted line). For **(E)** and **(H)** data are represented as mean  $\pm$  SEM.

### **Anterior Pole Cells Coalesce at the DV Median Plane**

Neoblast-derived progenitors have been observed to move from a specification location to their final destination for several tissue types, notably for the epidermis (Eisenhoffer et al., 2008; van Wolfswinkel et al., 2014) and the eye (Lapan and Reddien, 2011; 2012). To assess possible movement of dispersed pole progenitors along the DV axis into the anterior pole, we utilized bromodeoxyuridine (BrdU) labeling. BrdU is incorporated into neoblasts and can be used to trace the behavior of a cell cohort (Newmark and Sanchez Alvarado, 2000). Animals were amputated, immediately BrdU-pulsed, and analyzed in a regeneration time course (Figure 2D). The average distance of *foxD*<sup>+</sup>/BrdU<sup>+</sup> cells to the DV median plane was smaller at 60 and 72 hpa than at 48 hpa (Figure 2E), even as the number of *foxD*<sup>+</sup>/BrdU<sup>+</sup> cells per animal remained relatively constant (Figure 2F). These results are consistent with net movement of pole progenitors from being broadly dispersed on the DV axis into a coalesced anterior pole.

### **Anterior Pole Progenitor Specification Occurs at the Old Midline**

Anterior pole progenitor specification could in principle occur either at the ML median plane of the wound, such as might be the case if the blastema involves *de novo* pattern organization, or at the midline of pre-existing tissue. To distinguish between these possibilities, animals were subjected to either transverse, oblique, or sagittal amputations, and the expression of *notum*, *laminB*, and *slit* (which marks the midline (Cebrià et al., 2007)) was examined. In transversely amputated animals, the anterior pole formed at the pre-existing midline (yellow arrowheads), which was coincident with the ML median plane of the anterior-facing wound (white arrowheads) (Figure 3A, Figure S3A). Strikingly, in the oblique and sagittal amputations, the anterior pole progenitors formed at the pre-existing midline, even though this point was far from

the ML median plane of the wound. (Figure 3A, Figure S3A). Although the pole was shifted away from the ML median plane, with time these animals regenerated with the correct shape (Figure S3B). *foxD+/*smedwi-1+* cells (Figure 3B) were also shifted away from the ML median plane of the wound in oblique and sagittal fragments (Figure 3C). Instead, the pole-specialized neoblasts were present at the pre-existing *slit+* midline, suggesting that the anterior pole progenitor specification zone is biased to be within the pre-existing midline (Figure 3D).*

If pole progenitors are specified at a pre-existing midline, what happens to planarian fragments lacking a midline? To address this question, we generated fragments that had little-to-no pre-existing midline with parasagittal amputation (Figure S3D). As expected, the anterior pole in the parasagittal thick fragments regenerated at the pre-existing midline (Figure S3E). The thin fragments, which had no pre-existing midline, displayed new *slit* expression, followed by an anterior pole (Figure S3F). This result is consistent with the possibility that anterior pole formation happens at the midline, and that body fragments lacking a midline undergo a process of *de novo* midline formation prior to anterior pole formation.

### **The Plane of Symmetry in Asymmetric Fragments is Centered on the Anterior Pole**

The asymmetric formation of the anterior pole in amputated fragments lacking initial ML symmetry (Figure 3A) is consistent with the fact that obliquely amputated planarian body fragments produce head blastemas offset from the center of the wound face (Reddien and Sánchez Alvarado, 2004). We assessed the expression patterns of multiple patterning genes (*sFRP-1*, *ndl-2*, *wnt2*, *slit*, and *nlg7*) in these regenerating, asymmetric fragments at seven days post amputation. The plane of spatial expression symmetry for each of these patterning

molecules was centered at the regenerating anterior pole (Figure 3E, Figure S3C). The plane of symmetry during regeneration for many differentiated tissues, including the cephalic ganglia (*PC2+*), mechanosensory neurons (*cintillo+*), photoreceptor neurons (*opsin+*), GABAergic neurons (*gad+*), ciliated epidermis (*rootletin+*), secretory cells (*mag-1+*), and intestine (*madt+*), was also aligned with the location of the anterior pole (Figure 3E, Figure S3C). These results demonstrate for many tissues and gene expression domains that symmetry is centered around the pole, even if this position is offset from the ML midpoint of the wound face. These results are consistent with the role of the anterior pole in facilitating organization of new tissue pattern.

**Figure 3**

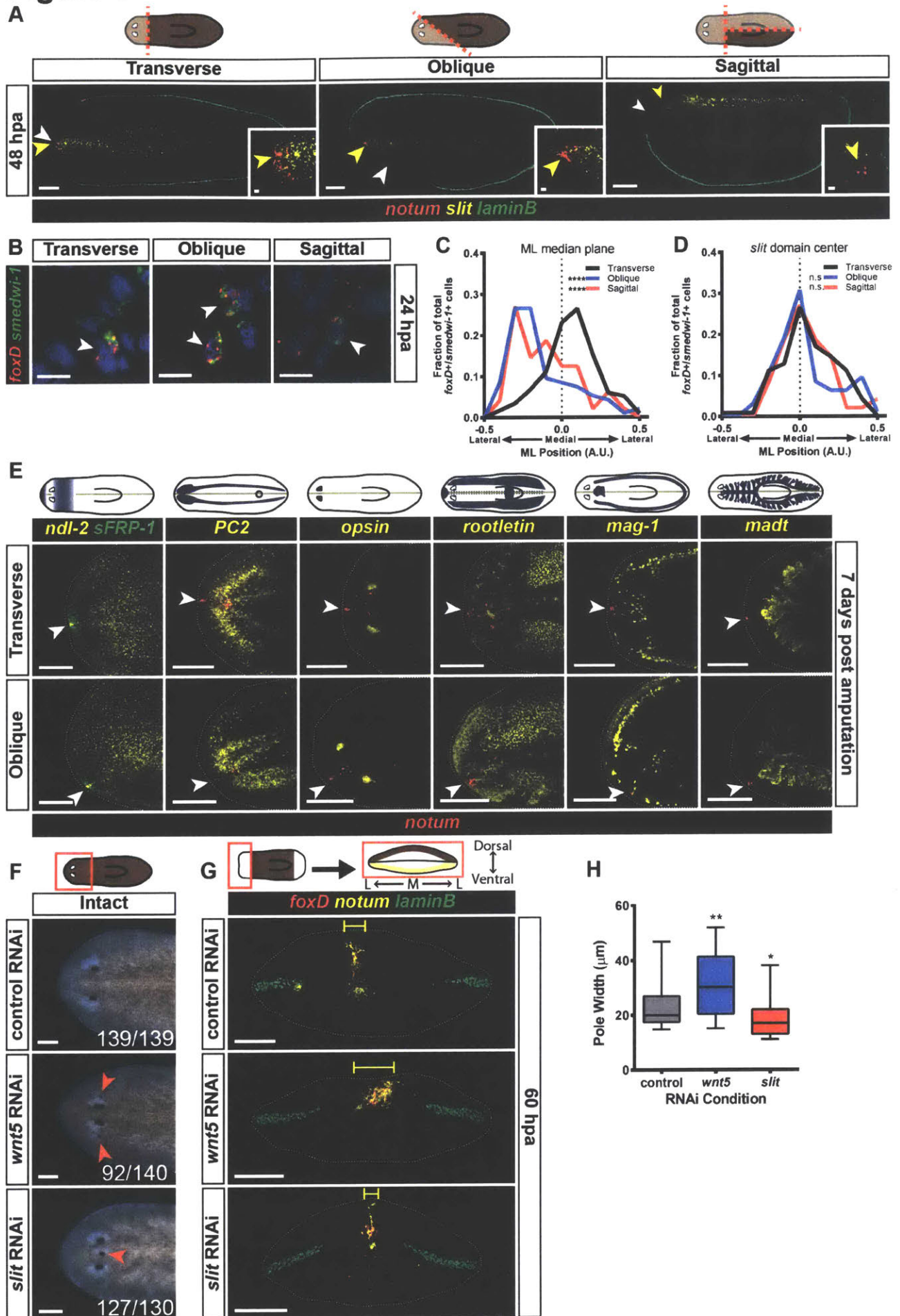


**Figure 3. Anterior pole formation occurs at the prior midline.**

(A) Triple FISH for *notum*, *slit* and *laminB* at 48 hpa for transverse, oblique or sagittal amputations. *notum*<sup>+</sup> cells appear near the *slit* domain in asymmetric wounds. White arrowheads, middle of anterior-facing wound; yellow arrowheads, middle of *slit* domain. Cartoon demonstrates surgery. Transverse 48 hpa, n=5/5; Oblique 48 hpa, n=10/10; Sagittal 48 hpa n=9/9. (B) Triple FISH for *foxD*, *smedwi-1* and *laminB* at 24 hpa for transverse, oblique or sagittal amputations. Nuclear signal (DAPI) is shown in blue. *foxD*<sup>+</sup>/*smedwi-1*<sup>+</sup> cells were quantified. (C-D) Distribution of *foxD*<sup>+</sup>/*smedwi-1*<sup>+</sup> cells along the ML axis at 24 hpa for transverse, oblique or sagittal amputations. (C) Reference is the ML median plane of the wound (dotted line). Transverse amputation distributions were centered on this point, oblique and sagittal distributions were offset. Data were compared by a Kolmogorov-Smirnov Test. Transverse vs Oblique \*\*\*\*p<0.0001 n>94 cells; Transverse vs Sagittal \*\*\*\*p<0.0001 n>48 cells. (D) Reference is the *slit* domain center (dotted line). Transverse, oblique and sagittal amputation distributions were centered on this point. Data were compared by a Kolmogorov-Smirnov Test. Transverse vs Oblique n.s. n>94 cells; Transverse vs Sagittal n.s. n>48 cells. (E) Triple FISH for *notum*, and *ndl-2* and *sFRP-1*, *PC2*, *opsin*, *rootletin*, *mag-1* or *madt* at 7 dpa for transverse and oblique amputations. White arrowheads, anterior pole. For clarity, ventral images (*PC2*) were vertically flipped. The plane of symmetry for gene expression was centered at the position of the anterior pole. (F) Live images at 28 days following inhibition of control gene, *wnt5* or *slit*. *wnt5(RNAi)* animals displayed ectopic lateral eyes and *slit(RNAi)* animals displayed ectopic medial eyes. Number of animals with phenotype, lower right. Red arrowheads, ectopic eyes. (G) Triple FISH for *foxD*, *notum* and *laminB* at 60 hpa following inhibition of control gene, *wnt5* or *slit*. *foxD*<sup>+</sup>/*notum*<sup>+</sup> cells occupied a wider area in *wnt5(RNAi)* animals, and a

narrower area in *slit(RNAi)* animals, compared to control RNAi animals. Yellow bracket, pole width. **(H)** Each animal was assigned a "pole width" score, which is the average distance of a cell to the center of its pole for that animal. *wnt5(RNAi)* animals had wider anterior poles and *slit(RNAi)* animals had narrower anterior poles. Data were compared by a Mann-Whitney test. control RNAi vs *wnt5* RNAi, \*\*p=0.0025, n>41 animals; control vs *slit* RNAi, \*p=0.0137, n>44 animals. For **(A)**, **(E)**, and **(F)** maximal intensity projections shown. Dorsal view, anterior is to the left. Scale bars, 200  $\mu$ L **(B)** single confocal slices shown. *en face* view of anterior blastema, dorsal is up. Scale bars, 10  $\mu$ L **(G)** maximal intensity projections shown. *en face* view of anterior blastema, dorsal is up. Scale bars, 200  $\mu$ L. See also Figure S3.



**Figure S3**

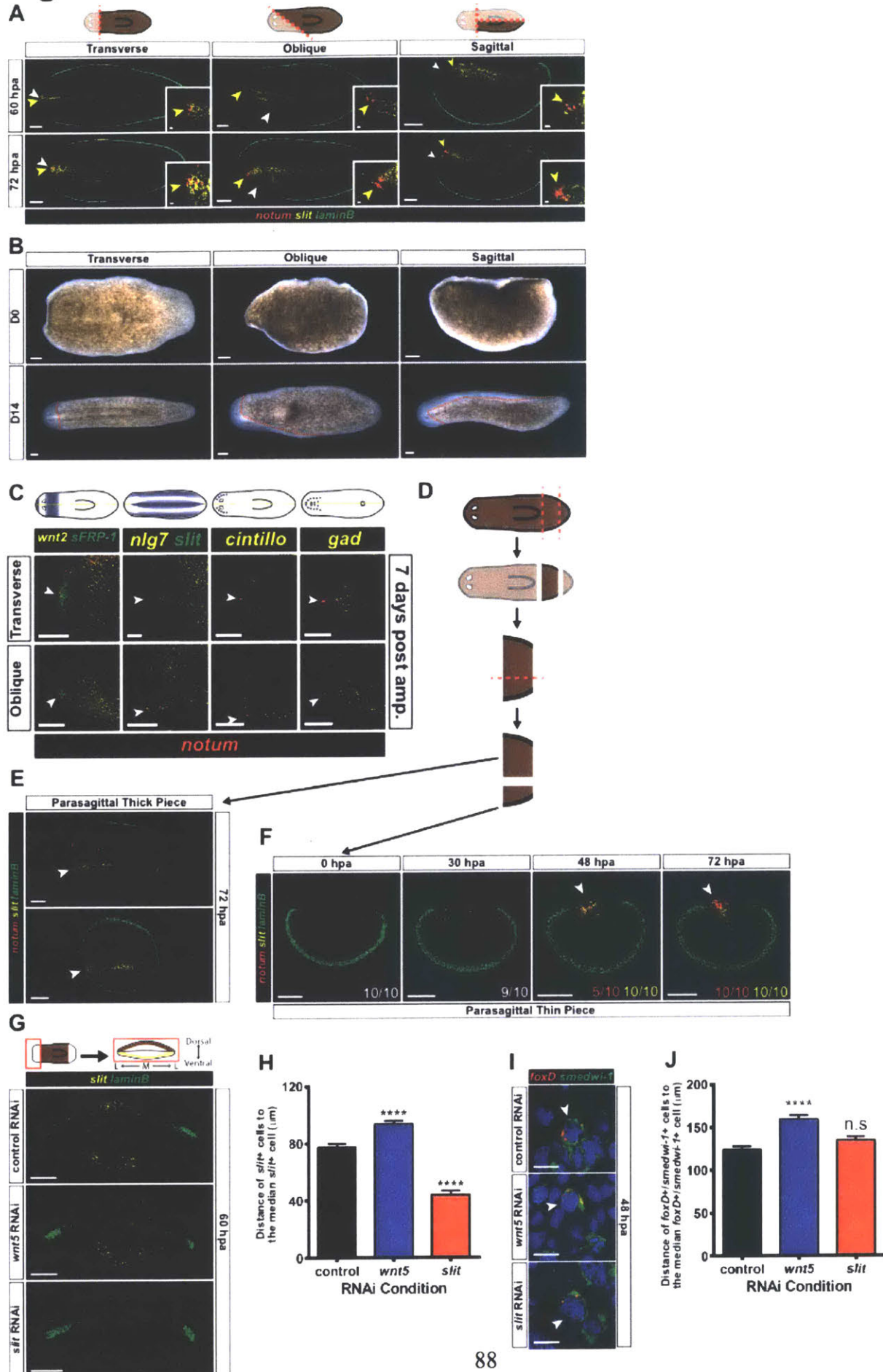


**Figure S3. Surgeries and *wnt5/slit* RNAi affect the ML axis. Related to Figure 3.**

(A) Triple FISH for *notum*, *slit* and *laminB* at 60 and 72 hpa for transverse, oblique or sagittal amputations. *notum*<sup>+</sup> cells appear near the *slit* domain in asymmetric wounds. White arrowheads, middle of anterior-facing wound; yellow arrowheads, middle of *slit* domain. Cartoon demonstrates surgery. Transverse 60 hpa, n=6/6; Oblique 60 hpa, n=11/11; Sagittal 60 hpa, n=10/10; Transverse 72 hpa, n=8/8; Oblique 72 hpa, n=12/12; Sagittal 72 hpa, n=20/20. (B) Live images at 0 and 14 days following transverse, oblique or sagittal amputation. Animals are capable of successfully regenerating from these amputations. (C) Triple FISH for *notum*, and *wnt2* and *sFRP-1*, *slit* and *nlg7*, *cintillo*, or *gad* at 7 dpa for transverse and oblique amputations. White arrowheads, anterior pole. For clarity, ventral images (*nlg7/slit* and *gad*) were vertically flipped. The plane of symmetry for gene expression was centered at the position of the anterior pole. (D) Cartoon depiction of the generation of thick and thin parasagittal pieces. (E) Triple FISH for *notum*, *slit* and *laminB* at 72 hpa for thick parasagittal pieces. White arrowheads, anterior pole. The anterior pole regenerates at the pre-existing midline. Two representative examples are shown. (F) Triple FISH for *notum*, *slit* and *laminB* at 0, 30, 48 and 72 hpa for thin parasagittal pieces. Immediately after the surgery, there is very little *slit* expression (10/10 animals). By 30 hpa, *slit* and wound-induced *notum* are expressed at the wound face (9/10 animals). At 48 hpa, some of the animals had begun to form a new anterior pole (5/10 animals), and all the animals had *slit* expression (10/10 animals). At 72 hpa all of the animals had formed a new anterior pole (10/10 animals), and all animals had *slit* expression extending into the fragment (10/10 animals). (G) Double FISH for *slit* and *laminB* at 60 hpa following inhibition of control gene, *wnt5* or *slit*. *slit*<sup>+</sup> cells occupy a wider area in *wnt5(RNAi)*, and a narrow area in *slit(RNAi)*, compared to control RNAi animals. (H) The distance between *slit*<sup>+</sup> cells and the

median cell is larger in *wnt5(RNAi)* animals and smaller in *slit(RNAi)* animals, as compared to control RNAi animals. Data are represented as mean  $\pm$  SEM and analyzed using a Student's t-test. control vs *wnt5(RNAi)*, \*\*\*\* $p < 0.0001$ ,  $n > 621$  cells; control vs *slit(RNAi)*, \*\*\*\* $p < 0.0001$ ,  $n > 454$  cells. **(I)** Double FISH for *foxD* and *smedwi-1* at 48 hpa following inhibition of control gene, *wnt5* or *slit*. Nuclear signal (DAPI) is shown in blue. *foxD*+/*smedwi-1*+ cells could be found and quantified. **(J)** The distance between *foxD*/*smedwi-1*+ cells and the median cell is larger in *wnt5(RNAi)* animals as compared to control RNAi animals. Data are represented as mean  $\pm$  SEM and analyzed using a Student's t-test. control vs *wnt5(RNAi)*, \*\*\*\* $p < 0.0001$ ,  $n > 510$  cells; control vs *slit(RNAi)*, n.s.,  $n > 496$  cells. For **(A-C)** and **(E-F)** maximal intensity projections shown. Dorsal view, anterior is to the left. Scale bars, 200  $\mu$ L **(G)** images shown are maximal intensity projections. Images are an *en face* view of the anterior blastema. Dorsal is up. Scale bars, 200  $\mu$  **(I)** images are a single confocal slice. Images are an *en face* view of the anterior blastema. Dorsal is up. Scale bars, 10  $\mu$ L.

## **Midline Patterning Molecules Affect the Medial Zone of Pole Progenitor Specification**

The appearance of pole progenitors at the prior (*slit*<sup>+</sup>) midline raised the possibility that the environment of the prior midline is permissive for pole progenitor specification at anterior-facing wounds. To test this possibility, animals were subjected to RNAi of *wnt5* and *slit*, which regulate the planarian ML axis (Cebrià et al., 2007; Gurley et al., 2010). *wnt5* negatively regulates the expression domain of *slit*. After 8 dsRNA feedings, *wnt5(RNAi)* animals displayed ectopic lateral eyes, and *slit(RNAi)* animals displayed ectopic medial eyes, confirming RNAi had perturbed medial-lateral pattern (Figure 3F). Furthermore, the *slit* expression domain was wider in *wnt5(RNAi)* animals and *slit* expression in *slit(RNAi)* animals was reduced and narrower than in controls (Figures S3G-H). Some *wnt5(RNAi)* animals had wider anterior poles than did control animals, whereas some of the *slit(RNAi)* animals had narrower poles than did control animals (Figures 3G-H). When we examined the distributions of pole-specialized neoblasts in these animals, we found that the distributions were wider in *wnt5(RNAi)* animals (Figures S3I-J). We conclude that the zone marked by the expression of *slit*, and defined by antagonistic roles for *wnt5* and *slit*, regulates the ML zone competent for pole progenitor specification at anterior-facing wounds.

## **Anterior Pole Progenitors Accumulate at the DV Median Plane of the Blastema**

We next sought to understand how the anterior pole is placed at a particular location along the DV axis. Of the many surgeries applied to planarians, few create asymmetry along this shortest of planarian axes. We developed a DV oblique cut involving transverse amputation and dorsal tissue removal, creating a wound with more dorsal than ventral tissue removed (Figure 4A).

Despite the severity of this wound, these animals eventually regenerated relatively normally (Figure S4A).

DV oblique animals formed a line of *laminB*<sup>+</sup> cells in the blastema that was shifted dorsally from the preexisting *laminB*<sup>+</sup> plane, consistent with a dorsal shift in the boundary formed between the dorsal and ventral epidermis during wound closure (Figure 4A-B). Early after DV oblique injury, pole progenitors were distributed along the DV axis; at later timepoints, the anterior pole coalesced far dorsal to the DV median plane of pre-existing tissue (Figure 4B-D). *laminB* expression in the blastema was used to estimate the DV boundary in the blastema at 72 hpa. Pole progenitors at 72 hpa were coincident with this new *laminB* expression plane (Figure 4E), suggesting that anterior pole progenitors accumulate near the approximate location of contact between the dorsal and ventral sides formed early during regeneration (DV boundary). At 7 days post injury, the expression gap in *ndl-2*, *sFRP-1* expression, and the location of the brain as visualized by *PC2* expression, were all shifted dorsally and retained their relative position to the anterior pole (Figure S4B).

### **Perturbation of Bmp Signaling Affects the DV Positioning of Pole Progenitors**

To determine if the pre-existing DV axis has a role in positioning anterior pole progenitors, animals were subjected to RNAi of *bmp4* and *smad1*, which normally promote dorsal tissue identity for the planarian DV axis (Molina et al., 2007; Orii and Watanabe, 2007; Reddien et al., 2007). As previously reported, the *laminB* expression domain was thickened with ectopic dorsal patches in both *bmp4* RNAi and *smad1* RNAi animals (Figure 4F, Figure S4C) (Gaviño and Reddien, 2011; Reddien et al., 2007). RNAi of *bmp4* and *smad1* causes ventralization; cells

responding to Bmp activity levels for localization should be shifted dorsally when that signal is reduced. Indeed, anterior pole progenitors were shifted dorsally at 48 hpa relative to *laminB*<sup>+</sup> cells in pre-existing tissue in both *bmp4* and *smad1* RNAi animals (Figure 4F). This result was confirmed by measuring the position of the anterior pole progenitors relative to the pre-existing DV median plane, and by examining their distributions (Figure 4G). Quantification of anterior pole progenitors at 72 hpa revealed that this dorsal bias persisted (Figure 4H). These results indicate that the correct DV localization of anterior pole progenitors requires Bmp signaling.

**Figure 4**

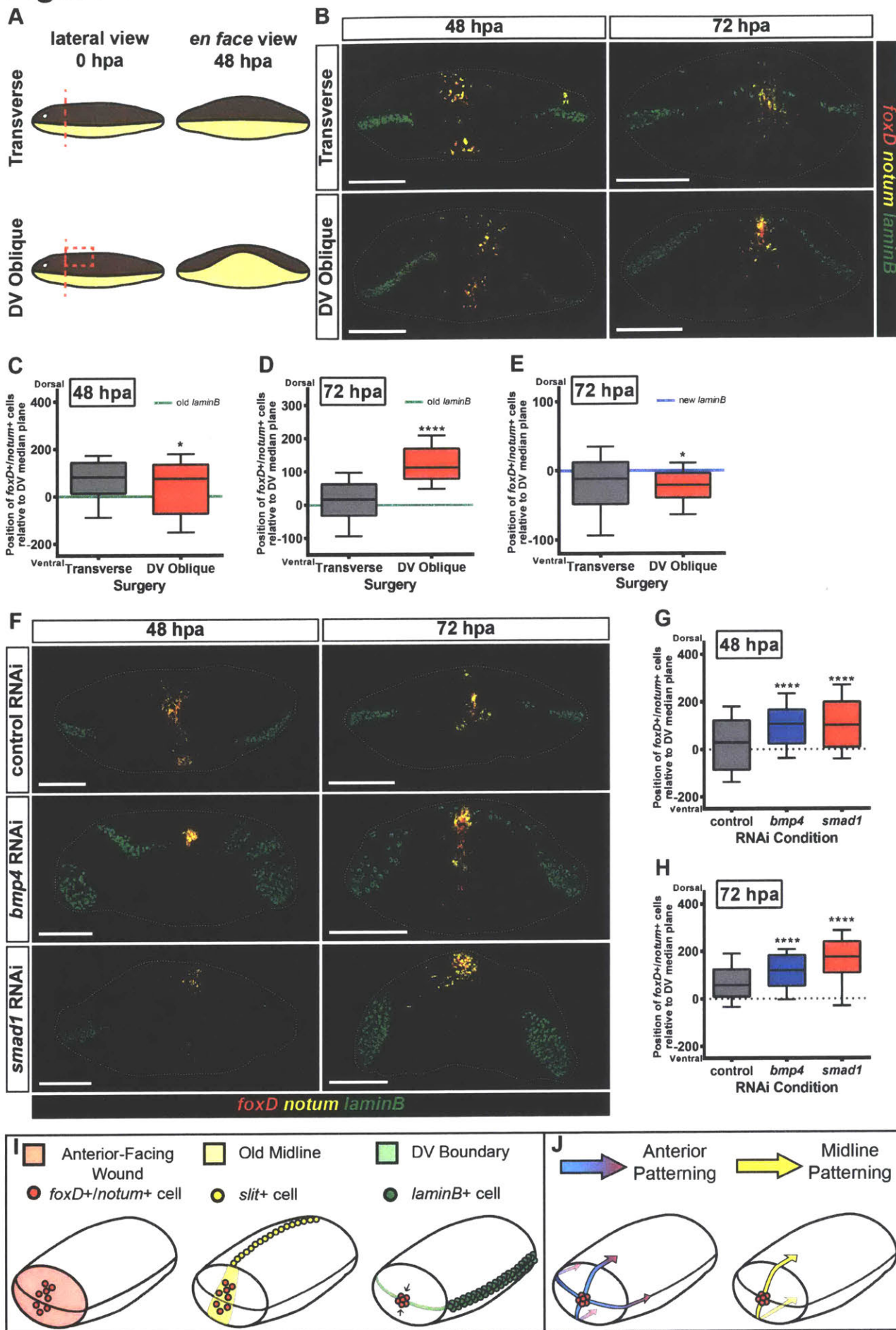


**Figure 4. The final location of the anterior pole is influenced by the DV axis.**

(A) Left panel: Cartoon of a transverse and DV oblique amputation. To generate DV oblique fragments, animals had a transverse amputation followed by a precise removal of dorsal tissue. Lateral view, dorsal is up. Right panel: In order to close the wound following a DV oblique cut, ventral tissue must migrate further to make contact with dorsal tissue and seal the wound. *en face* view, dorsal is up. (B) Triple FISH for *foxD*, *notum* and *laminB* at 48 and 72 hpa following transverse or DV oblique amputation. *foxD*<sup>+</sup>/*notum*<sup>+</sup> cells accumulate at the DV boundary (*laminB*<sup>+</sup>) over time. (C-E) The distribution of *foxD*<sup>+</sup>/*notum*<sup>+</sup> cells on the DV axis. The transverse and DV oblique conditions were compared by a Mann-Whitney test. (C) At 48 hpa, *foxD*<sup>+</sup>/*notum*<sup>+</sup> cells were broader in DV oblique animals, but not dorsally shifted. \**p*<0.0417, *n*>228 cells. (D) At 72 hpa, *foxD*<sup>+</sup>/*notum*<sup>+</sup> cells were shifted dorsally in DV oblique animals. \*\*\*\**p*<0.0001, *n*>297 cells. (E) At 72 hpa, *foxD*<sup>+</sup>/*notum*<sup>+</sup> cells were close to the DV boundary. \**p*<0.0152, *n*>230 cells. (F) Triple FISH for *foxD*, *notum* and *laminB* at 48 and 72 hpa following inhibition of control gene, *bmp4* or *smad1*. *foxD*<sup>+</sup>/*notum*<sup>+</sup> cells were shifted dorsally in *bmp4*(RNAi) and *smad1*(RNAi) as compared to control RNAi animals. (G-H) The distribution of *foxD*<sup>+</sup>/*notum*<sup>+</sup> cells on the DV axis. Data were compared by a Mann-Whitney test. (G) At 48 hpa, *foxD*<sup>+</sup>/*notum*<sup>+</sup> cells were dorsally shifted following inhibition of *bmp4* or *smad1*. control RNAi vs *bmp4* RNAi, \*\*\*\**p*<0.0001, *n*>346 cells; control RNAi vs *smad1* RNAi, \*\*\*\**p*<0.0001, *n*>354 cells. (H) At 72 hpa, *foxD*<sup>+</sup>/*notum*<sup>+</sup> cells were dorsally shifted following inhibition of *bmp4* or *smad1*. control RNAi vs *bmp4* RNAi, \*\*\*\**p*<0.0001, *n*>295 cells; control RNAi vs *smad1* RNAi, \*\*\*\**p*<0.0001, *n*>295 cells. For (B) and (F) maximal intensity projections shown. *en face* view of anterior blastema, dorsal is up. Scale bars, 200 μL. For (C-D) and (G-H) the reference point for these coordinates is the DV median plane, which is estimated

using old *laminB* expression (green or dotted line). For **(E)** the reference point for these coordinates is the DV boundary in the blastema, which was estimated using new *laminB* expression (blue line). **(I)** Anterior pole formation relies on three landmarks at wounds in order to integrate the pattern of the new and pre-existing tissues: an anterior-facing wound, the prior midline, and the boundary between the dorsal and ventral sides of the animal. **(J)** Once the anterior pole is formed, it acts to help pattern the AP and ML axes of the regenerating head. See also Figure S4.



**Figure S4**

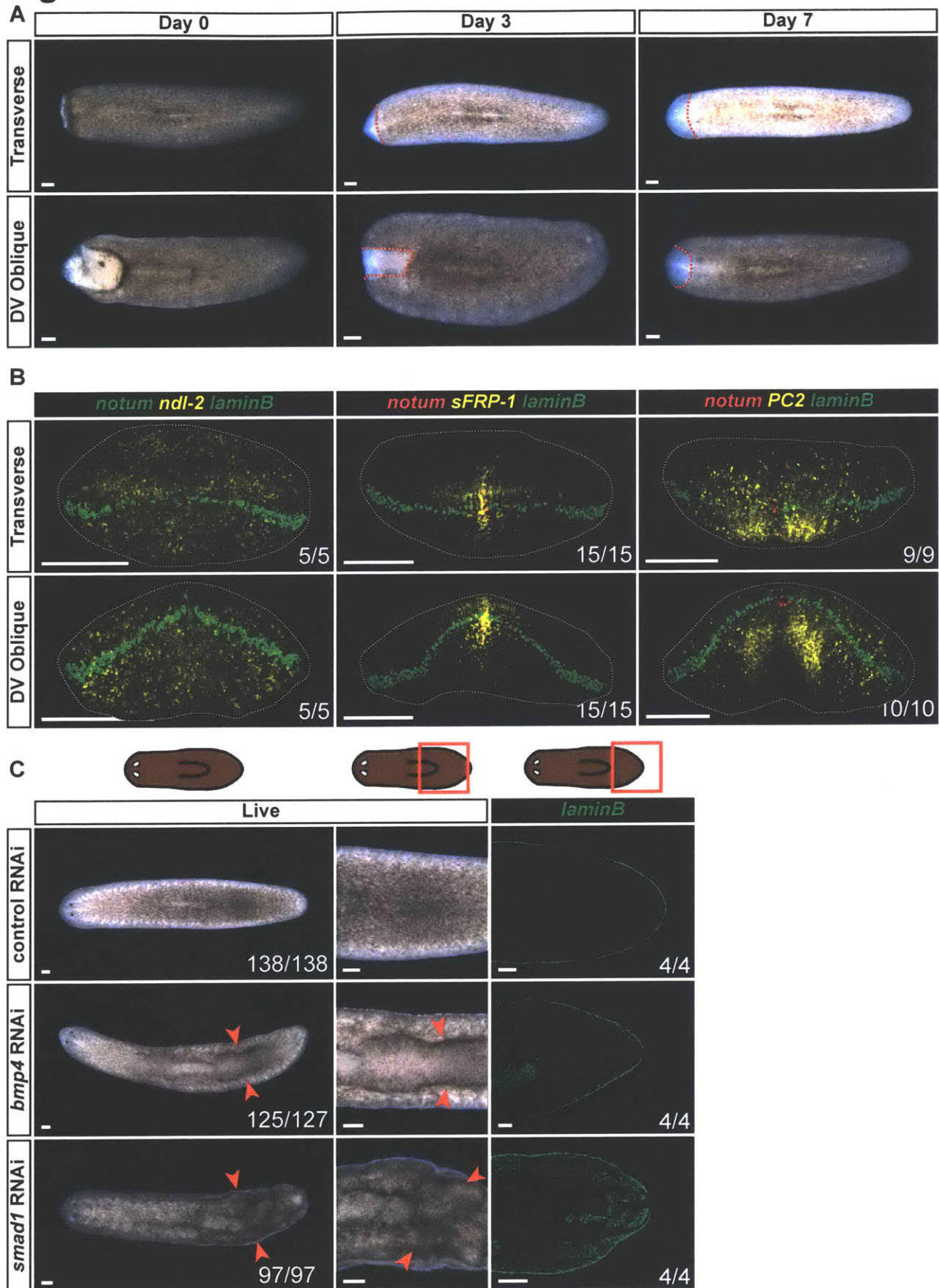


**Figure S4. DV oblique cuts and Bmp pathway inhibition affect the DV axis. Related to Figure 4.**

(A) Live images at 0, 3 and 7 days following transverse or DV oblique amputation. Animals are capable of restoring form after these injuries. Red dotted line, old tissue/blastema boundary. (B) Triple FISH for *notum* and *ndl2*, *notum* and *sFRP-1*, or *notum* and *PC2*, and *laminB* at 7 dpa for transverse and DV oblique amputations. Gene expression domains and tissue architecture appear to maintain their spatial relationship with the anterior pole. Number of animals, lower right. (C) Left columns: Live images at 28 days following inhibition of control gene, *bmp4* or *smad1*. *bmp4(RNAi)* and *smad1(RNAi)* animals display ridges on their dorsal side. Red arrowheads, dorsal ridges. Right Column: Single FISH for *laminB* at 28 days following inhibition of control gene, *bmp4* or *smad1*. Patches of ectopic *laminB* expression can be found on the dorsal sides of *bmp4(RNAi)* and *smad1(RNAi)* animals. Number of animals, lower right. For (A) and (C), dorsal view, anterior is to the left. For (B), *en face* view of the anterior blastema, dorsal is up. For all images, maximal intensity projections shown. Scale bars, 200  $\mu$ L.

## Conclusions

One of the central challenges of regeneration is having a system that is capable of responding to injuries with different wound site architectures to produce a correctly patterned animal. Regenerative tissue outgrowths (blastemas) likely initiate pattern formation by a mechanism distinct from what occurs at the beginning of embryogenesis given the drastically different starting conditions for these processes. Given prior RNAi data (Scimone et al., 2014; Vázquez-Doorman and Petersen, 2014; Vogg et al., 2014) and the head tip transplantation results, the anterior pole likely has an important role in determining how the planarian head blastema organizes its pattern. Our findings suggest that the position of anterior pole regeneration relies on three cues: an anterior-facing wound (Scimone et al., 2014; Vázquez-Doorman and Petersen, 2014; Vogg et al., 2014), the pre-existing midline, and the DV boundary in the blastema (Figure 4I). The positioning of the pole at the midline during regeneration can allow ML pattern of new tissue to align with ML pattern of pre-existing tissue. Coordinating AP axis information with a DV axial plane to set a point of tissue organization and growth has parallels to other biological systems, such as in *Drosophila* imaginal discs (Diaz-Benjumea and Cohen, 1993) (Diaz-Benjumea and Cohen, 1995). Positioning of an organizer at the DV median plane in regeneration could facilitate a vector of growth and pattern formation on the AP axis perpendicular to the old DV axis. Planarians use positional information actively as adults for maintenance and restoration of axial pattern (Reddien, 2011). We conclude that the process of anterior pole formation during regeneration integrates axial cues at wounds, providing a mechanism to coordinate patterning and growth during head regeneration in a manner coherent with pre-existing tissue pattern (Figure 4J).

## Tables

Gene Symbol	Reference	Pubmed ID	NCBI Accession Number
<i>bmp4</i>	Molina 2007	17905225	EF633689
<i>cintillo</i>	Oviedo 2003	12557210	AY067542
<i>follistatin</i>	Roberts-Galbraith 2013	23297191	KC161222
<i>foxD</i>	Vogg 2014	24704339	KC577557
<i>gad</i>	Nishimura 2008	18440152	AB332029
<i>laminB</i>	Tazaki 2002	12203092	AY067086
<i>mag-1</i>	Zayas 2010	20865784	HM803280
<i>madt</i>	Wenemoser 2010	20599901	EG413862
<i>ndl-2</i>	Scimone 2016	27063937	KT983961
<i>nlg7</i>	Molina 2009	19174194	FJ471489
<i>nlg8</i>	Molina 2009	19174194	FJ471490
<i>notum</i>	Petersen 2011	21566195	JF725701
<i>opsin</i>	Sanchez Alvarado 1999	10220416	AF112361
<i>PC2</i>	Collins 2010	20967238	BK007043
<i>rootletin</i>	Glazer 2010	19852954	AY068190
<i>sFRP-1</i>	Petersen 2008	18063755	EU296635
<i>slit</i>	Cebria 2007	17553481	DQ336176
<i>smad1</i>	Molina 2007	17905225	EF633692
<i>smedwi-1</i>	Reddien 2005	16311336	DQ186985
<i>wnt2</i>	Petersen 2008	18063755	EU296634
<i>wnt5</i>	Adell 2009	19211673	FJ463749
<i>zic-1</i>	Vogg 2014	24704339	KF751216

## **Materials and Methods**

### **Animals and radiation treatment**

Asexual *Schmidtea mediterranea* strain (CIW4) were maintained in 1x Montjuic planarian water at 20°C as previously described (Sánchez Alvarado et al., 2002). Animals were starved 7–14 days prior experiments were used. Irradiated animals were exposed to a 6,000 rads dose of radiation using a dual Gammacell-40 <sup>137</sup>cesium source and amputated two days after irradiation. Animals were selected to be size-matched within an experiment, for all experiments.

### **Double-stranded RNA synthesis for RNAi experiments**

Double stranded RNA (dsRNA) was synthesized as previously described (Rouhana et al., 2013). Briefly, PCR templates of sequences for the forward and reverse of the target genes were prepared with a 5' flanking T7 promoter (TAATACGACTCACTATAGGG). The forward and reverse templates (16uL) were mixed, in separate reactions, with 1.6 uL of 100mM rNTPs (Promega); 0.6 uL of 1M dithiothreitol (DTT; Promega); 4 uL of T7 polymerase; and 24 uL of 5x Transcription optimized buffer (Promega). Reactions were incubated for 2h at 37 C and then supplemented with RNase-free DNase for 45 minutes. RNA was purified by ethanol precipitation, and finally resuspended in 24 uL of milliQ H<sub>2</sub>O. RNA was analyzed on 1% agarose gel. RNA for forward and reverse strands were combined and annealed by heating the reactions in a thermo-cycler to 90 C and lowering gradually the temperature to 20 C.

## **RNAi**

Animals were starved for at least 7 days prior to the first feeding. The food mixture was as follows: 26  $\mu\text{L}$  of 100% homogenized beef liver, 12  $\mu\text{L}$  of dsRNA, and 2  $\mu\text{L}$  of red food coloring. Animals were fed twice a week.

## **Transplantation and Microsurgery**

Transverse trunk fragments were generated by amputation beneath the auricles and immediately posterior to the pharynx. Oblique fragments were generated by a single diagonal cut made from the right side of the animal adjacent to the right eye to the left side of the animal below the pharynx. Sagittal fragments were made by amputating the head and performing a single sagittal cut. Transplantation of pole and flank pieces was as follows. Large (10-12 mm long) animals were selected for the procedure. Donors were lethally irradiated (6000 rads) 24 hours prior to transplantation and then were incubated in a 1:500 dilution of DiI (2  $\mu\text{L}$ ). Thirty minutes prior to transplantation the DiI solution was removed and the donors were transferred to fresh plates. Hosts were anesthetized in 0.2% chloretone diluted in planarian water for 5 minutes, and briefly rinsed in Holtfreter's on a filter paper on ice moistened with Holtfreter's (Santos, 1929). A glass capillary tube of 0.75 mm interior diameter and 0.7 mm exterior diameter (FHC, Bowdoin, ME, USA) were used to remove host tissue from the future transplantation site posterior to the pharynx (Figure S1D) (Guedelhofer and Sánchez Alvarado, 2012). Donors were placed on a filter paper on top of a petri-dish lid over ice moistened with Holtfreter's and either a pole fragment or flank fragment was excised (Figure S1B). Because donors were labeled with DiI, the donor fragments were easily visualized under a fluorescent microscope (Figure S1C). The pole or flank fragment was moved with a pipette from the donor to the host, and a pair of surgical

scalpels were used to force the pole or flank fragment into the host (Figure S1E). The host was then placed in a recovery chamber as described previously (Guedelhofer and Sánchez Alvarado, 2012). Twenty-four hours after transplantation, hosts were moved from the recovery chamber into a petri dish with planaria water. Live animals were examined under a fluorescent microscope to look for DiI signal (Figure S1G).

### **Fixations**

Animals were fixed and labeled as previously described (King and Newmark, 2013). In brief, animals were killed in 5% N-acetyl-cysteine in PBS for 5 minutes and then fixed in 4% formaldehyde for 20 minutes at room temperature. Fixative was removed and worms were rinsed 1X with PBSTx (PBS + 0.3% Triton X-100). PBSTx was replaced with preheated Reduction solution for 10 minutes at 37°C. Animals were dehydrated by a methanol series and stored in methanol at -20°C.

### **Whole-mount *in situ* hybridizations**

RNA probes were synthesized and nitroblue tetrazolium/5-bromo-4-chloro-3-indolyl phosphate (NBT/BCIP) colorimetric whole-mount *in situ* hybridizations (ISH) were performed as described (Pearson et al., 2009). Fluorescence *in situ* hybridizations (FISH) were performed as described (King and Newmark, 2013) with minor modifications. Briefly, animals were killed in 5% NAC and treated with proteinase K (4  $\mu$ L) serum PBSTx solution when anti-DIG or anti-DNP antibodies were used, and in 1% Roche Western Blocking Reagent PBSTx solution when an anti-FITC antibody was used. Post-antibody binding washes and tyramide development were performed as described (King and Newmark, 2013). Peroxidase inactivation with 1% sodium

azide was done for 90 minutes at RT. Most specimens were counterstained with DAPI overnight (Sigma, 1  $\mu$ L)

### **BrdU labeling and immunofluorescence**

BrdU (Sigma) was administered by soaking fragments starting 1 hour following amputation for 2 hours in planaria H<sub>2</sub>O containing 25 mg/ml BrdU and 3% DMSO; animals were then chased in Instant Ocean dissolved at 5 g/L until they were fixed. For BrdU labeling, samples were pretreated by incubation in 2N HCl (+0.5% triton-X-100) for 45 minutes followed by brief neutralization in 0.1M sodium borate. BrdU was detected with mouse anti-BrdU (BD Biosciences) followed by goat anti-Mouse IgG HRP Conjugate (Life Technologies), blocked in 0.6% BSA, 1% Western Blocking Reagent (Roche), and 5mM thymidine in PBSTx(0.3%). The BrdU signal was developed as previously described (Pearson et al., 2009) using the Cy5 tyramide.

### ***en face* mounting**

Following staining, animals were placed in a petri dish with PBSTx and the anterior blastemas were cut off using a sharp scalpel. The anterior blastemas were placed on a slide with the cut edge down. A coverslip was placed over the same and Vectashield was allowed to flow in from the side.

### **Microscopy and image analysis**

Fluorescent images were taken with a Zeiss LSM700 Confocal Microscope. Light images were taken with a Zeiss Discovery Microscope. For *en face* images, the marking of cell positions was

performed using Fiji/ImageJ. A text file containing the positions of all the cells, and 5 reference positions (Figure S2A), was exported from Fiji/ImageJ. Reference point 1 is the dorsal most point, reference point 2 is the ventral most point, reference points 3 and 4 are the right and left sides, respectively, and reference point 5 is the estimated DV boundary in the blastema. This file was imported into MATLAB, which was used to perform the following transformations:

Coordinate Transformation I: The mean of reference points 1 and 2 was subtracted from all coordinates. This moves the distribution so that rotation will be around this point.

Coordinate Rotation: Matrix multiplication was used to rotate the coordinates so that reference point 1 was directly vertical.

Coordinate Transformation II: The x-value mean of reference points 3 and 4 was used to subtract from the X coordinates, and the y-value of reference point 5 was used to subtract from the Y coordinates. This places the origin of the data at the middle between the right and left sides of the fragment, and at the DV boundary.

The transformed coordinates, as well as measurements of distances between the coordinates and various landmarks were exported into an Excel document for further analysis. The histogram function in Excel was used on the X coordinates to generate the histograms for Figures 1D, 2B, 3C-D, S2C, S2F. The Y coordinates were plotted to generate Figures 1E, 2C, 4C-E, 4G-H, S2D, and S2G. The absolute values of the Y coordinates were used to generate the distances from the DV boundary in Figures 1F, 2E, S2E, S2H, and S2I.

## **Graphs and statistical analysis**

All graphs and statistical analysis were done using the Prism software package (GraphPad Inc., La Jolla, CA). Comparisons between the means of two populations were done by a Student's t-test. Comparisons between two distributions were done using a Mann-Whitney test. Comparisons between two rows in a contingency table were done using Fisher's exact test. Significance was defined as  $p < 0.05$ .

## **Acknowledgements**

We thank the members of the Reddien Lab for comments and discussion. D.J.L. is supported by the National Institute of General Medical Sciences (T32GM007753) and by the Paul and Daisy Soros Fellowship for New Americans. P.W.R. is an Investigator of the Howard Hughes Medical Institute and an associate member of the Broad Institute of Harvard and MIT. We acknowledge support from the NIH (R01GM080639).

## References

- Cebrià, F., Guo, T., Jopek, J., and Newmark, P.A. (2007). Regeneration and maintenance of the planarian midline is regulated by a *islit/i* orthologue. *Developmental Biology* 307, 394–406.
- Chandebois, R. (1985). Intercalary regeneration and level interactions in the fresh-water planarian *Dugesia lugubris*. *Roux's Archives Biology* 53, 390–396.
- Diaz-Benjumea, F.J., and Cohen, S.M. (1993). Interaction between dorsal and ventral cells in the imaginal disc directs wing development in *Drosophila*. *Cell* 75, 741–752.
- Diaz-Benjumea, F.J., and Cohen, S.M. (1995). Serrate signals through Notch to establish a Wingless-dependent organizer at the dorsal/ventral compartment boundary of the *Drosophila* wing. *Development (Cambridge, England)* 121, 4215–4225.
- Driever, W., and Nüsslein-Volhard, C. (1988). A Gradient of *bicoid* Protein in *Drosophila* Embryos. *Cell* 54, 83–93.
- Dubois, F. (1949). Contribution à l'étude de la migration des cellules de régénération chez les Planaires dulcicoles (Bulletin Biologique de la France et de le Belgique).
- Eisenhoffer, G.T., Kang, H., and Sánchez Alvarado, A. (2008). Molecular analysis of stem cells and their descendants during cell turnover and regeneration in the planarian *iSchmidtea mediterranea/i*. *Cell Stem Cell* 3, 327–339.
- Gaviño, M.A., and Reddien, P.W. (2011). A Bmp/Admp Regulatory Circuit Controls Maintenance and Regeneration of Dorsal-Ventral Polarity in Planarians. *Current Biology : CB* 21, 294–299.
- Gaviño, M.A., Wenemoser, D., Wang, I.E., and Reddien, P.W. (2013). Tissue absence initiates regeneration through Follistatin-mediated inhibition of Activin signaling. *Elife* 2, e00247.
- Guedelhofer, O.C., and Sánchez Alvarado, A. (2012). Amputation induces stem cell mobilization to sites of injury during planarian regeneration. *Development (Cambridge, England)* 139, 3510–3520.
- Gurley, K.A., Elliott, S.A., Simakov, O., Schmidt, H.A., Holstein, T.W., and Sánchez Alvarado, A. (2010). Expression of secreted Wnt pathway components reveals unexpected complexity of the planarian amputation response. *Developmental Biology* 347, 24–39.
- Hill, E.M., and Petersen, C.P. (2015). Wnt/Notum spatial feedback inhibition controls neoblast differentiation to regulate reversible growth of the planarian brain. *Development (Cambridge, England)* 142, 4217–4229.
- Kato, K., Orii, H., Watanabe, K., and Agata, K. (1999). The role of dorsoventral interaction in the onset of planarian regeneration. *Development* 126, 1031–1040.

- King, R.S., and Newmark, P.A. (2013). In situ hybridization protocol for enhanced detection of gene expression in the planarian *iSchmidtea mediterranea*. *BMC Developmental Biology* 13, 8.
- Lapan, S.W., and Reddien, P.W. (2011). *idlx/i* and *isp6-9/i* Control Optic Cup Regeneration in a Prototypic Eye. *PLoS Genet* 7, e1002226.
- Lapan, S.W., and Reddien, P.W. (2012). Transcriptome Analysis of the Planarian Eye Identifies *iovo/i* as a Specific Regulator of Eye Regeneration. *Cell Reports* 2, 1–14.
- Molina, M.D., Saló, E., and Cebrià, F. (2007). The BMP pathway is essential for re-specification and maintenance of the dorsoventral axis in regenerating and intact planarians. *Developmental Biology* 311, 79–94.
- Newmark, P.A., and Sanchez Alvarado, A. (2000). Bromodeoxyuridine Specifically Labels the Regenerative Stem Cells of Planarians. *Developmental Biology* 220, 142–153.
- Orii, H., and Watanabe, K. (2007). Bone morphogenetic protein is required for dorso-ventral patterning in the planarian *Dugesia japonica*. *Development, Growth & Differentiation* 49, 345–349.
- Pearson, B.J., Eisenhoffer, G.T., Gurley, K.A., Rink, J.C., Miller, D.E., and Sánchez Alvarado, A. (2009). Formaldehyde-based whole-mount in situ hybridization method for planarians. *Dev. Dyn.* 238, 443–450.
- Petersen, C.P., and Reddien, P.W. (2011). Polarized *notum* Activation at Wounds Inhibits Wnt Function to Promote Planarian Head Regeneration. *Science* 332, 852–855.
- Reddien, P.W. (2005). SMEDWI-2 Is a PIWI-Like Protein That Regulates Planarian Stem Cells. *Science* 310, 1327–1330.
- Reddien, P.W. (2011). Constitutive gene expression and the specification of tissue identity in adult planarian biology. *Trends in Genetics* 27, 277–285.
- Reddien, P.W., and Sánchez Alvarado, A. (2004). Fundamentals of Planarian Regeneration. *Annu. Rev. Cell Dev. Biol.* 20, 725–757.
- Reddien, P.W., Bermange, A.L., Kicza, A.M., and Sánchez Alvarado, A. (2007). BMP signaling regulates the dorsal planarian midline and is needed for asymmetric regeneration. *Development (Cambridge, England)* 134, 4043–4051.
- Roberts-Galbraith, R.H.R., and Newmark, P.A.P. (2013). Follistatin antagonizes Activin signaling and acts with Notum to direct planarian head regeneration. *Proc Natl Acad Sci U S A* 110, 1363–1368.
- Rouhana, L., Weiss, J.A., Forsthoefel, D.J., Lee, H., King, R.S., Inoue, T., Shibata, N., Agata, K., and Newmark, P.A. (2013). RNA interference by feeding in vitro synthesized double-stranded RNA to planarians: methodology and dynamics. *Developmental Dynamics : an Official Publication of the American Association of Anatomists* 242, 1–43.

- Santos, F.V. (1931). Studies on transplantation in planaria. *Physiological Zoology*.
- Santos, F.V. (1929). Studies on transplantation in planaria. *Biological Bulletin* 57, 188–197.
- Sánchez Alvarado, A., Newmark, P.A., Robb, S.M., and Juste, R. (2002). The *Schmidtea mediterranea* database as a molecular resource for studying platyhelminthes, stem cells and regeneration. *Development (Cambridge, England)* 129, 5659–5665.
- Scimone, M.L., Lapan, S.W., and Reddien, P.W. (2014). A *forkhead* Transcription Factor Is Wound-Induced at the Planarian Midline and Required for Anterior Pole Regeneration. *PLoS Genet* 10, e1003999.
- Spemann, H., and Mangold, H. (1924). Über Induktion von Embryonalanlagen durch Implantation artfremder Organisatoren. *Archiv Fur Entwicklungsmechanik Der Organismen* 100, 599–638.
- Sugino, H. (1937). Transplantation experiments in *Planaria gonocephala*. *Jour. Zool* 7, 373–439.
- Tazaki, A., Kato, K., Orii, H., Agata, K., and Watanabe, K. (2002). The body margin of the planarian *Dugesia japonica* : characterization by the expression of an intermediate filament gene. *Dev Genes Evol* 212, 365–373.
- van Wolfswinkel, J.C., Wagner, D.E., and Reddien, P.W. (2014). Single-Cell Analysis Reveals Functionally Distinct Classes within the Planarian Stem Cell Compartment. *Cell Stem Cell* 15, 1–14.
- Vásquez-Doorman, C., and Petersen, C.P. (2014). *zic-1* Expression in Planarian Neoblasts after Injury Controls Anterior Pole Regeneration. *PLoS Genet* 10, e1004452.
- Vogg, M.C., Owlarn, S., Pérez Rico, Y.A., Xie, J., Suzuki, Y., Gentile, L., Wu, W., and Bartscherer, K. (2014). Stem cell-dependent formation of a functional anterior regeneration pole in planarians requires *Zic* and *Forkhead* transcription factors. *Developmental Biology* 390, 136–148.
- Wagner, D.E., Wang, I.E., and Reddien, P.W. (2011). Clonogenic Neoblasts Are Pluripotent Adult Stem Cells That Underlie Planarian Regeneration. *Science* 332, 811–816.



## **CHAPTER 3**

### **Nuclear receptor NR4A patterns the ends of the planarian anterior-posterior axis**

Dayan J. Li, Peter W. Reddien



## Abstract

Positional information is fundamental to adult metazoan regeneration and homeostasis. The mechanisms by which pattern is established and maintained in adult tissues, however, are poorly understood. In planarians, signaling factors produced by muscle cells help generate body-wide positional identity (Witchley et al., 2013). At the ends of the planarian anterior-posterior (AP) axis, positional identity is determined by the anterior and posterior poles (Adell et al., 2009; Gurley et al., 2010; Petersen and Reddien, 2008; 2009; 2011; Reddien, 2011). Regarded as putative adult organizers, planarian poles are defined by the expression of genes important for head and tail patterning (Adell et al., 2009; Currie and Pearson, 2013; Gaviño et al., 2013; Gurley et al., 2010; Hayashi et al., 2011; März et al., 2013; Petersen and Reddien, 2008; 2009; 2011; Roberts-Galbraith and Newmark, 2013; Scimone et al., 2014; Vásquez-Doorman and Petersen, 2014; Vogg et al., 2014). Using tissue fragment and single-cell RNA sequencing, we comprehensively identified the anterior and posterior pole transcriptomes and identified new pole-expressed genes encoding predicted transcription factors, cell surface receptors, and a secreted protein. One of these genes, *nr4A*, was required for maintaining the localization of both the anterior and posterior poles to the extreme ends of the primary (AP) body axis. *nr4A* encodes a nuclear receptor and is expressed predominantly in planarian muscle. Consistent with its activity in the muscle, *nr4A* regulates the expression of multiple muscle markers and patterning genes that have regionalized expression domains in the head and the tail. Upon *nr4A* inhibition, head and tail-restricted gene expression domains in muscle shift away from head and tail tips towards the midbody. This shift is followed by progressively posterior ectopic formation of anterior differentiated cell types in the head and progressively anterior ectopic formation of

posterior differentiated cell types in the tail. We propose that *nr4A* promotes pattern at the extreme anterior and posterior ends of the planarian body through restriction of the expression domains of patterning molecules in body-wall muscle to the tips of the AP axis.

## Introduction

Metazoans display a staggering diversity of developmental modes and adult forms. Processes that govern the generation of form, collectively known as patterning, act to precisely modulate cell number, location, and identity to produce distinct body shapes and tissue organizations. How activity at the cellular level translates into pattern at the morphological level is a question of active investigation.

The challenges of tissue patterning are prominent in regenerative organisms, which must faithfully and consistently replace and re-pattern tissues after a multitude of injuries. In addition, many regenerative organisms must maintain correct body pattern during the course of tissue turnover. Planarians are freshwater flatworms capable of remarkable feats of whole-body regeneration and offer as a model system the opportunity to generate important insights into the molecular mechanisms of patterning.

In planarians, patterning has been most extensively studied along the anterior-posterior (AP) axis spanning from the head (anterior) to the tail (posterior). RNA interference approaches have identified evolutionarily conserved pathways that pattern the planarian AP axis (Adell et al., 2010; Forsthoefel and Newmark, 2009; Reddien, 2011). Notably, Wnt/ $\beta$ -catenin signaling regulates the head-versus-tail regeneration choice made at transverse amputation planes and

maintain the polarity of the AP axis during homeostatic tissue turnover (Gurley et al., 2008; Iglesias et al., 2008; Petersen and Reddien, 2008). Genes encoding several ligands and cell surface receptors of the Wnt and FGFRL pathways are expressed in specific domains along the AP axis (Gurley et al., 2010; Reddien, 2011). Inhibition of many of these genes, such as *wnt1* and *ndk* (an *FGFRL* gene), resulted in tail and head patterning defects (Adell et al., 2009; Cebrià et al., 2002; Gurley et al., 2010; Petersen and Reddien, 2009). In addition, cooperation between Wnt and FGFRL pathways maintains AP axial identity. Inhibition of *wntP-2* and another *FGFRL* gene *ndl-3* led to the formation of ectopic mouths and pharynges in the trunk, and inhibition of *fz5/8-4*, *wntA*, and *ndk* resulted in posterior ectopic eyes in the head (Lander and Petersen, 2016; Scimone et al., 2016). These genes, with constitutive regionalized expression and a role in patterning, are called position control genes, or PCGs (Reddien, 2011). All of these PCGs are predominantly expressed in the planarian body-wall muscle (Scimone et al., 2016; Witchley et al., 2013). The widespread presence of PCGs across the planarian body plan leads to a model whereby the planarian muscle serves as a source of positional information that patterns surrounding tissues, for instance by influencing the localization and/or specification of resident stem cells called neoblasts (Reddien, 2011; Witchley et al., 2013; Wurtzel et al., 2017).

A few of the PCGs are expressed at the opposing ends of the AP axis, defining regions called the anterior and posterior poles that function as putative organizers in planarian head and tail patterning, respectively (Adell et al., 2009; Gurley et al., 2010; Petersen and Reddien, 2008; 2009; 2011; Reddien, 2011). These adult organizers bear molecular and functional similarities to the organizers governing axial patterning during vertebrate embryogenesis, the classic example being the Spemann-Mangold organizer in amphibians (Lemaire and Kodjabachian, 1996; Spemann and Mangold, 1924). In planarians, the anterior pole is located at the midline of the

head tip and is specified by the expression of transcription factor genes *foxD* and *zic1* (Scimone et al., 2014; Vásquez-Doorman and Petersen, 2014; Vogg et al., 2014). Anterior pole cells also express *islet1* (Hayashi et al., 2011; März et al., 2013), *pitx* (Currie and Pearson, 2013; März et al., 2013), *notum* (Petersen and Reddien, 2011), and *follistatin* (Gaviño et al., 2013; Roberts-Galbraith and Newmark, 2013), the latter two encoding Wnt and TGF- $\beta$  inhibitors, respectively. Inhibition of each these genes resulted in head regeneration defects, including stunted heads with decreased or absent expression of anterior PCGs and midline collapse involving cyclopia and fused brain lobes (Currie and Pearson, 2013; Gaviño et al., 2013; Hayashi et al., 2011; März et al., 2013; Roberts-Galbraith and Newmark, 2013; Scimone et al., 2014; Vásquez-Doorman and Petersen, 2014; Vogg et al., 2014). Consistent with the organizing activity of the anterior pole, recent transplantation experiments demonstrated that a graft of the head tip containing the anterior pole is capable of inducing a correctly patterned head outgrowth (with a midline and a pair of eyes) in the tail region (Oderberg et al., 2017). The posterior pole, located at the midline of the tail tip, is defined by the expression of *islet1* (Hayashi et al., 2011; März et al., 2013), *pitx* (Currie and Pearson, 2013; März et al., 2013), *wnt11-2* (Adell et al., 2009; Gurley et al., 2010), and *wnt1* (Petersen and Reddien, 2008; 2009). RNAi of each of these posterior pole genes also resulted in stunted tails and midline collapse involving fused ventral nerve cords (Adell et al., 2009; Currie and Pearson, 2013; Gurley et al., 2010; Hayashi et al., 2011; März et al., 2013; Petersen and Reddien, 2008; 2009).

Given that the planarian poles function as adult organizers, their comprehensive genetic characterization will help elucidate the various roles they may play in patterning the head and the tail. To accomplish this, we determined the transcriptomes of the planarian anterior and posterior poles via tissue fragment and single-cell RNA sequencing. We identified a host of new genes

expressed at the poles, greatly expanding the current known repertoire of genes with enriched expression at the ends of the planarian AP axis. We uncovered a novel and intriguing patterning role for one of these genes, which encodes a planarian ortholog of the NR4A nuclear receptor family, and is expressed predominantly in body-wall muscle. Inhibition of *nr4A* by RNA interference (RNAi) resulted in patterning abnormalities in both the head and the tail. These included ectopic posterior eyes and other neuron classes in the head and ectopic epidermal and secretory cell presence in the head and the tail. Differentiated tissue changes were accompanied by changes in the domains of expression of several PCGs, including the pole markers *notum* and *wnt1*. *nr4A* represents a new planarian patterning gene encoding a member of the nuclear receptor family of transcription factors that helps regulate tissue pattern at both extreme ends of the AP body axis.

## Results

### RNA sequencing identifies new genes expressed at the anterior and posterior poles

To comprehensively identify genes expressed in the planarian poles, we performed RNA sequencing of anterior and posterior poles of both uninjured animals and regenerating trunks 72 hours post amputation (hpa). For the anterior pole in uninjured animals, we cut head tips into three fragments that were isolated for RNA sequencing - a midline piece containing the pole and two flanking pieces to use as controls (Fig. 1A). Similar cuts were made in the anterior blastema (an unpigmented outgrowth of differentiating tissue) of 72hpa trunks (Fig. 1A). Differential gene expression analysis identified 203 genes with significantly higher ( $p_{\text{adj}} < 0.05$ ) expression in

pole-containing pieces compared to flanking pieces from intact animals. In the anterior blastema, 86 genes had pole-enriched expression ( $p_{\text{adj}} < 0.05$ ). Among the 51 genes with enriched expression in the poles of both uninjured and regenerating animals were previously published anterior pole genes *foxD*, *notum*, *zic1*, and *follistatin* (Fig. 1A, Table S1 and S2).

To obtain the posterior pole transcriptome, we cut pole-containing fragments from the tail tip of uninjured animals and from the posterior blastema of 72hpa trunks (Fig. S1A). We isolated single cells by FACS and used the expression of the posterior pole marker *wnt1* and of the muscle marker *collagen* to identify pole cells (*wnt1*<sup>+</sup>; *collagen*<sup>+</sup>) and non-pole muscle cells (*wnt1*<sup>-</sup>; *collagen*<sup>+</sup>) by qRT-PCR (Fig. S1A). In total, we screened cDNA from close to 1000 total cells and identified 11 posterior pole cells (6 from uninjured animals and 5 from blastemas) and 90 non-pole muscle cells (43 from uninjured animals and 47 from blastemas) as controls (Fig. S1B). Using Single-Cell Differential Expression (SCDE) analysis (Kharchenko et al., 2014) to compare the single-cell transcriptomes, we identified 198 genes with significantly higher expression ( $p < 0.05$ ) in posterior pole cells compared to non-pole muscle cells (Fig. S1B). Of those, known posterior pole genes *wnt1*, *pitx*, and *islet1* were in the top 16% of genes ranked by enrichment in posterior pole cells (Table S3).

We selected 133 anterior pole candidate genes and 96 posterior pole candidate genes for a whole-mount *in situ* hybridization screen based on their high fold enrichment in pole cells and similarity of their predicted protein products to cell surface receptors, secreted factors, and transcription factors from other organisms. From the screen, we identified 12 new genes expressed in the anterior pole (Fig. 1B) and 10 new genes expressed at the posterior pole (Fig. S1C). These included genes encoding a secreted factor (*kallmann1*), cell surface receptors (*ror1*, *ephr4*, *ephr5*, *pcdh9*, *dcc*, *ddr2*), and transcription factors (*islet2*, *musculin*, *nr4A*) (Fig. 1B and

S1C). Some of these genes, such as *kallmann1*, *ephr5*, and *dd\_20026\_01* were expressed at both anterior and posterior poles (Fig. 1B and S1C). We confirmed the expression of the new anterior pole genes in anterior pole cells via their co-expression with the anterior pole marker *notum* (Fig. 1C). Overall, our pole RNA sequencing approach identified a host of new genes expressed at the anterior and posterior poles, significantly expanding the current repertoire of genes with enriched expression at the extreme ends of the planarian anterior-posterior axis.

**Figure 1**

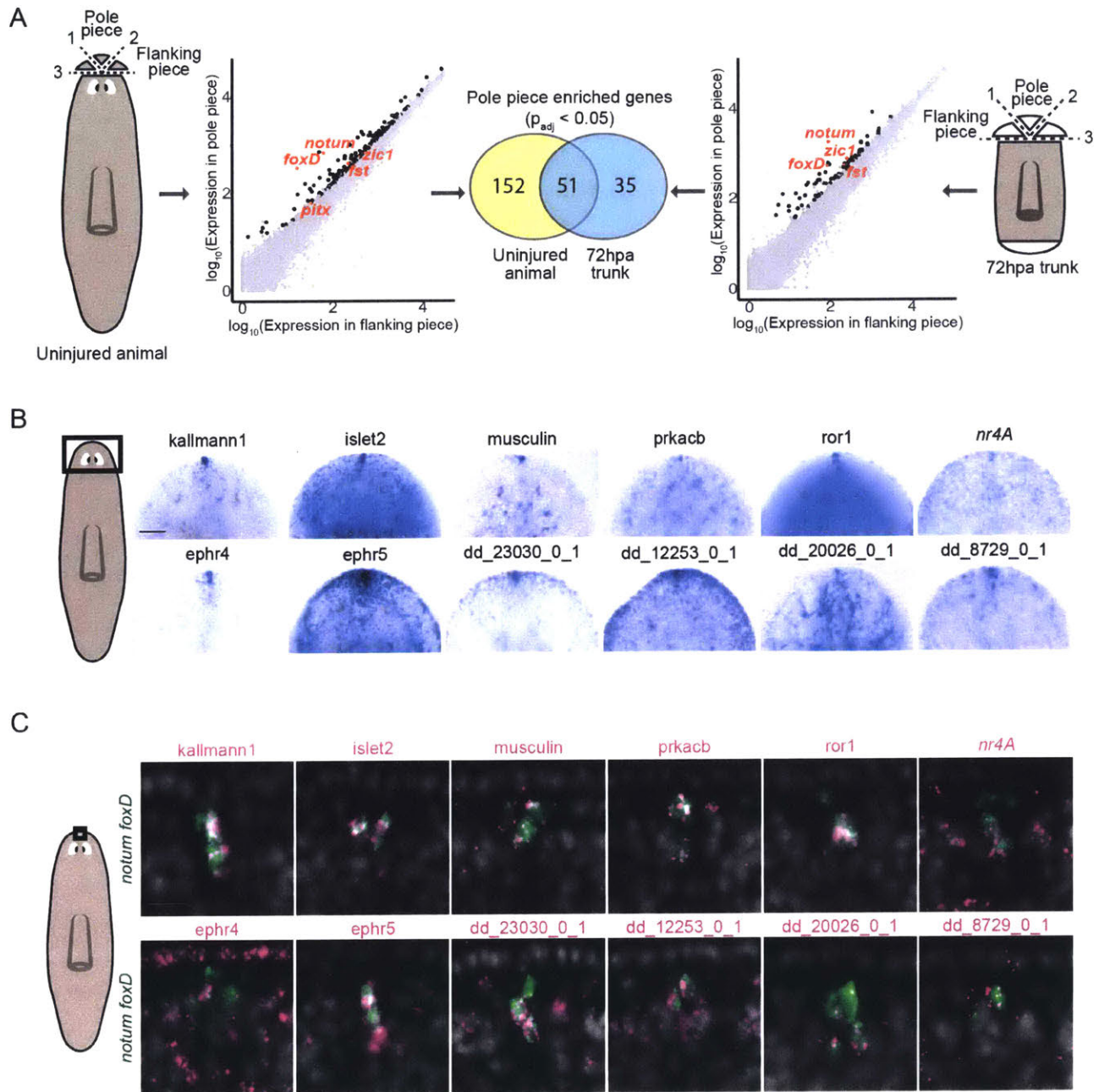
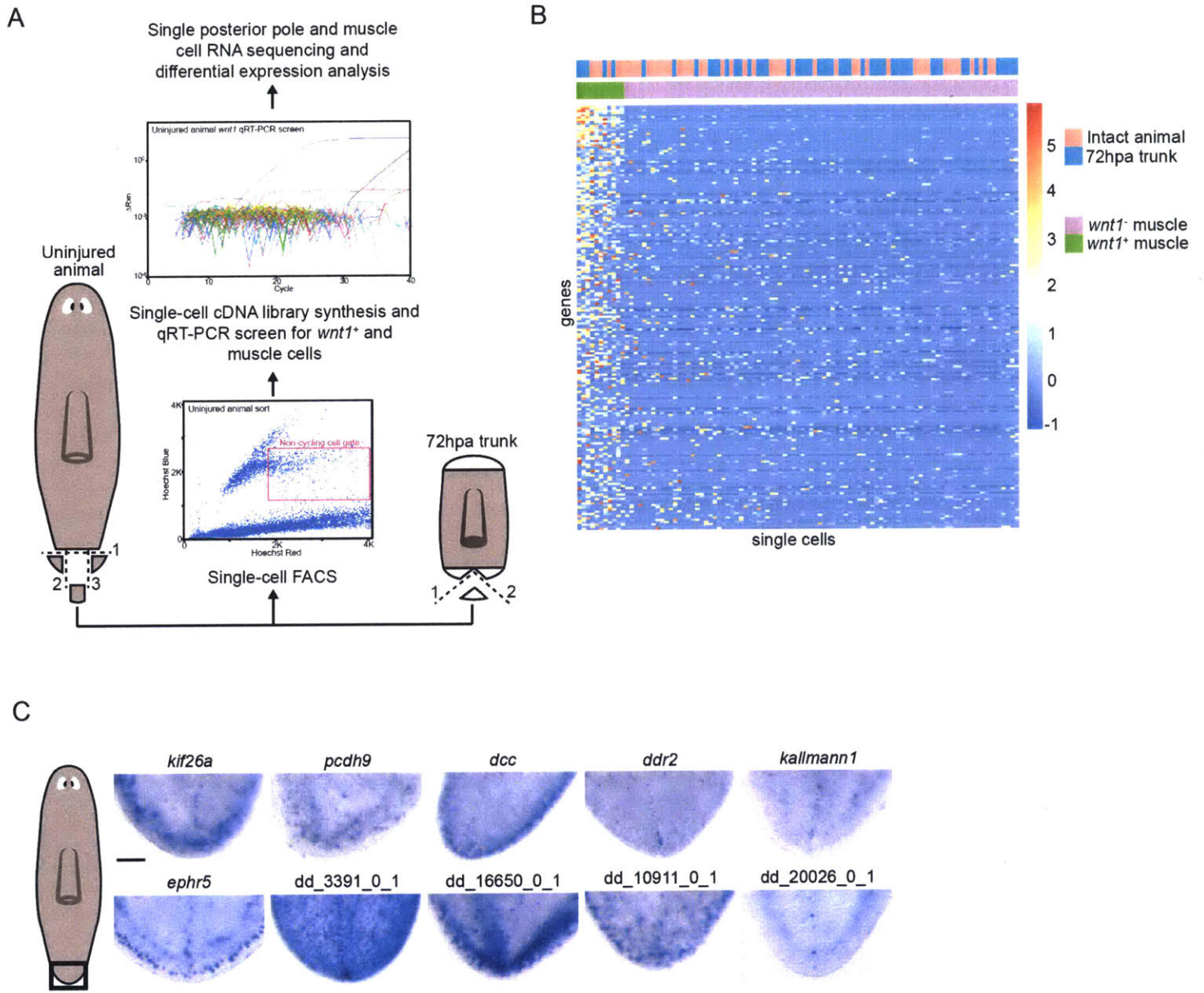


**Figure 1. Bulk RNA sequencing of anterior pole-containing head fragments and anterior pole candidate *in situ* screen.** (A) Anterior pole bulk RNA sequencing approach: Wedge-shaped fragments containing the anterior pole (pole pieces) and adjacent fragments without the pole (flanking pieces) were excised from head tips of intact animals and anterior blastemas of regenerating trunks 72 hours post amputation (cartoons; dotted lines represent cut planes, and dotted line numbers indicate cut sequence). Pole pieces and flanking pieces were separately processed for cDNA library synthesis and RNA sequencing. Scatter plots for intact animal pole and regenerating animal pole data show the normalized transcript counts per gene in pole pieces (y-axis) versus flanking pieces (x-axis). Each data point in the plot represents a gene; black data points represent genes that had enriched expression in pole pieces versus flanking pieces ( $p_{adj} < 0.05$ ); red data points and labels represent the known anterior pole genes. Venn Diagram shows the number of anterior pole-enriched genes in intact animals and regenerating trunks and the number of anterior pole-enriched genes common in both. (B) Head expression of anterior pole candidates from RNA sequencing is shown by whole-mount *in situ* hybridization. Gene names represent best human BLAST; numerical names indicate the transcript number with no human homology. Area imaged is indicated by the box in the cartoon on the left. Scale bar represents 100 $\mu$ m. (C) Co-expression of anterior pole gene candidates with pole markers *notum* and *foxD* is shown by FISH. Pooled *notum* and *foxD* RNA probes are in green; anterior pole candidates in magenta. Area imaged is indicated by the box in the cartoon on the left. Scale bar represents 10 $\mu$ m.

# Supplemental Figure 1



**Supplemental Figure 1. Single-cell RNA sequencing of posterior pole-containing tail fragments and posterior pole candidate *in situ* screen.** (A) Posterior pole single-cell RNA sequencing approach: Posterior pole containing pieces were excised from tail tips of intact animals and posterior blastemas of regenerating trunks 72 hours post amputation (cartoons; dotted lines represent cut planes, and dotted line numbers indicate cut sequence). Excised fragments were then dissociated and single cells were sorted onto 96-well plates via fluorescence-activated cell sorting (FACS). The magenta rectangular box on the FACS plot represents the FACS gate from which differentiated, non-dividing cells were sorted. Individual cells were then used to synthesize single-cell cDNA libraries, which were screened by qRT-PCR for their *wnt1* and *collagen* expression (qRT-PCR plot). Representative FACS and qRT-PCR plots from uninjured animal tail fragments are shown. Cells with *wnt1* expression (11) and cells with *collagen* but no *wnt1* expression (90) were selected for single-cell cDNA library synthesis, sequencing, and differential expression analysis via SCDE (see Methods). (B) Heatmap of all 101 single cells sequenced (columns: 11 *wnt1*<sup>+</sup>;*collagen*<sup>+</sup> posterior pole cells and 90 *wnt1*<sup>-</sup>;*collagen*<sup>+</sup> muscle cells) was generated by clustering by normalized transcript counts of the genes (rows) differentially expressed in posterior pole cells over non-pole muscle cells ( $p < 0.05$ ) (C) WISH of the tail expression of posterior pole candidates from RNA sequencing: Gene names represent best human BLAST; numerical names indicate the transcript number with no human homology. *kallmann1*, *ephr5*, and *dd\_20026\_0\_1* were identified from bulk anterior pole RNA sequencing to also have expression in posterior pole region. Area imaged is indicated by the box in the cartoon on the left. Scale bar represents 50 $\mu$ m.

### ***nr4A* is required for head and tail patterning**

We utilized RNAi to determine the functions of new pole genes and identified a striking phenotype following inhibition of a gene encoding the planarian homolog to the NR4A nuclear receptor protein family, which we have named *nr4A* (Fig. S2). RNAi of *nr4A* resulted in the progressive formation of posterior ectopic eyes in uninjured animals (Fig. 2A). The *nr4A(RNAi)* animals caused the distance between the original eyes and the head tip to progressively decrease, and just posterior to the original eyes, an additional eye pair emerged. Then, as time progressed, the original and second pair of eyes became closer to the head tip and a third pair of eyes posterior to the second eye pair appeared, resulting in an animal with 6 eyes. This is a patterning phenotype not previously described to occur following inhibition of any other planarian gene, suggesting a novel patterning function for *nr4A*. *nr4A(RNAi)* uninjured animals also eventually developed dorsal tissue protrusions at their tail tips, suggesting a tissue organization requirement for this gene might exist in both the head and the tail (Fig. 2A). After transverse amputation of heads and tails, *nr4A(RNAi)* trunk fragments animals were capable of regenerating heads with normal eye number and location and slightly pointed tails (Fig. 2A).

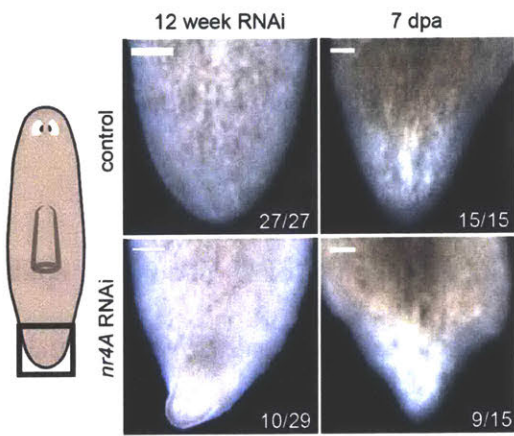
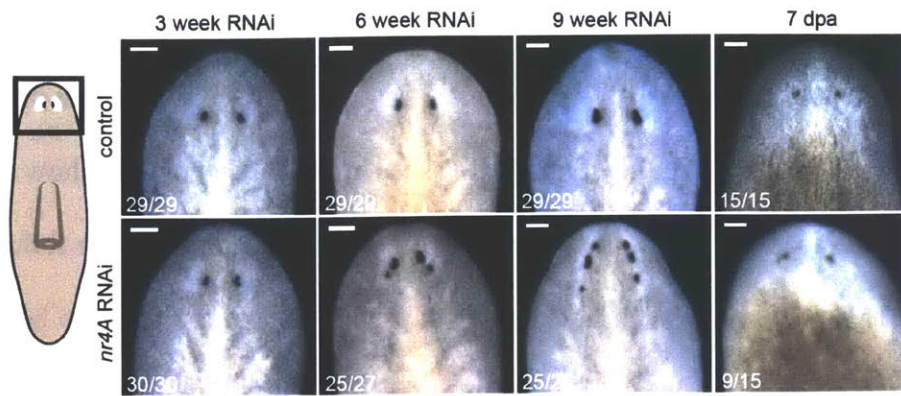
Detailed fluorescence *in situ* hybridization (FISH) analysis of the homeostasis phenotype using differentiated tissue markers revealed patterning abnormalities of multiple differentiated tissues in both the head and the tail. In addition to ectopic eyes, labeled by an RNA probe to *opsin*, the heads of *nr4A(RNAi)* animals developed ectopic internal foci of a class of "DV boundary" epidermal cells normally restricted in their distribution to the animal periphery at the DV-median plane (NB.22.1e<sup>+</sup> and *laminB*<sup>+</sup>) cells (Fig. 2B). These interior DV boundary cells appeared near the animal midline in between the eyes (Fig. 2B). *mag-1* expression marks secretory "marginal adhesive gland" cells that are normally restricted to a prepharyngeal zone

posterior to the eyes and posteriorly from this zone along the body margin. The prepharyngeal zone of *mag-1*<sup>+</sup> cells was expanded in *nr4A(RNAi)* animals (Fig. 2B). FISH with neural markers *chAT* and *A5 neural* - genes expressed in the inverted "U"-shaped cephalic ganglia – show a loss of the head region between the apex of the head and the anterior aspect of the brain following *nr4A* RNAi (Fig. 2B). This phenotype is consistent with the shortening of the distance between the original eyes and the apex of the head. Furthermore, these markers demonstrated that the brain became posteriorly expanded following *nr4A* RNAi. Taken together, these results suggest that *nr4A* inhibition causes a loss of head tip identity, and a progressive more posterior expansion of differentiated tissues.

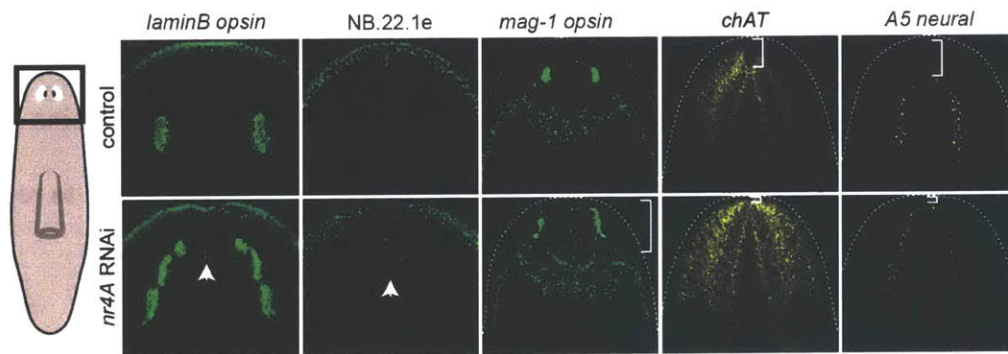
Similar to the changes we observed in the head, ectopic foci of DV boundary epidermal cells (*NB.22.1e*<sup>+</sup> and *laminB*<sup>+</sup>) appeared internally in the tails of *nr4A(RNAi)* animals. The secretory *mag-1*<sup>+</sup> cells normally are restricted to the body margin all around the periphery of tails. Following *nr4A* RNAi ectopic *mag-1*<sup>+</sup> cells appeared internally along the midline of tails (Fig. 2C), resulting in aberrant tail tip identity. The mislocalization of differentiated tissues in RNAi animals indicates that *nr4A* normally restricts tissues to their proper domains at the extremes ends of the AP axis. To our knowledge, this is the first planarian gene found to regulate the homeostatic pattern of differentiated tissues in both the head and the tail.

**Figure 2**

**A**



**B**



**C**

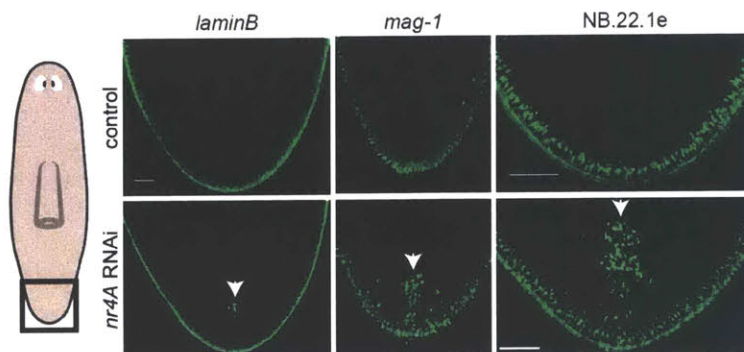
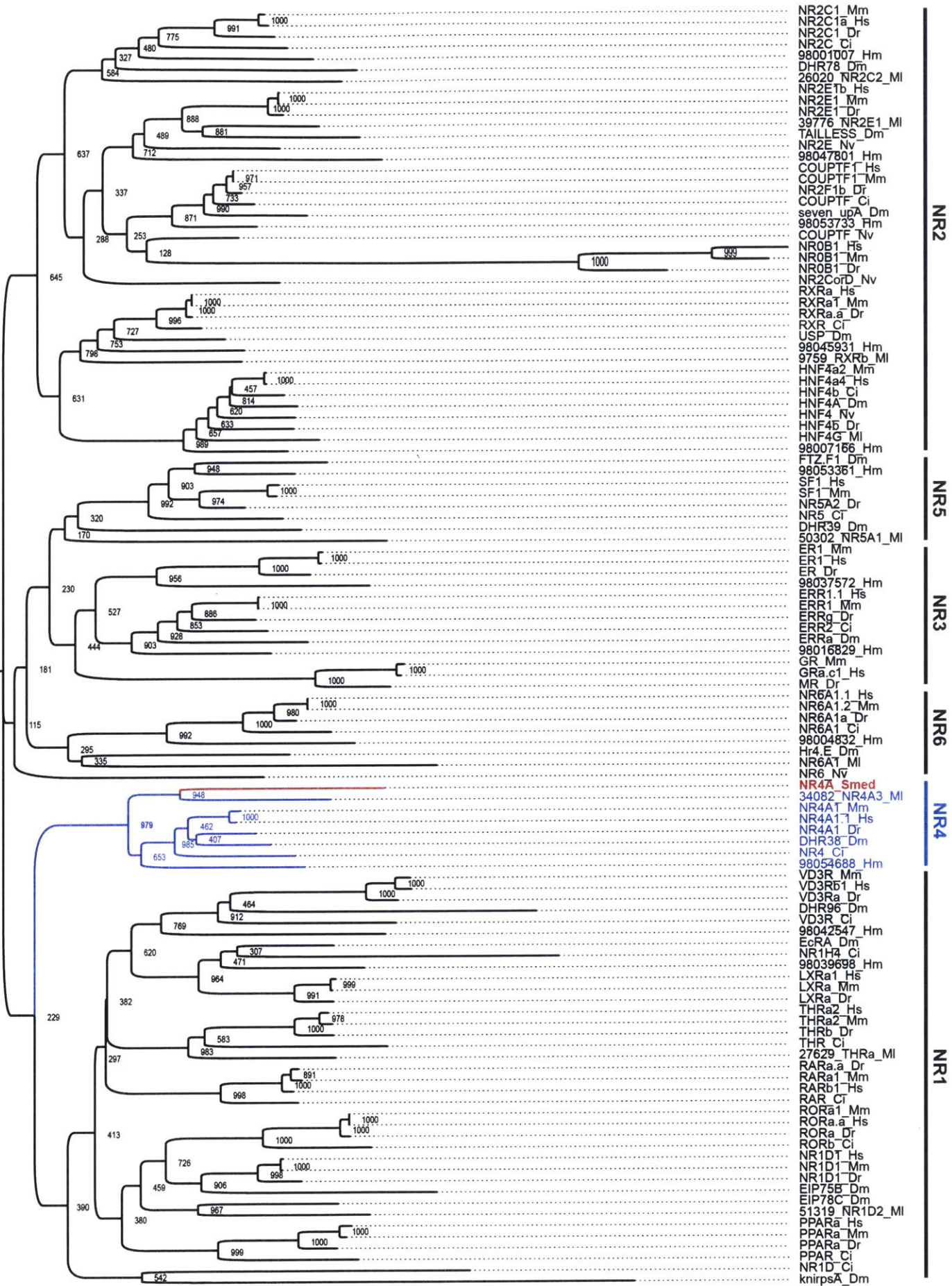


**Figure 2. *nr4A* RNAi leads to head and tail patterning defects.** (A) Live images of animals at different time points during control and *nr4A* RNAi showing progressive development of posterior ectopic eyes and tail knobs in uninjured animals, and complete head and tail regeneration at 7 days post amputation (7 dpa), with slightly pointed tails in regenerating *nr4A(RNAi)* animals. Numbers below the images indicate proportions of observed phenotype over total number of animals. Image scale bars represent 150 $\mu$ m. (B) FISH with differentiated tissue markers showed ectopic marker expression in the heads of *nr4A(RNAi)* animals (arrow head) and loss of head tip identity (bracket). Animals analyzed were from 9 weeks of RNAi. Images are representative of results seen in >4 animals per panel. Markers for photoreceptors (*opsin*), epidermal cells at the dorsal-ventral boundary (*laminB*, *NB.22.1e*), and marginal adhesive gland secretory cells (*mag-1*) are shown in green. Markers for neurons (*chAT*, *A5 neural*, and *PKD2*) are shown in yellow. Area imaged is indicated by the box in the cartoon on the left. Dotted white lines indicate anterior borders of the heads. Scale bars for images with green markers represent 100 $\mu$ m; scale bars for images with yellow marker represent 200 $\mu$ m. (C) FISH with differentiated tissue markers showed ectopic marker expression in the tails of *nr4A(RNAi)* animals (arrow head). Animals analyzed were from 9 weeks of RNAi. Images are representative of results seen in >4 animals per panel. Markers for epidermal cells at the dorsal-ventral boundary (*laminB*, *NB.22.1e*) and marginal adhesive gland secretory cells (*mag-1*) are shown in green. Area imaged is indicated by the box in the cartoon on the left. Scale bars represent 100 $\mu$ m.

# Supplemental Figure 2



**Supplemental Figure 2. Phylogenetic analysis of *Schmidtea mediterranea nr4A*.** Tree showing the protein sequence of the translated *Schmidtea mediterranea nr4A* mRNA (NR4A\_Smed) along with representative protein sequences from each of the six nuclear receptor subfamilies annotated on the right from *Homo sapiens* (Hs), *Mus musculus* (Mm), *Danio rerio* (Dr), *Ciona intestinalis* (Ci), *Drosophila melanogaster* (Dm), *Macrostomum lignano* (Ml), and *Nematostella vectensis* (Nv). Protein sequences were aligned by their DNA-binding and ligand-binding domains via Neighbor-Joining Method. Numbers at the nodes denote the number of trees consistent with branch placements at those nodes from 1000 bootstrap replicates. The blue-colored clade denotes the NR4A subfamily, with the red-colored branch denoting the *Schmidtea mediterranea* NR4A.

### ***nr4A* is expressed in muscle and maintains head muscle fiber integrity**

Planarian muscle cells, marked by *collagen* expression, have a widespread role in regionally expressing genes that regulate body-wide patterning (Witchley et al., 2013). Consistent with its patterning function, we found that *nr4A* was predominantly expressed in the planarian muscle in both intact animals and regenerating blastemas (Fig. 3). Although its expression was enriched in the head, *nr4A* is also expressed broadly throughout the body, including in posterior pole cells as well as the anterior pole (Fig. 1C, 3A, and S3). Furthermore, mapping *nr4A* expression onto single-cell expression data clustered by tissue types (Wurtzel et al., 2015) showed that *nr4A* is most highly expressed in muscle cells, with some expression in neoblasts (Fig. 3B). In regenerating animals, *nr4A* expression is observed in the regenerating blastemas as early as 48 hpa and increases in levels at 72 hpa (Fig. 3C). At 7 days of regeneration, its enriched expression in the head and broad expression in the tail becomes similar to that in uninjured animals (Fig. 3C). The dynamics of *nr4A* expression throughout regeneration is similar to those of many patterning genes (Wenemoser et al., 2012; Wurtzel et al., 2015), and is consistent with its role in head and tail patterning.

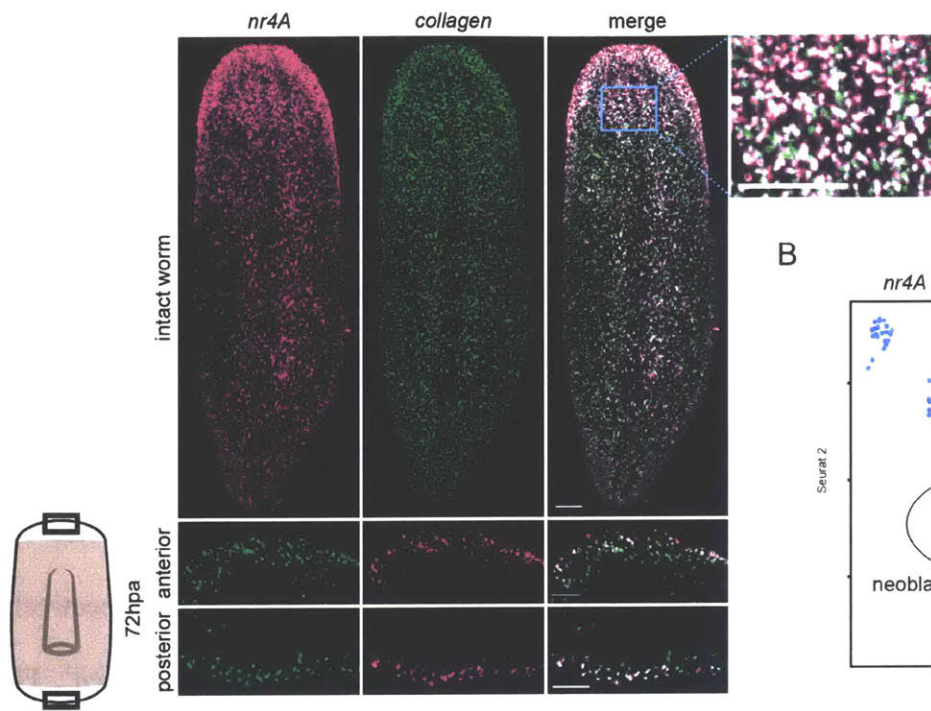
Because *nr4A* encodes a transcription factor with enriched expression in muscle, we examined the appearance of muscle fibers in *nr4A(RNAi)* animals using the 6G10 muscle antibody (Ross et al., 2015) that labels the various circular, diagonal, longitudinal, and dorsal-ventral planarian body-wall muscle fibers. Strikingly, we observed a loss of body-wall muscle fibers on both the dorsal and ventral sides of the head in *nr4A(RNAi)* animals compared to control animals (Fig. 4A). Longitudinal, circular, and diagonal muscle fibers were severely reduced at head tips (Fig. 4A). We did not however observe similar muscle fiber disruptions in the tails of *nr4A(RNAi)* animals (Fig. 4B). The loss of muscle fibers at the head tips of

*nr4A(RNAi)* animals was accompanied by a reduction in the number of *collagen*<sup>+</sup> muscle cells (Fig. 4C). *collagen*<sup>+</sup> muscle cell number in the tail tips was not affected (Fig. 4D). The loss of muscle fibers and reduction in *collagen*<sup>+</sup> cells are events that happen during the late stages of the phenotype, as similar analyses of *nr4A(RNAi)* animals at an earlier time point (4 weeks of RNAi) showed no changes in muscle fibers or *collagen*<sup>+</sup> cell numbers compared to control animals (Fig. S4A, B).

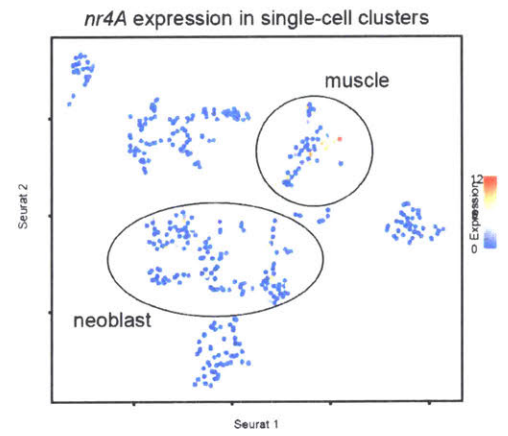
To determine whether the decrease in the number of *collagen*<sup>+</sup> cells at the head tips resulted from a decrease in muscle cell number, we assayed apoptosis and new muscle cell production using a TUNEL assay (Fig. S4C) and EdU incorporation (Fig. S4D), respectively. Quantification of apoptotic cells (Fig. S4C) and new muscle cells (EdU<sup>+</sup> and *collagen*<sup>+</sup>, Fig. S4D) in the head showed no dramatic differences between control and *nr4A(RNAi)* animals, suggesting that the loss of muscle fiber number is a gradual process impacted by subtle changes in the rate muscle cell turnover. While RNAi of genes like *myoD* and *tropomyosin* important in broad muscle function resulted in regeneration and body-wide morphology defects (Reddien et al., 2005), RNAi of *nr4A* led to muscle loss specifically at the head tip. This supports the observation that rather than being required for general muscle cell function, *nr4A* plays a specific role at the ends of the AP axis, where it acts to pattern the head and the tail. The specific and widespread expression of *nr4A* in planarian muscle, along with its importance in long-term head tip muscle fiber integrity, led us to hypothesize that the patterning defects observed in *nr4A(RNAi)* animals are caused by impairment in muscle cell gene expression or function at the ends of the AP axis, such as in the maintenance of regionalized expression of important patterning genes.

Figure 3

A



B



C

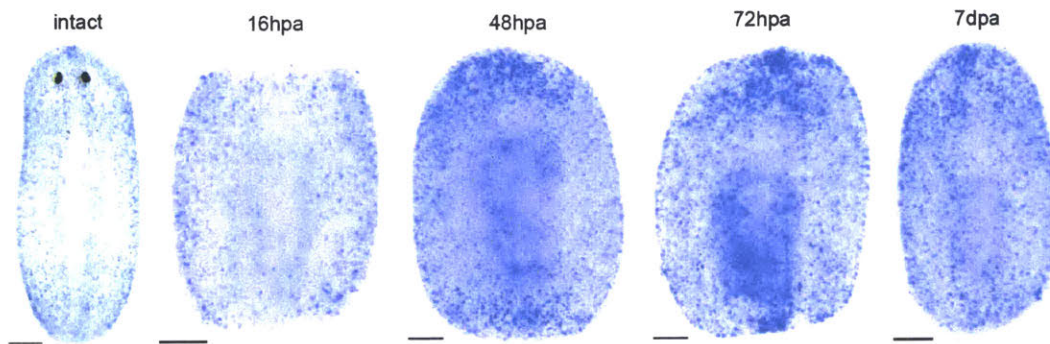
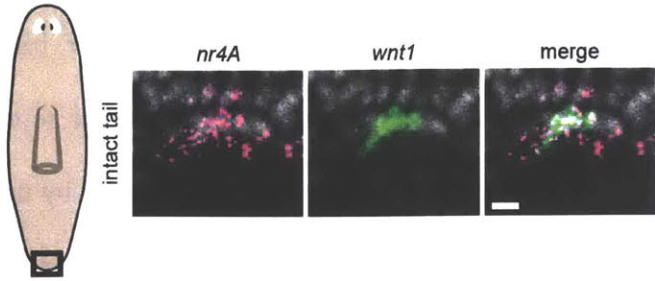


**Figure 3. Planarian *nr4A* expression.** (A) FISH using RNA probes for *nr4A* (magenta) and *collagen* (green) in intact animals (top panel) and in anterior and posterior blastemas of regenerating trunks 72 hours post amputation (72hpa, bottom panel). Images are representative of results seen in >4 animals. Areas imaged in regenerating animals are indicated by the boxes in the cartoon on the left. Scale bar on intact animal image represents 100 $\mu$ m; scale bars on regenerating blastema images represent 50 $\mu$ m. (B) Expression of *nr4A* mapped on the t-SNE plot of cell type clusters generated by Seurat showed that *nr4A* is highly expressed in muscle cells, with some expression in neoblasts. (C) WISH of *nr4A* probe during regeneration and in intact animal showed *nr4A* expression to be absent during the wound-response phase (16 hours post amputation – 16hpa) and increasingly concentrated at the anterior and posterior poles during regeneration (48 and 72 hpa). In regenerated heads (7 days post amputation – 7dpa, and intact), *nr4A* expression was also higher in the head tips at the anterior pole.

### Supplemental Figure 3



**Supplemental Figure 3. *nr4A* is expressed in the posterior pole.** FISH showed the expression of *nr4A* in the posterior pole via the co-localization of the *nr4A* probe (magenta) and the *wnt1* probe (green) in cells at the tail tip of intact animals (area imaged indicated by box in the cartoon). Scale bar represents 10 $\mu$ m.



Figure 4

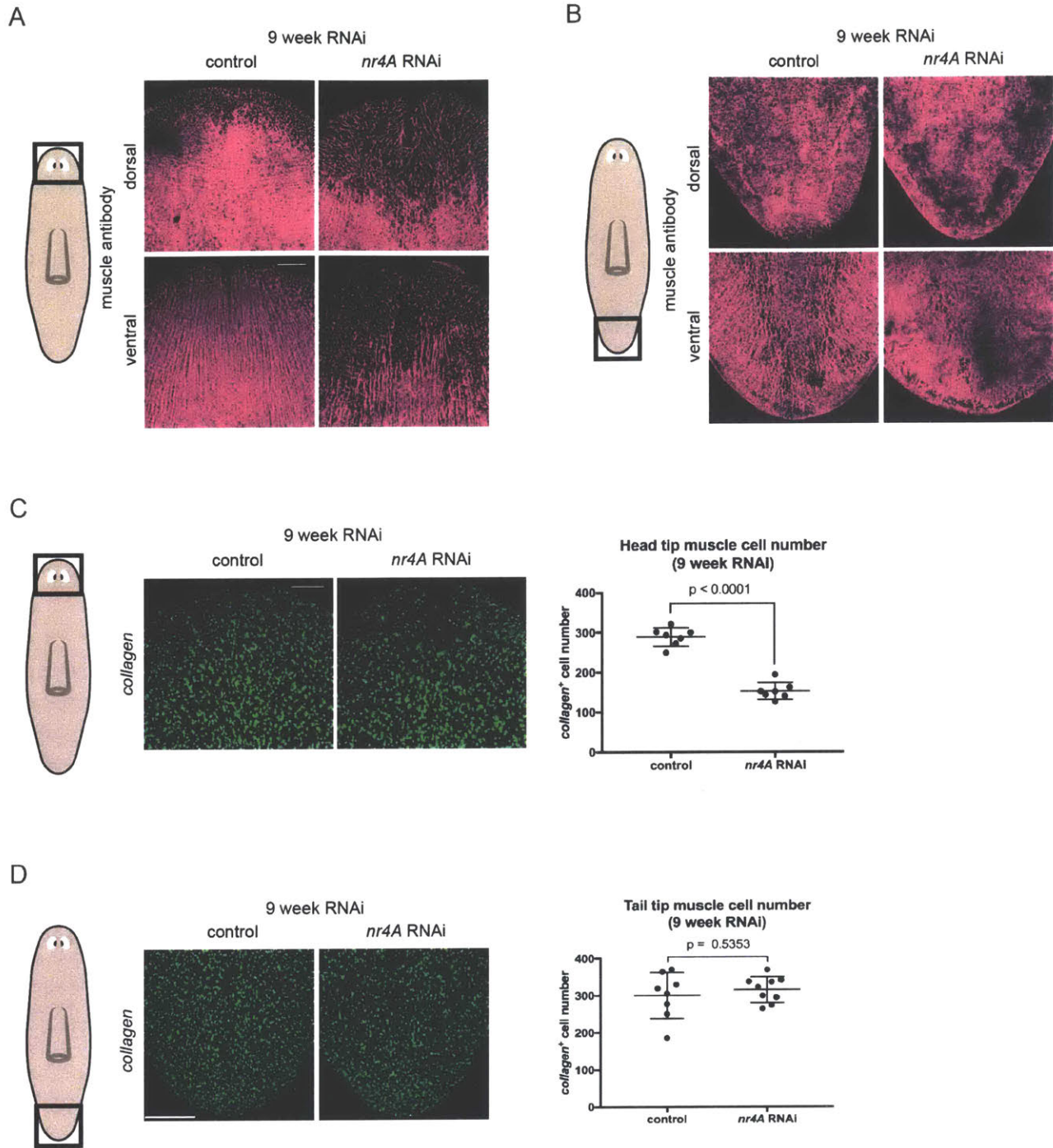


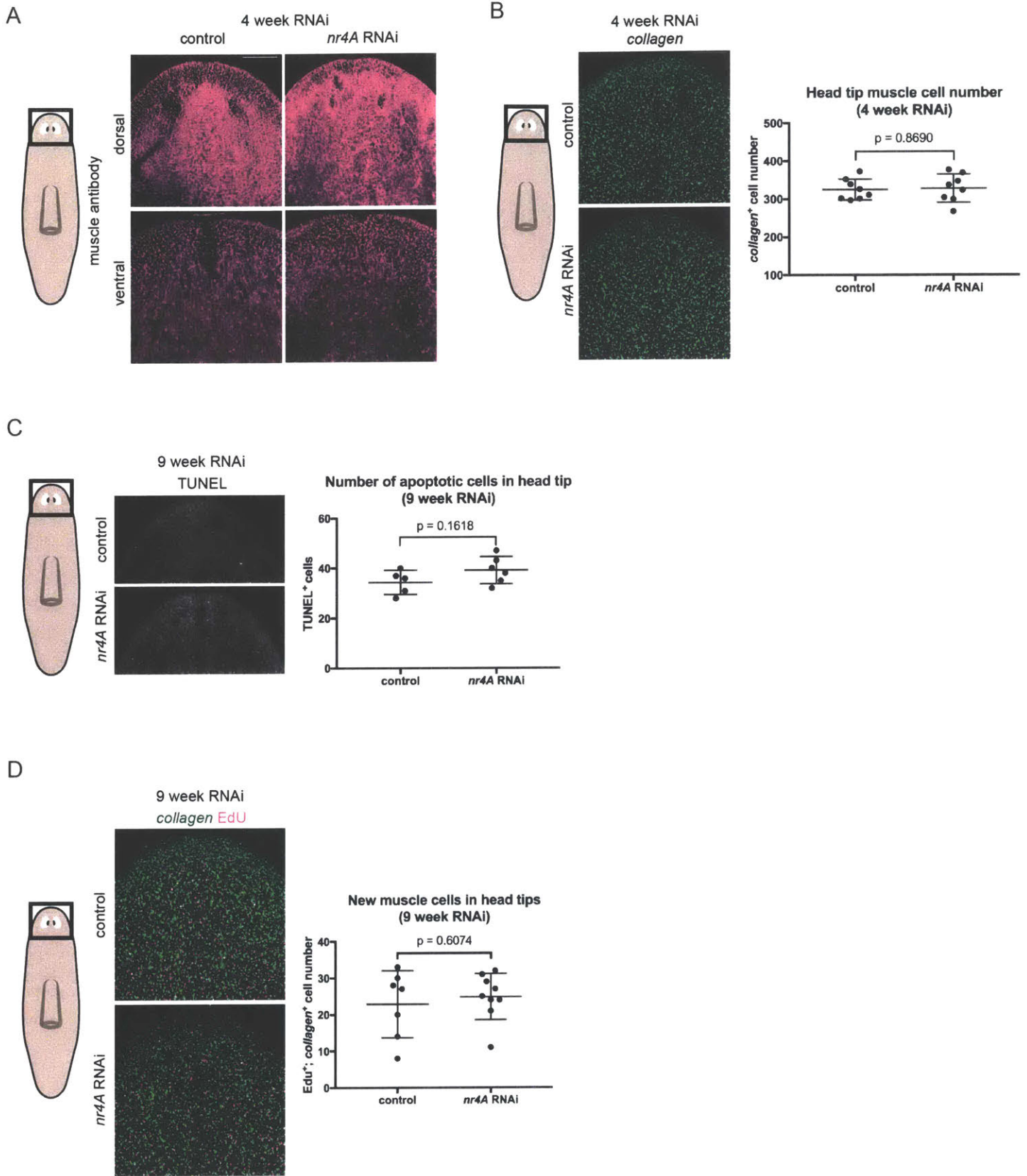
**Figure 4. *nr4A* maintains *collagen*<sup>+</sup> cell number and muscle fiber integrity at the head tip.**

(A) Muscle antibody (6G10) fluorescence stain showed loss of muscle fibers on both the dorsal and ventral sides of the head tips of *nr4A(RNAi)* animals compared to muscle fibers in the heads of control animals. All animals were analyzed at 9 weeks of RNAi. Images are representative of results seen in >4 animals per panel. Area imaged is indicated by the box in the cartoon on the left. Scale bars represent 200 $\mu$ m. (B) Muscle antibody (6G10) fluorescence stains showed no significant changes in muscle fibers on both the dorsal and ventral sides of the tail tips of *nr4A(RNAi)* animals compared to muscle fibers in the tails of control animals. All animals were analyzed at 9 weeks of RNAi. Images are representative of results seen in >4 animals per panel. Area imaged is indicated by the box in the cartoon on the left. Scale bars represent 150 $\mu$ m. (C) Muscle cells at the head tips stained by muscle marker *collagen* were decreased in number in *nr4A(RNAi)* animals compared to control animals. Plot shows quantification of *collagen*<sup>+</sup> muscle cell number in a 150 $\mu$ m wide by 100 $\mu$ m high rectangular area centered around the midline of the tip of the heads in control and *nr4A(RNAi)* animals. Quantification showed a significant decrease in muscle cell number at the head tips of *nr4A(RNAi)* animals at 9 weeks of RNAi. All animals were analyzed at 9 weeks of RNAi. Images are representative of results seen in >4 animals per panel. Area imaged is indicated by the box in the cartoon on the left. Scale bars represent 200 $\mu$ m. (D) Muscle cells at the tail tips stained by muscle marker *collagen* were comparable in number in *nr4A(RNAi)* animals compared to controls. Plot shows quantification of *collagen*<sup>+</sup> muscle cell number in a 150 $\mu$ m wide by 100 $\mu$ m high rectangular area centered around the midline of the tip of the tails in control and *nr4A(RNAi)* animals. Quantification did not show a significant difference in tail tip muscle cell number between control and *nr4A(RNAi)* animals. All animals

were analyzed at 9 weeks of RNAi. Images are representative of results seen in >4 animals per panel. Area imaged is indicated by the box in the cartoon on the left. Scale bars represent 150 $\mu$ m.



# Supplemental Figure 4



**Supplemental Figure 4. *nr4A* RNAi did not lead to changes in muscle at early time points or in apoptosis and new muscle cell specification at the head tip.** (A) Muscle antibody (6G10) fluorescence stain did not show a loss of muscle fibers at the head tips of 4 week *nr4A(RNAi)* animals compared to muscle fibers in control heads. Images are representative of results seen in >4 animals per panel. Area imaged is indicated by the box in the cartoon on the left. Scale bars represent 200µm. (B) Muscle cells at the head tips stained by muscle marker *collagen* were comparable in number in 4 week *nr4A(RNAi)* animals compared to control animals. Plot shows quantification of *collagen*<sup>+</sup> muscle cell number in a 150µm wide by 100µm high rectangular area centered around the midline of the tip of the heads in control and *nr4A(RNAi)* animals. Quantification did not show a significant difference in head tip muscle cell number between control and *nr4A(RNAi)* animals at 4 weeks of RNAi. Images are representative of results seen in >4 animals per panel. Area imaged is indicated by the box in the cartoon on the left. Scale bars represent 200µm. (C) TUNEL assay showed that *nr4A* RNAi did not lead to changes in the number of apoptotic cells (yellow) at the head tip between control and *nr4A(RNAi)* animals. TUNEL-positive cell quantification at the head tip showed no statistically significant difference between control and *nr4A(RNAi)* animals. The number of TUNEL-positive cells was counted in a condition-blind fashion within a 550µm x 550µm region centered around the midline of head tips. TUNEL assay was performed on animals at 9 weeks of RNAi. Images are representative of results seen in >4 animals per panel. Area imaged is indicated by the box in the cartoon on the left. Scale bars represent 100µm. (D) EdU incorporation assay showed no difference in new muscle cell production – EdU<sup>+</sup> (magenta) and *collagen*<sup>+</sup> (green) co-localization – in the heads of control and *nr4A(RNAi)* animals. Quantification of EdU<sup>+</sup> and *collagen*<sup>+</sup> cells revealed no statistically significant difference between control and *nr4A(RNAi)* animals. The number of

double EdU<sup>+</sup> and collagen<sup>+</sup> cells were counted in a condition-blind fashion within a 640µm x 640µm region centered around the midline of head tips. For the EdU incorporation, animals were fed once with EdU mixed with liver and fixed 8 days after. EdU incorporation assay was performed on animals at 9 weeks of RNAi. Images are representative of results seen in >4 animals per panel. Area imaged is indicated by the box in the cartoon on the left. Scar bars represent 100µm.

### ***nr4A* regulates the expression of muscle-specific markers and head and tail PCGs**

To identify the downstream targets of *nr4A*, we collected head and tail tissue regions at several time points following the initiation of *nr4A* RNAi, before gross anatomical changes could be detected (Fig. 5A). We performed RNA sequencing on these head and tail fragments to detect gene expression changes over the course of *nr4A* inhibition.

Over all time points analyzed, we identified 55 genes with significant expression changes in the head ( $p_{adj} < 0.05$ ) in least one time point in *nr4A*(RNAi) animals compared to control animals. Of those 55 genes, 48 were downregulated and 7 were upregulated in their expression (Fig. 5B). In the tail, 41 genes were differentially expressed in *nr4A*(RNAi) animals compared to control animals, with 36 genes downregulated and 5 genes upregulated in their expression (Fig. 5B). The majority (31/55) of the genes with *nr4A*-dependent expression in the head were genes known to display muscle-enriched expression from single-cell RNA sequencing data (Wurtzel et al., 2015). The expression of all but one those genes was downregulated by *nr4A* RNAi (Fig. 5B). Similarly, a large proportion (19/41) of *nr4A*-dependent genes in the tail were known to have enriched expression in muscle, with all but three being downregulated in their expression by *nr4A* RNAi. Among the *nr4A*-dependent muscle markers were several that encoded components of the extracellular matrix, such as collagens and a metalloproteinase (Fig. 5B).

As expected, the number of genes significantly affected by *nr4A* inhibition increased over time, reflecting the progressive and cumulative nature of the RNAi phenotype. At the earliest time point analyzed, all of the *nr4A*-dependent genes in the head and the tail were muscle markers (Fig. 5B), indicating that the earliest changes in *nr4A* RNAi were restricted to muscle cells, with later changes in non-muscle specific gene expression likely reflecting indirect effects of muscle cell perturbation (Fig. 5B). In fact, two of the earliest *nr4A* targets, *col21a1* and *qki*,

were downregulated in their expression in both the head and the tail. These were two of the 16 genes that were significantly regulated by *nr4A* in both the head and the tail. A high proportion (11/16) of them were muscle markers.

We performed a FISH screen of many of these head and tail *nr4A*-dependent genes and verified the decrease in their expression following *nr4A* RNAi (Fig. 5C). Some of these genes, including *col21a1*, *dd\_508\_0\_1*, *psap11*, and *hspb1* were expressed broadly in control animals. Others, like *mmp19*, *dd\_2972\_0\_1*, *ca12*, and *pcdh11y*, displayed enriched expression in heads and tails. Notably, *nr4A* RNAi reduced the expression of the epidermal gene *vim* only at the head and tail tips, largely sparing its expression in the rest of the body.

In addition to regulating many muscle markers, *nr4A* RNAi also perturbed the expression of AP PCGs (Fig. 5B). In the head, *ndl-5* expression was significantly downregulated starting at week 4 of RNAi. In the tail, *wnt11-1* expression became upregulated as early as week 2 of RNAi. Conversely, *nlg-8* expression was downregulated by *nr4A* RNAi starting at week 3. All of these genes encode components of signaling pathways – FGFR, Wnt, and Bmp signaling for *ndl-5*, *wnt11-1*, and *nlg-8* respectively – that have been implicated in patterning (Adell et al., 2010; Forsthoefel and Newmark, 2009; Molina et al., 2007; Reddien, 2011). The changes in expression of these genes with regionalized expression in muscle following *nr4A* RNAi are highly suggestive of a broad disruption of PCG expression programs that accompany the disruption of muscle marker expression. Because these transcriptional perturbations precede the ectopic differentiated tissue phenotype and muscle loss observed, we hypothesized that they might underlie the differentiated cell patterning changes in the head and the tail we observed at later time points of *nr4A* RNAi.



**Figure 5**

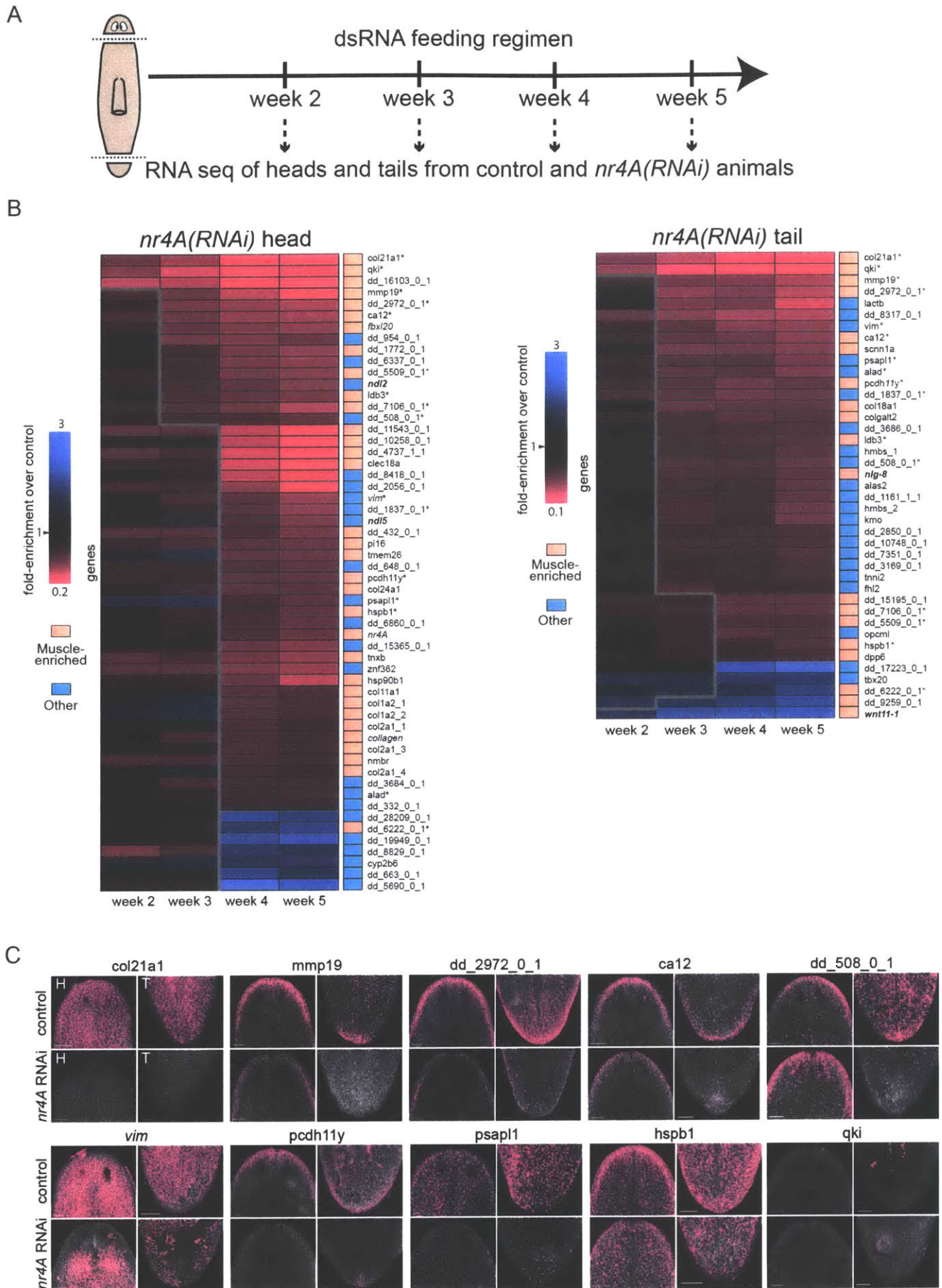


**Figure 5. *nr4A* regulates the expression of muscle-specific markers and head and tail PCGs.**

(A) RNA sequencing approach of control and *nr4A(RNAi)* animals: Heads and tails of animals at weeks 2, 3, 4, and 5 of control and *nr4A(RNAi)* were amputated and processed for RNA sequencing. Amputation planes are shown as dotted lines in the cartoon on the left. Three biological replicates of heads and tails were collected per time point, with six animals pooled within each biological replicate. Gene expression in *nr4A(RNAi)* heads and tails were compared with gene expression in *control(RNAi)* heads and tails, respectively, within each RNAi time point. (B) LEFT – Heat map generated from the fold expression values of genes differentially expressed in the heads of *nr4A(RNAi)* versus *control(RNAi)* animals. Columns represent individual RNAi time points and rows represent individual genes. Heat map region to the right of the thick gray line indicates statistically significant ( $p_{\text{adj}} < 0.05$ ) expression changes over control. Genes are ordered from top to bottom by the time at which their expression significantly changed, with early-response genes at the top and the late-response genes at the bottom. Far-right column indicates whether each gene had muscle-specific expression, with salmon color denoting muscle-enriched expression in single-cell analysis and cyan denoting expression that was not muscle-enriched (Wurtzel et al., 2015). Some genes, like *ndl-5* and *ndl-2* are highly expressed in muscle but were not identified by single-cell analysis to be muscle markers. Non-italicized gene names are best human BLAST hits; genes with no homology were named by their Dresden assembly transcript ID numbers (beginning with “dd”); previously published *Schmidtea mediterranea* genes and *nr4A* with its orthology determined by phylogenetic analysis are in lowercase italics; gene names in bold are PCGs; gene names in asterisk are genes that were also significantly changed in their expression in *nr4A(RNAi)* tails. RIGHT – Heat map generated from the fold expression values of genes differentially expressed in the tails of *nr4A(RNAi)* versus

*control(RNAi)* animals. Heat map region to the right of the thick gray line indicates statistically significant ( $p_{\text{adj}} < 0.05$ ) expression changes over control. Gene naming conventions are the same as for the *nr4A*-dependent genes in the head. (C) Whole-mount FISH with probes for genes with expression downregulated by *nr4A* RNAi in both the head and the tail. All animals were analyzed at 9 weeks of RNAi. DAPI in grey stains the cell nuclei. H denotes head; T denotes tail. Scale bars represent 150 $\mu\text{m}$ .

### ***nr4A* maintains proper PCG expression at the head and tail tips**

The changes in *ndl-5*, *nlg-8*, and *wnt11-1* expression in RNA sequencing data from *nr4A(RNAi)* animals led us to extensively examine the expression patterns of various head and tail PCGs via FISH of RNAi animals. The expression of several genes like *ndl-4*, *sFRP-1*, *notum*, and *foxD* at the anterior end of the anterior-posterior axis defines the head tip compartment (Fig. 6A). In uninjured *nr4A(RNAi)* animals, these expression domains were retracted from the head tip and expanded posteriorly (Fig. 6A, *nr4A RNAi*). Notably, inhibition of *nr4A* eliminated the cluster of *foxD*<sup>+</sup> and *notum*<sup>+</sup> anterior pole cells at the head tip and led to the appearance of ectopic anterior pole cells scattered between the eyes (Fig. 6A). Similarly, the expression domains of PCGs that are broadly expressed in the head and pre-pharyngeal regions, *ndl-2*, *ndl-5*, *ndl-3*, and *wnt-2*, also shifted posteriorly from the head tip following *nr4A RNAi* (Fig. 6A). The reduction of *ndl-5* expression at the head tip of *nr4A(RNAi)* animals corroborates the decrease in *ndl-5* expression levels we observed in the RNA sequencing data. Additionally, the expression domains of midline markers *slit* and *ephR1* were broadened medial-laterally and disorganized in the head of *nr4A(RNAi)* animals (Fig. 6A). Unlike the expression domains of other head PCGs examined, *ndk* expression was not excluded from the head tip in *nr4A(RNAi)* animals (Fig. 6A).

In the tail of *nr4A(RNAi)* animals, we confirmed the decrease in *nlg-8* expression and the increase in *wnt11-1* expression levels observed in the RNA sequencing data (Fig. 6B). Specifically, the tail tip expression domain of *nlg-8* was lost and there was anterior expansion of the *wnt11-1* expression domain (Fig. 6B). We also observed expression changes in two other *wnt* genes that mark the tail tip. In control animals, *wnt11-2* is expressed in a gradient emanating from a high-density expression cluster at the midline of the tail tip (Fig. 6B). Inhibition of *nr4A* eliminated that cluster and broadened the expression gradient anteriorly (Fig. 6B). *wnt1*, a

marker for the posterior pole, is normally expressed linearly along the midline of the tail tip. Similar to its effect on *npl-8* expression, *nr4A* RNAi eliminated *wnt1* expression at its posterior-most domain, leaving a gap between the tip of the tail and the new posterior end of *wnt1* expression (Fig. 6B).

Amputated *nr4A(RNAi)* animals were able to regenerate anterior poles by 72hpa (Fig. 6C). However, at 7dpa the anterior pole cell cluster was absent from the head tip and instead was disorganized and posteriorly shifted (Fig. 6C). This anterior pole positioning phenotype is similar to the anterior pole phenotype we observed in uninjured *nr4A* RNAi (Fig. 6A).

Taken together, the posteriorly expanded expression domains of head tip genes (*foxD*, *notum*, *ndl-4*, and *sFRP-1*) and the anteriorly shifted expression domains of tail tip genes (*wnt11-1* and *wnt11-2*), along with the loss of expression of several other PCGs at the head and tail tips, suggest that head and tail tip regional identities are shifted away from the ends of the animal. This is consistent with the appearance of ectopic expression foci of differentiated cell markers for epidermal and secretory cells normally confined to the dorsal-ventral boundary at head and tail tips in *nr4A(RNAi)* animals. Such changes in regionalized muscle gene expression, along with the appearance of ectopic differentiated tissues, support our observation that *nr4A* inhibition causes loss of head and tail tip identities at the extreme ends of the AP axis.



**Figure 6**

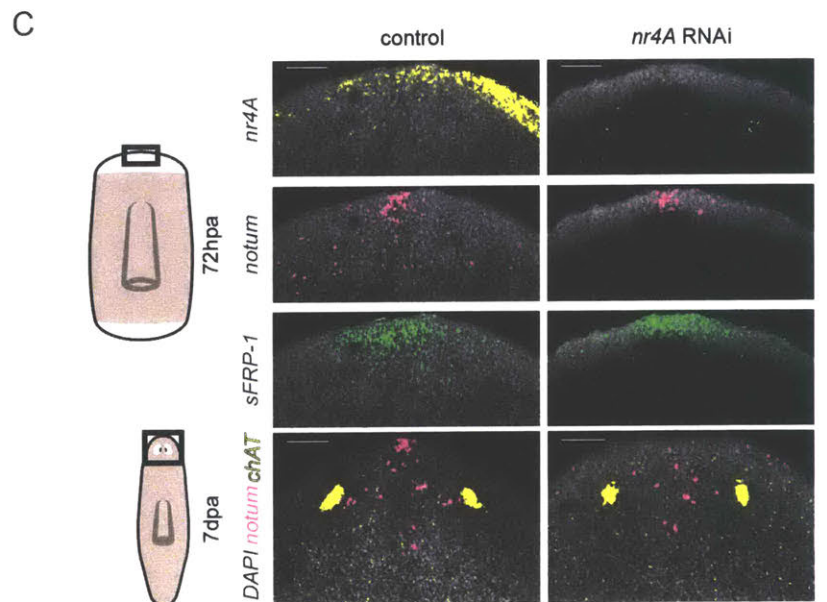
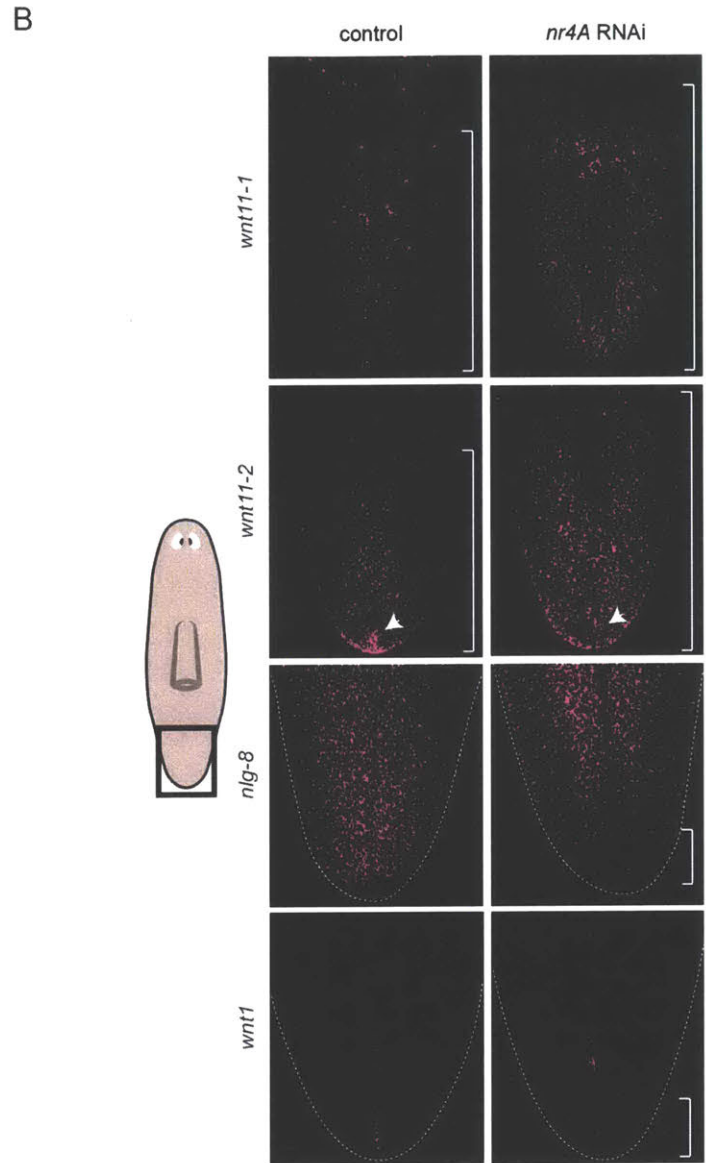
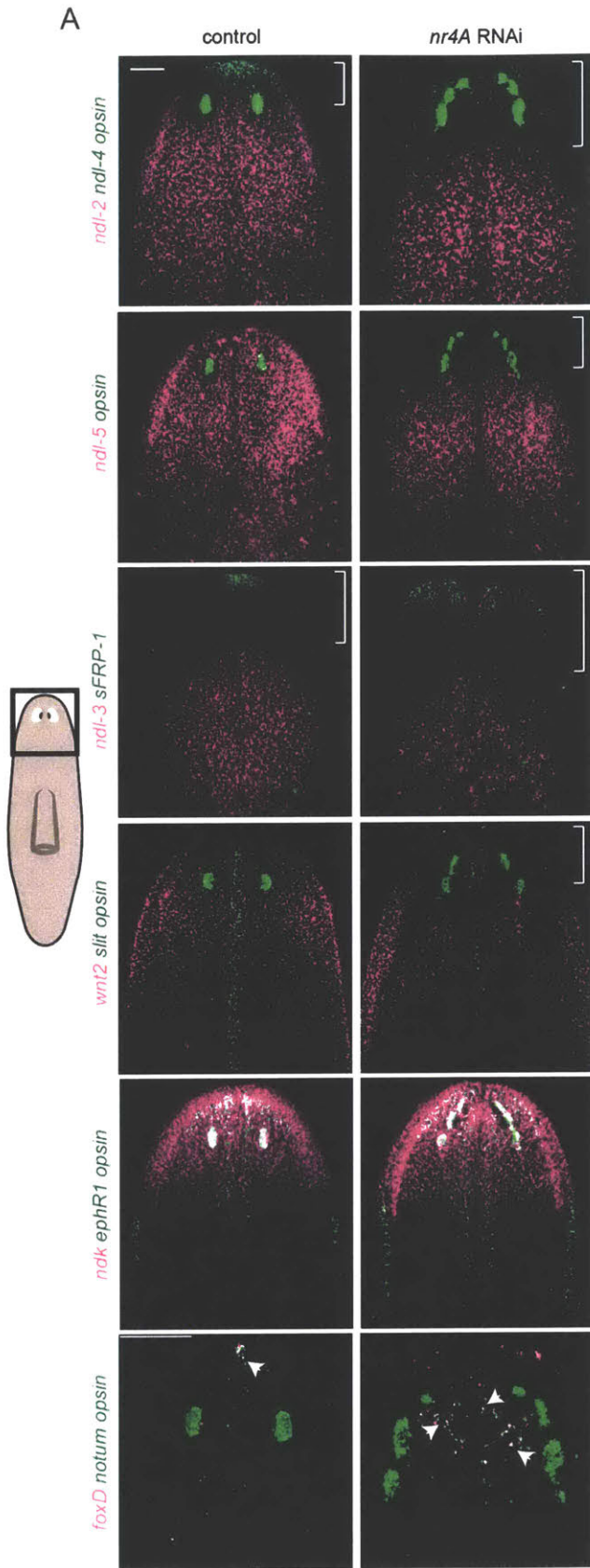


**Figure 6. *nr4A* maintains proper PCG expression at the head and tail tips.** (A) FISH of head PCG probes in control and *nr4A(RNAi)* animals at 9 weeks of RNAi showed retraction of expression domains of *ndl-2*, *ndl-5*, *ndl-3*, and *wnt2* away from the head tip. *ndk*, expression domain, however, was retained at the head tip and became slightly broadened posteriorly in *nr4A* RNAi. *ndl-4* and *sFRP-1* expression, normally anterior to the photoreceptors, broadened posteriorly and decreased at the head tip. Anterior pole cells (*notum*<sup>+</sup>; *foxD*<sup>+</sup>) were absent from the head tip and became scattered around the midline in between the eyes in *nr4A* RNAi. The head domain of midline markers *slit* and *ephR1* also became disorganized in *nr4A* RNAi. Images are representative of results seen in >4 animals per panel. Area imaged is indicated by the box in the cartoon on the left. Scale bars represent 200μm. (B) FISH of tail PCG probes in control and *nr4A(RNAi)* animals at 9 weeks of RNAi showed anterior expansion of expression domains of *wnt11-1* and *wnt11-2*. At their posterior-most domain in the tail, *nlg-8* and *wnt1* expression was absent in *nr4A(RNAi)* animals. Area imaged is indicated by the box in the cartoon on the left. Scale bar represents 100μm. (C) FISH with probes for *notum* and *sFRP-1* at the anterior blastema 72 hours post amputation (72hpa) showed that the anterior pole and the anterior domain of the blastema was properly regenerated in *nr4A(RNAi)* animals compared to control animals. At 7 days post amputation, *notum*<sup>+</sup> cells became absent from the tip and scattered in between the eyes, even though no ectopic photoreceptors are present at this point. Images are representative of results seen in >4 animals per panel. Area imaged is indicated by the box in the cartoon on the left. Scale bars represent 100μm.

## ***nr4A* inhibition causes early anterior and posterior pole shifts that precede changes in differentiated tissues**

Although long-term inhibition of *nr4A* caused expression changes in both PCGs and other tissue markers, our RNA sequencing data of *nr4A(RNAi)* animals showed that changes in PCG expression occurred before anatomical abnormalities appeared (e.g., ectopic eyes). To explore the *nr4A* RNAi phenotype progression in more detail, we analyzed head and tail PCG expression at early RNAi time points. Notably, *notum* expression posteriorized and became scattered between the eyes as early as two weeks of RNAi, preceding changes in the expression of head PCGs (*ndl-2*, *ndl-4*, *ndl-5*, *sFRP-1*) and the differentiated marginal adhesive gland cell marker *mag-1* (Fig. 7A, S5A). A head-on view of the anterior pole cells and muscle fibers at the head tips demonstrated that *notum*<sup>+</sup> cells are normally nestled at the nexus of AP, dorsal-ventral (DV), and medial-lateral (ML) axes where longitudinal, diagonal, circular, and dorsal-ventral muscle fibers converge. In *nr4A(RNAi)* animals however, *notum*<sup>+</sup> cells were scattered and dispersed from this point (Fig. 7B). Consistent with our findings that muscle fiber loss at the head tip occurs at late stages of the phenotype, we observed no apparent differences in head tip muscle fibers between control and *nr4A(RNAi)* animals after two weeks of RNAi (Fig. 7B, S5B).

Anterior shifting of the position of the posterior pole, marked by the expression of *wnt1*, became evident by 3 weeks of RNAi (Fig. 7C). The clustered expression of *wnt11-2* at the tail tip decreased and its graded expression expanded anteriorly at this time point (Fig. 7C). However, no changes in *mag-1*<sup>+</sup> expression were apparent, indicating, like the case for the anterior head tip, that PCG pattern changes precede differentiated tissue shifting in *nr4A(RNAi)* animals (Fig. 7C).

After just one week of *nr4A* RNAi, a time long before other detectable defects emerged, we observed a quantifiable increase in the distance between *notum*<sup>+</sup> cells and the head apex (Fig.

8A, B, and S6A, non-irradiated). To test whether the mislocalized *notum*<sup>+</sup> cells were newly generated cells, we utilized lethal irradiation (6,000 rads of gamma irradiation) to kill all cycling cells (neoblasts), which produce all new cell types in adult planarians including pole cells (Wagner et al., 2011). Because irradiation ultimately leads to head loss and death, we could only examine the early aspects of the *nr4A* phenotype, one week after initiation of RNAi, with this approach. Eliminating neoblasts suppressed the early shift of *notum*<sup>+</sup> cells in *nr4A(RNAi)* animals (Fig. 8A, B, irradiated), indicating that *nr4A* inhibition caused specialized neoblasts for new pole cells to become incorporated at ectopic regions of the head instead of the apex. We also imaged newly produced progeny of neoblasts by detecting perduring protein of the neoblast-expressed *smedwi-1* gene. *smedwi-1* transcripts are absent from neoblast progeny cells but SMEDWI-1 protein persists into newly differentiated neoblast descendant cells (Wenemoser and Reddien, 2010). We detected the presence of SMEDWI-1 protein in the ectopic *notum*<sup>+</sup> and *foxD*<sup>+</sup> pole cells in *nr4A(RNAi)* animals after two and nine weeks of RNAi, respectively (Fig. 8C).

Together, these data show that *nr4A* is important in maintaining the correct location of the anterior pole cells at the tip of the head. Inhibiting *nr4A* expression causes new anterior pole cells to be localized away from the tip of the head and more posteriorly. This change in pole cell localization is followed by anterior shifts of the posterior pole in the tail, all of which occur before other PCG shifts and the appearance of ectopic differentiated tissues such as *mag-1*<sup>+</sup> secretory cells and eyes.

**Figure 7**

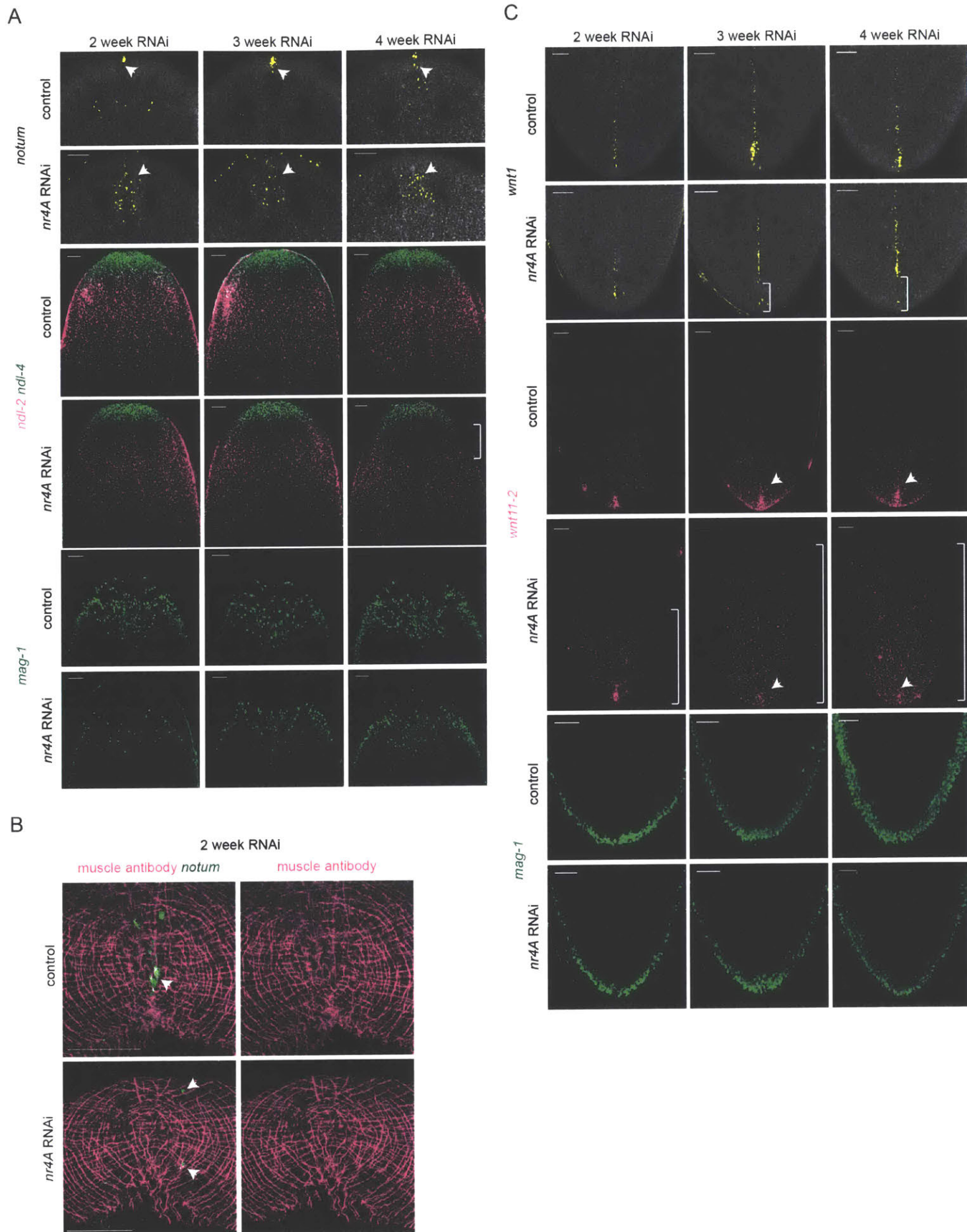


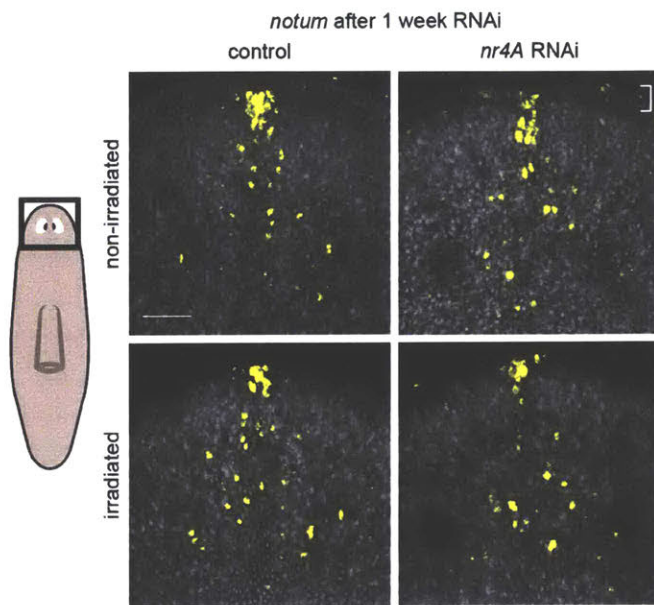
**Figure 7. Time course of early PCG changes in *nr4A* RNAi.** (A) FISH images of head regions of animals at 2, 3, and 4 weeks of RNAi showed early changes in the anterior pole in *nr4A* RNAi. Compared to those in control RNAi, *notum*<sup>+</sup> cells in *nr4A* RNAi were absent from the tip of the head and became scattered posteriorly between the eyes and along the head rim starting at 2 weeks of RNAi, eventually appearing as a loose cluster in between the eyes by 4 weeks of RNAi. The retraction of *ndl-2* expression domain away from the tip of the head did not become apparent until 4 weeks of RNAi. In contrast, *ndl-4* and *mag-1* expression patterns remained unchanged in *nr4A* RNAi compared to control RNAi at all early time points sampled. Images are representative of results seen in >4 animals per panel. Scale bars represent 100µm. (B) Head-on images of the head tips showed that *nr4A* RNAi leads to the loss of anterior pole (*notum*<sup>+</sup>) cells at the vertex of the head, where muscle fibers (stained by muscle antibody 6G10) coalesce. Ectopic *notum*<sup>+</sup> cells (arrow heads) are seen around the apex. Anterior pole changes were not accompanied by changes in muscle fibers at the head apex. All animals were analyzed at 2 weeks of RNAi. Images are representative of results seen in >4 animals per panel. Scale bars represent 50µm. (C) FISH images of tail regions of animals at 2, 3, and 4 weeks of RNAi showed early changes in the posterior pole in *nr4A* RNAi. The gap in expression of *wnt1* at the most posterior aspect of its expression domain became apparent at 3 weeks of *nr4A* RNAi compared to control RNAi. Similarly, the clustered expression of *wnt11-2* at the midline of the tip of the tail was lost at 3 weeks of *nr4A* RNAi, accompanied by the anterior expansion of its graded expression domain in the tail. In contrast, no ectopic *mag-1* expression in the tails of *nr4A*(RNAi) animals was seen at all time points sampled. Images are representative of results seen in >4 animals per panel. Scale bars represent 100µm.



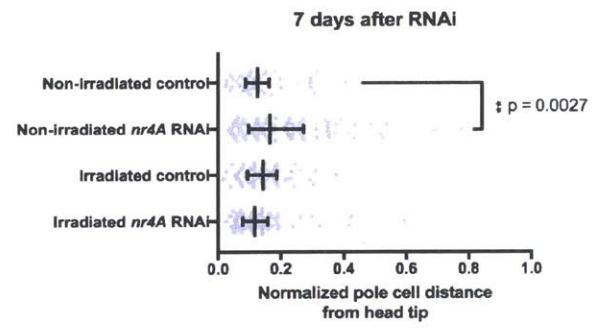
**Supplementary Figure 5. Time course of early head PCG changes in *nr4A* RNAi.** (A) FISH images of head regions of animals at 2, 3, and 4 weeks of RNAi showed posteriorly retracted and decreased in *ndl-5* expression starting at 3 weeks of *nr4A* RNAi compared to control. In contrast, *sFRP-1* expression domain remained unchanged. Images are representative of results seen in >4 animals per panel. Scale bars represent 100 $\mu$ m. (B) Head-on images of the head tips of additional animals showing the loss of pole (*notum*<sup>+</sup>) cells from the apex of the head in *nr4A* RNAi, with muscle fibers (stained by muscle antibody 6G10) remaining unchanged compared with control RNAi. Scale bars represent 100 $\mu$ m.

Figure 8

A



B



C

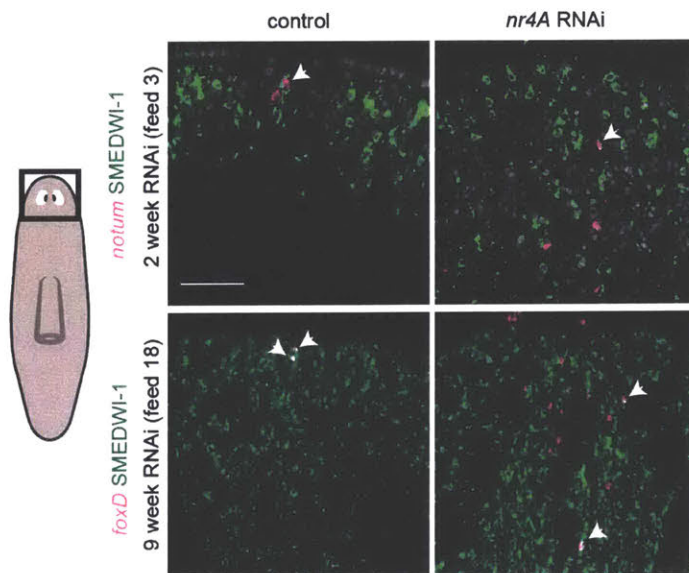
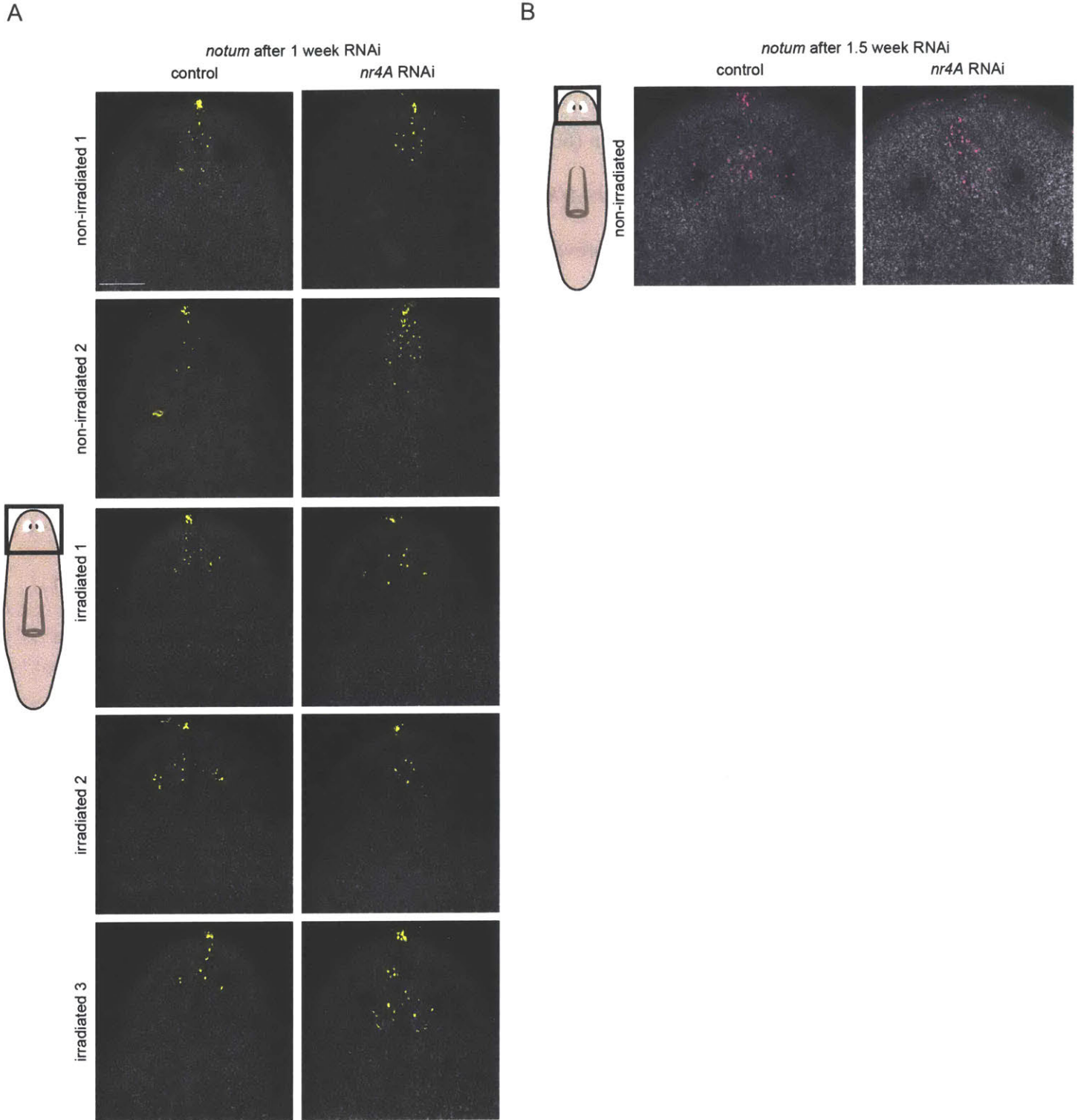


**Figure 8. Early anterior pole shifts in *nr4A* RNAi are neoblast-dependent.** (A) FISH images of anterior pole (*notum*<sup>+</sup>) cells in animals fixed 7 days after one *nr4A* or control RNAi feeding and 8 days after lethal gamma irradiation (6000 rads): Without irradiation, a slight posterior shift of the anterior pole was observed in *nr4A(RNAi)* animals compared to *control(RNAi)* animals. Eliminating neoblasts with irradiation prevented the anterior pole shift in *nr4A(RNAi)* animals. Images are representative of results seen in >4 animals per panel. Area imaged is indicated by the box in the cartoon on the left. Scale bar represents 50µm. (B) Quantification of the anterior pole shift using the distance between *notum*<sup>+</sup> cells and the head apex (the middle of the tip of the head) normalized by the distance between the eyes showed that the statistically significant increase in average pole cell distance from the head apex in *nr4A(RNAi)* animals was suppressed by irradiation. At least 5 animals were analyzed per condition. (C) Fluorescence stains with *notum* probe (magenta) and SMEDWI-Antibody (SMEDWI-Ab, green) showed that some of the ectopic anterior pole cells were newly generated cells (*notum*<sup>+</sup>; SMEDWI-Ab<sup>+</sup>, arrow heads) at both early (2 week RNAi) and late (9 week RNAi) stages of the *nr4A* RNAi phenotype. Area imaged is indicated by the box in the cartoon on the left. Scale bar represents 50µm.

# Supplemental Figure 6



**Supplemental Figure 6. Early anterior pole shift in *nr4A* RNAi is repressed by irradiation.**

(A) FISH images of anterior pole (*notum*<sup>+</sup>) cells in additional animals fixed 7 days after one *nr4A* or control RNAi feeding and 8 days after lethal gamma irradiation (6000 rads) showed that the posterior shift in the anterior pole was suppressed by the elimination of neoblasts. Area imaged is indicated by the box in the cartoon on the left. Scale bar represents 100μm. (B) FISH image of anterior pole (*notum*<sup>+</sup>) cells in *control* and *nr4A(RNAi)* animals after 1.5 weeks of RNAi showed a greater degree in the shift of the locations of anterior pole cells from the apex of the head to the head rim and more posteriorly in between the eyes. Area imaged is indicated by the box in the cartoon on the left. Scale bars represent 50μm.

## Discussion

### Anterior and posterior pole transcriptomes

The planarian anterior and posterior poles have been subjects of intense recent study because of their roles in patterning the head and the tail (Owlarn and Bartscherer, 2016; Reddien, 2011). Multiple studies have identified anterior and posterior pole transcription factors that regulate proper head and tail formation during regeneration (Hayashi et al., 2011; März et al., 2013; Scimone et al., 2014; Vásquez-Doorman and Petersen, 2014; Vogg et al., 2014; Currie and Pearson, 2013; März et al., 2013). Given their locations along the midline and at the extreme ends of the AP axis, together with the expression of transcription factors that establish and maintain the poles during regeneration and throughout homeostasis, the poles have been regarded as adult organizers (Scimone et al., 2014; Vásquez-Doorman and Petersen, 2014; Vogg et al., 2014; Vogg et al., 2016).

Using bulk and single-cell RNA sequencing, we identified many new genes expressed in the anterior and posterior poles, including ones expressed in both. Although the roles of many of these genes remain to be explored, their identities can help elucidate aspects of pole biology. For example, *kallmann1*, which encodes an extracellular matrix protein implicated in defects in olfactory neuron migration in humans (Rugarli, 1999; Rugarli et al., 1993), is interesting for its specific expression in both anterior and posterior pole cells. Another gene specifically expressed in the anterior pole, *musculin*, encodes a transcription factor that could be investigated to determine how anterior pole gene expression is regulated. A large number of the new anterior and posterior pole genes we identified encode cell surface receptors (e.g., *ephr4*, *ephr5*, *ror1*,

*pcdh9*, *ddr2*, *dcc*), and these are good candidates for future work on the processes of pole formation (e.g. pole cell aggregation, migration) or signal transduction with surrounding cells. Genes with unique functions in organizers in development and regeneration are of interest for understanding how these regions form and pattern neighboring tissue, and RNA sequencing approaches like the one defined here could identify the transcriptomes of these regulatory regions of embryos and animals broadly.

### ***nr4A* as a new patterning gene**

From our pole transcriptome screen, we have identified *nr4A*, a gene specifically expressed in muscle, as a new regulator of AP axial patterning. *nr4A* genes are widely conserved in the animal kingdom, and to our knowledge this is the first time that a member of the NR4A family of nuclear receptors has been found to influence tissue patterning.

In the field of developmental biology and regeneration, little is known about the role of members of the NR4A subfamily of transcription factors. NR4A subfamily members belong to the broader superfamily of nuclear receptors specific to metazoans, possibly acquired to accommodate the need for endocrine signaling in increasingly complex body systems (Bridgham et al., 2010; Escriva et al., 2004). Although members of many other subfamilies of nuclear receptors bind to steroid hormones, retinoic acids, fatty acids, and prostaglandins, NR4A family members are orphan receptors that are thought to regulate transcription in a ligand-independent manner (Bridgham et al., 2010)(Paulsen et al., 1992). Whereas vertebrates possess three NR4A members (NR4A1, NR4A2, and NR4A3), protostomes only have one (Bertrand et al., 2004).

DHR38, the *Drosophila* ortholog of the mammalian NR4A family of nuclear receptors, mediates an atypical ligand-independent ecdysteroid signaling pathway responsible for the dramatic insect developmental transitions such as molting and metamorphosis (Baker et al., 2003). In vertebrates, the three members of the *NR4A* family are immediate-early stress response genes induced by a host of physiological signals such as growth factors, cytokines, prostaglandins, neurotransmitters, and phorbol esters (Maxwell and Muscat, 2006; Safe et al., 2016). *NR4A1*, *NR4A2*, and *NR4A3* are expressed in a variety of tissues such as the brain, liver, gonads, skeletal muscle, kidney, fat, lung, and endocrine glands (Maxwell and Muscat, 2006). Their functions have been implicated in the development of regulatory T cells and dopaminergic neurons, and the metabolism in various cells, such as liver cell gluconeogenesis, and apoptosis (Maxwell and Muscat, 2006; Safe et al., 2016) (Sekiya et al., 2013).

The most striking aspect of the activity of the planarian *nr4A* is its patterning role at the ends of the AP axis. *nr4A* RNAi inhibited *vim* expression and induced ectopic epidermal and adhesive gland marker expression only in the head and tail. *nr4A* was expressed strongly in the head and tail, but was also expressed in muscle cells throughout the body. RNA sequencing data from *nr4A(RNAi)* animals revealed that the predominant downstream targets of *nr4A* were genes specifically expressed in muscle cells, the majority of which encode extracellular matrix (ECM) components (collagens and metalloproteinase) and signaling proteins. Several of these genes predicted to encode ECM components displayed enriched expression in the head and tail tips. Though it is unknown which genes are transcriptional direct targets of the NR4A protein, genes that experienced changes in expression early in the course of RNAi (e.g. *col21a1*, *qki*, *mmp19*, etc) are more likely to be directly dependent on *nr4A*. Both RNA sequencing and *in situ* hybridization data from *nr4A(RNAi)* animals showed that *nr4A* inhibition perturbed not only

muscle itself, but ultimately also other differentiated tissues such as the epidermis and adhesive gland cells. That these tissue changes followed *nr4A*-mediated changes in expression of several known PCGs lends further support to the model whereby muscle cells communicate with and dictate – directly or indirectly – the identity and/or location of other surrounding differentiated tissues.

### **A model for the *nr4A* RNAi phenotype**

As the longest axis of the planarian body plan, the AP axis is formed by a continuum of distinct and overlapping PCG expression domains spanning from the head tip to the tail tip. These gene expression domains generate varying anatomical identities along the AP axis, for example by promoting eye specification in the head and pharynx specification in the midbody (Lander and Petersen, 2016; Scimone et al., 2016).

In light of this positional information map superimposed on existing adult anatomy, we propose that in long-term *nr4A(RNAi)* animals the ectopically posterior tissues in the head and the ectopically anterior tissues in the tail manifest from a shift of the AP PCG pattern from the ends of the AP axis (Fig. 9). Specifically, the AP PCG axis termini demarcated by the anterior and posterior poles are scaled away from the AP anatomical termini (head and tail tips) (Fig. 9). As the phenotype progresses, the retraction of AP PCG expression domains from the ends of the AP anatomical axis culminates in the encroachment of new differentiated tissues produced from neoblasts during homeostatic tissue turnover towards the midbody of the animal (Fig. 9). The end product is an anatomically frameshifted animal containing old tissues juxtaposed to new tissues farther away from the termini of the AP axis (Fig. 9). This model depends on the PCG

and anatomical axis frameshift happening before differentiated tissue changes, as observed. As early as one week after *nr4A* RNAi, the anterior pole began to scale away from the head tip, followed by the posterior pole scaling away from the tail tip at 3 weeks of RNAi (Fig. 6A, C). Between 3 and 4 weeks of RNAi, a host of other head and tail PCGs became progressively excluded from head and tail tips, respectively (Fig. 6A, C). This all occurred before we detected ectopic eyes, gland, or DV boundary epidermal cell marker expression between 5 and 11 weeks of RNAi (Fig. 2, 4, 7). We conclude that *nr4A* is a novel adult patterning gene that helps muscle promote the patterning of both the anterior and posterior extreme ends of the primary planarian body axis.

**Figure 9**

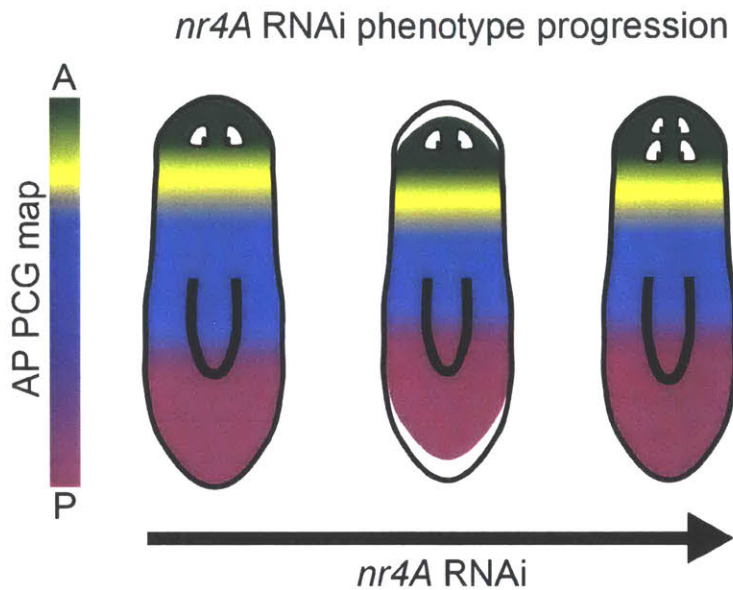


**Figure 9. A model for the progression of *nr4A* RNAi phenotype.** Distinct and overlapping gene expression domains that maintain pattern along the AP axis during homeostasis are represented by the AP PCG map color gradient. As *nr4A* RNAi phenotype progresses (left to right), the AP PCG gradient is scaled away from the head and tail tips and towards the midbody (middle animal). This is followed by the specification of new tissues away from the ends of planarian AP axis, for example, resulting in the formation of ectopic posterior eyes in the head (right-most animal).

**Supplemental Table 1.** Anterior pole enriched genes in uninjured animals

Contig ID	foldChange	padj	Human accession	Human name	E-value
dd Smed v4 23249 0 1	20.0757009	1.8338E-26	NP_997188	FOXD	2E-53
dd Smed v4 12485 0 1	14.0008448	7.4345E-29	NP_001921	DHPS	2E-141
dd Smed v4 24180 0 1	10.8219834	3.6705E-31	NP_848588	NOTUM	8E-73
dd Smed v4 74605 0 1	9.49864762	0.01941079	XP_005252952		2E-17
dd Smed v4 23400 0 2	7.44349338	3.9799E-06	NP_001171886		6.8
dd Smed v4 47419 0 1	6.84697692	0.00231786	NP_001252541		5E-17
dd Smed v4 13188 0 1	6.32451826	2.9603E-33	NP_000207	KAL1	1E-21
dd Smed v4 16209 0 1	6.0865619	3.5797E-05	NP_110388	WNT4	8E-38
dd Smed v4 49372 0 1	5.57039053	2.883E-14	XP_005253612		2E-79
dd Smed v4 39577 0 1	4.34360238	0.01867111			none
dd Smed v4 13875 0 1	4.2765903	3.7412E-11			none
dd Smed v4 27668 0 1	4.12043304	4.1688E-47	XP_005247264		3E-60
dd Smed v4 8201 0 2	3.99039792	1.2972E-19	XP_005253612		0
dd Smed v4 25387 0 1	3.90646639	5.1062E-48	NP_001664		3E-106
dd Smed v4 20026 0 1	3.84193987	8.1864E-05	NP_001120963		3.1
dd Smed v4 35379 0 1	3.77853799	1.4245E-14	NP_665804	ISL2	1E-21
dd Smed v4 22615 0 1	3.64402765	3.9218E-17	NP_001171548		8E-11
dd Smed v4 39545 0 1	3.60183337	6.0883E-22	XP_005245808		9E-37
dd Smed v4 5147 0 1	3.43152993	2.2614E-15	XP_005262583		5.3
dd Smed v4 16070 0 1	3.32953379	0.00024146	NP_005089	MSC	6E-12
dd Smed v4 40708 0 1	3.12235979	6.0966E-07			none
dd Smed v4 19949 0 1	3.10901094	3.2842E-08	NP_078858	FAT4	2.6
dd Smed v4 93315 0 1	2.79853427	2.8699E-06	NP_005530	INPP5A	2.3
dd Smed v4 8371 0 1	2.79771124	1.4159E-16	NP_002721	PRKACA	2E-168
dd Smed v4 1574 6 101	2.76881916	0.03795801	XP_005268774		0.7
dd Smed v4 13823 0 1	2.64464803	8.0044E-29	NP_005609		2E-84
dd Smed v4 10673 0 1	2.48667461	0.00089819	XP_005274075		2E-48
dd Smed v4 15506 0 1	2.44677756	0.00018028	NP_003059	SNAI2	3E-38
dd Smed v4 4427 0 1	2.44322394	0.01486315			none
dd Smed v4 13985 0 1	2.40780117	0.00091943	NP_003006	SFRP5	2E-37
dd Smed v4 12269 0 2	2.39502018	0.00403468			none
dd Smed v4 348 0 1	2.31531687	5.9094E-08	NP_000934	PPIC	1E-46
dd Smed v4 12111 0 1	2.3135299	1.3121E-07	NP_003053	SLIT3	0
dd Smed v4 12269 0 3	2.30410926	0.01076241			none
dd Smed v4 1242 0 1	2.14713568	5.2506E-07	NP_000934	PPIC	5E-47
dd Smed v4 12650 0 1	2.12952826	0.02436734	NP_001124157		3E-45
dd Smed v4 14635 0 1	2.08594432	1.8045E-09	NP_001445	FOXJ1	1E-34
dd Smed v4 380 0 1	2.08259433	0.0081274			none
dd Smed v4 23030 0 1	2.07849028	3.9242E-08	NP_899068		1.8
dd Smed v4 8829 0 1	2.06951909	3.8115E-12	NP_002622	PGD	0

dd Smed v4 13975 0 3	2.03621752	0.00126145	NP_003237	THBS1	0.00000007
dd Smed v4 12426 0 1	2.03103167	0.00258139			none
dd Smed v4 10089 0 1	2.03076549	1.6081E-11			none
dd Smed v4 1949 0 1	2.00541697	3.9218E-17	NP_001107594		8.9
dd Smed v4 13814 0 1	1.96344422	0.04849472	NP_597715	ZFP90	4.8
dd Smed v4 12653 0 1	1.96174927	6.142E-05	XP_005246500		0
dd Smed v4 18393 0 2	1.95566146	7.5897E-06	NP_734465		4E-37
dd Smed v4 28398 0 1	1.94946584	0.0242333	NP_005421	WNT1	3E-59
dd Smed v4 17589 0 1	1.93864069	5.0222E-08	NP_000208	KCNA1	8E-140
dd Smed v4 28076 0 1	1.93300887	0.0047544	NP_001265130		1E-13
dd Smed v4 18393 0 3	1.9311254	1.2785E-05	NP_734465		3E-37
dd Smed v4 24483 0 1	1.92441593	1.007E-05			none
dd Smed v4 15253 0 1	1.91491965	0.00872335	NP_005020	PITX3	2E-42
dd Smed v4 14647 0 1	1.91029842	0.00994655	XP_005257115		0.007
dd Smed v4 16571 0 1	1.90715785	9.373E-12	NP_003459	FZD5	0
dd Smed v4 4196 0 3	1.8968666	6.0319E-12	XP_005258157		0.012
dd Smed v4 13065 0 1	1.89141655	9.6819E-08	NP_002498	NGFR	0.58
dd Smed v4 36844 0 1	1.88985455	0.00506415	NP_057658	DRD2	1E-19
dd Smed v4 9584 0 2	1.87450677	1.0478E-07	NP_006341	FST	0.000000001
dd Smed v4 8393 0 1	1.87378926	1.2054E-05	NP_056226	SUMF2	8E-63
dd Smed v4 1538 0 1	1.8704468	0.01426759	NP_543007		9.4
dd Smed v4 12635 0 1	1.86775255	3.696E-05			none
dd Smed v4 7911 0 1	1.84425208	1.0415E-11	NP_005003	ROR1	8E-137
dd Smed v4 4196 0 1	1.8426563	6.0683E-11	XP_005258155		0.003
dd Smed v4 16928 0 1	1.83425041	1.5642E-10	NP_004433		0
dd Smed v4 18393 0 4	1.82691769	0.00018028	NP_734465		3E-37
dd Smed v4 4196 0 4	1.82656769	1.1953E-10	XP_005258155		0.019
dd Smed v4 18393 0 1	1.79407671	0.00037309	NP_734465		4E-37
dd Smed v4 8375 0 1	1.78133203	2.3781E-09			none
dd Smed v4 4196 0 2	1.7791524	9.6884E-10	XP_005258155		0.004
dd Smed v4 18952 0 1	1.76304222	0.0220518	NP_112599	SCRT1	1E-75
dd Smed v4 23771 0 1	1.7608536	0.00056099	NP_000327	SCNN1B	1E-11
dd Smed v4 9584 0 1	1.75223107	0.02186196	NP_006341		0.000000001
dd Smed v4 9204 0 2	1.7473412	0.03274855	NP_001036816	TPM3	3.5
dd Smed v4 13154 0 1	1.74483798	0.03176913	XP_005262301		0.0000008
dd Smed v4 25969 0 1	1.73697524	0.01572296	NP_001005515		0.031
dd Smed v4 8504 0 1	1.72995145	3.244E-08	NP_004813	NTN1	6E-103
dd Smed v4 9584 0 3	1.72576546	1.1345E-05	NP_006341		0.000000001
dd Smed v4 50035 0 1	1.70931475	0.00913631	XP_005251742		2E-87
dd Smed v4 17072 0 1	1.70821048	0.02795007	NP_002223	KCNA3	9E-29
dd Smed v4 17352 0 1	1.66105533	0.00609918	XP_005256194		2E-38
dd Smed v4 24722 0 1	1.66009583	0.01118254	NP_001020119	FNBP1L	1.3

dd Smed v4 17154 0 1	1.65870971	0.00116087	XP_005271074		1E-180
dd Smed v4 10555 0 1	1.65654039	3.244E-08	NP_001185546		2.4
dd Smed v4 2493 0 3	1.6528485	8.9976E-06	NP_001138548	EML4	0.0003
dd Smed v4 7063 0 1	1.65008179	1.5167E-06	NP_001077075		5E-56
dd Smed v4 5057 0 1	1.65000933	2.4896E-05	XP_005270333		9.3
dd Smed v4 12010 0 1	1.64645386	0.00053978	XP_005274075		2E-50
dd Smed v4 5242 0 1	1.63113607	0.00012507	NP_938080	GALNT10	9E-171
dd Smed v4 4284 0 1	1.62465451	1.1062E-07	XP_005251788		2E-56
dd Smed v4 15482 0 1	1.59346889	0.01426759			none
dd Smed v4 7030 0 1	1.58642918	9.4246E-06			none
dd Smed v4 13975 0 1	1.58598526	6.624E-07	NP_001265354		7E-36
dd Smed v4 9747 0 1	1.58392881	0.00940814			none
dd Smed v4 11650 0 1	1.57992468	0.00615402	NP_009128	FZD10	7E-114
dd Smed v4 16483 0 1	1.57961777	3.3577E-05	XP_005246431		3E-114
dd Smed v4 6034 0 1	1.57828991	9.765E-05			none
dd Smed v4 17402 0 1	1.57243582	0.00582906	NP_001710	BMP7	7E-31
dd Smed v4 16438 0 1	1.57215118	0.01236627	NP_057440		0.00002
dd Smed v4 39721 0 1	1.54772946	0.0094563	XP_005251498		7E-52
dd Smed v4 15181 0 1	1.53837713	0.00266037	NP_116754		2E-75
dd Smed v4 29263 0 1	1.53301644	0.00188307	NP_065907	TSHZ3	0.49
dd Smed v4 8804 0 2	1.5316596	0.00010402	NP_006473	DYRK2	0.95
dd Smed v4 3381 0 1	1.52310527	1.6273E-05	XP_005246885		5E-25
dd Smed v4 7063 0 2	1.51718948	0.00015649	NP_001077075		2E-57
dd Smed v4 8804 0 3	1.51639669	0.00136106	XP_005254555		2.9
dd Smed v4 10791 0 1	1.51574138	0.03543635	NP_060017	FOXRED1	6E-105
dd Smed v4 22585 0 1	1.51378623	0.00189913	NP_003404	ZIC3	7E-85
dd Smed v4 20159 0 1	1.50414421	0.01354765	NP_057440		6E-27
dd Smed v4 12038 0 1	1.50355316	0.00568861			none
dd Smed v4 19076 0 1	1.50076937	0.00883887	XP_005263218		0.004
dd Smed v4 10150 0 1	1.49663233	0.03194886			none
dd Smed v4 8804 0 1	1.48971287	0.00045542	NP_006473	DYRK2	0.96
dd Smed v4 9196 0 1	1.48720792	0.00388962			none
dd Smed v4 13570 0 1	1.48193672	0.00226098	NP_078858	FAT4	4E-58
dd Smed v4 29517 0 1	1.48022386	0.01793118	NP_001191332		2E-92
dd Smed v4 19322 0 1	1.47626777	0.01169906	NP_057196	PKD2L1	3E-64
dd Smed v4 10730 0 2	1.47468751	0.00170516	NP_003719	UNC5C	6E-89
dd Smed v4 13474 0 1	1.47366421	0.03300051	NP_001017363		1E-68
dd Smed v4 12269 0 1	1.47245367	0.00021318			none
dd Smed v4 39713 0 1	1.4711156	0.00955529	NP_653213	LOXHD1	2E-14
dd Smed v4 6254 0 1	1.46790082	0.00388962	NP_006614	PHGDH	1E-109
dd Smed v4 15217 0 1	1.46706444	0.02021419	NP_004967	KCNC1	4E-55
dd Smed v4 12182 0 1	1.46681257	0.02080111	NP_000737	CHRNA7	1E-116

dd Smed v4 20556 0 1	1.46545966	0.01292298	NP 116749		3E-43
dd Smed v4 10237 0 1	1.45464932	0.0081274	NP 003556	ULK1	7E-77
dd Smed v4 13071 0 1	1.44884081	0.00506933	NP 150094	CSMD1	5E-27
dd Smed v4 12208 0 1	1.44593285	0.00077634	NP 001239264		0.69
dd Smed v4 9230 0 2	1.44576008	0.00091943	XP 005254787		4E-40
dd Smed v4 15626 0 1	1.44515077	0.00101351	NP 001240766		1E-95
dd Smed v4 18385 0 1	1.44450601	0.01071848	NP 001029		0.00000001
dd Smed v4 22398 0 1	1.43836969	0.04683779	NP 001073347	CNGA3	0
dd Smed v4 11681 0 1	1.43452265	0.00492594	NP 055916	GLT25D2	6E-98
dd Smed v4 8806 0 2	1.43310627	0.00353972	XP 005267687		3E-160
dd Smed v4 7632 0 3	1.43310487	0.02997569	NP 001129108		1E-111
dd Smed v4 15272 0 1	1.43239954	0.00174202	XP 005250039		4E-38
dd Smed v4 1970 0 1	1.43117029	0.04329763	XP 005251136		2E-48
dd Smed v4 8489 0 2	1.42884202	0.01061888	XP 005251890		4E-11
dd Smed v4 12208 0 2	1.42834915	0.00208362	NP 001239264		0.72
dd Smed v4 7144 0 1	1.42699869	0.03490493	NP 653182	C14orf149	1E-66
dd Smed v4 14018 0 1	1.42631194	0.01224971			none
dd Smed v4 8806 0 1	1.42628131	0.00363636	XP 005267683		3E-159
dd Smed v4 9677 0 1	1.42614202	0.00439239	NP 001265548		6E-66
dd Smed v4 7545 0 1	1.42446791	0.02803986	NP 114141	HMCN1	6E-46
dd Smed v4 10613 0 1	1.42344891	0.00878168	NP 061181	SVOP	8E-67
dd Smed v4 12595 0 1	1.42078889	0.0052445	NP 055978	TRIM9	2E-123
dd Smed v4 3381 0 2	1.4174696	0.00116042	NP 001243779		3E-25
dd Smed v4 12229 0 1	1.41744639	0.00682198	NP 775180		2E-50
dd Smed v4 4752 0 1	1.41603817	0.00102009	NP 065706	JPH3	9E-94
dd Smed v4 6746 0 1	1.41509093	0.0092338	NP 000207	KAL1	8E-38
dd Smed v4 12407 0 1	1.41406084	0.01480389	XP 005270910		1E-157
dd Smed v4 9120 0 1	1.41378786	0.01145008	NP 001123498	FAM115C	7E-23
dd Smed v4 6048 0 4	1.41346986	0.01053353	XP 005257785		1E-25
dd Smed v4 8959 0 1	1.41121007	0.00413543	XP 003960332		0.00004
dd Smed v4 9230 0 1	1.40725885	0.00325106	XP 005254787		6E-40
dd Smed v4 9009 0 2	1.40616574	0.00173416	NP 060009	DNAH3	0
dd Smed v4 6182 0 1	1.40505251	0.03274855	NP 005771	LHFP	5E-16
dd Smed v4 9009 0 1	1.40461769	0.00157119	NP 060009	DNAH3	0
dd Smed v4 12674 0 3	1.40452616	0.03138514	XP 005272339		6E-22
dd Smed v4 7614 0 1	1.40400911	0.0091829	NP 443139	TMEM132B	0.0003
dd Smed v4 16808 0 1	1.39822321	0.00315906	XP 005246888		0.0000009
dd Smed v4 3418 0 1	1.39692767	0.00150724	XP 005246675		0.6
dd Smed v4 1772 0 1	1.39684026	0.00103576	NP 733765	ATP2A2	0
dd Smed v4 6048 0 3	1.39529981	0.00609918	XP 005257785		5E-26
dd Smed v4 12674 0 2	1.39400021	0.03777427	XP 005272339		1E-21
dd Smed v4 2493 0 2	1.39397135	0.00245526	NP 001008707	EML1	0

dd Smed v4 6048 0 2	1.39333855	0.00678953	XP 005257785		3E-33
dd Smed v4 2493 0 1	1.38911016	0.00272172	NP 004425		0
dd Smed v4 12629 0 1	1.38910055	0.00682281			none
dd Smed v4 5037 0 1	1.38905536	0.00725028	NP 963851		1E-119
dd Smed v4 508 0 2	1.38693234	0.0043886	NP 005992		0
dd Smed v4 508 0 3	1.38531143	0.0047544	NP 116093	TUBA1C	0
dd Smed v4 15531 0 1	1.37924613	0.01963443	NP 009060	ZIC2	6E-79
dd Smed v4 12674 0 1	1.3792059	0.04208104	XP 005272339		1E-21
dd Smed v4 10730 0 1	1.37752262	0.02648904	NP 003719	UNC5C	2E-91
dd Smed v4 5781 0 1	1.37750459	0.03423574	NP 001158067	PDZRN4	3E-18
dd Smed v4 181 0 1	1.37305626	0.00353972	XP 005260608		1E-16
dd Smed v4 508 0 1	1.3683871	0.00874508	NP 005992		0
dd Smed v4 6597 0 1	1.36445708	0.00904772	NP 005838	SLC23A1	6E-83
dd Smed v4 3527 0 2	1.36326126	0.00615402	XP 005245918		7E-27
dd Smed v4 13399 0 1	1.36303355	0.0092338	NP 001244949		1E-128
dd Smed v4 8690 0 1	1.36286991	0.01113036	NP 071426	LRRC4	6E-10
dd Smed v4 10734 0 1	1.36036468	0.00742491	NP 001269810		3E-54
dd Smed v4 19860 0 1	1.35314047	0.03936914	XP 005263267		2E-57
dd Smed v4 14162 0 1	1.34915722	0.04624038	XP 005264701		5E-179
dd Smed v4 8833 0 1	1.34826993	0.01071848	XP 005276090		3E-19
dd Smed v4 2072 0 29	1.34421439	0.03950284	NP 001191333		0
dd Smed v4 11502 0 1	1.34234567	0.03932899	NP 065871	PREX1	3.3
dd Smed v4 508 0 4	1.33802957	0.02181739	NP 116093	TUBA1C	0
dd Smed v4 11744 0 1	1.328788	0.02033781	NP 003728	DCHS1	4E-82
dd Smed v4 6809 0 1	1.32683795	0.02648904	NP 066010	ANO8	7E-112
dd Smed v4 718 0 1	1.32391061	0.02159219	NP 001257329		0
dd Smed v4 9407 0 1	1.32121946	0.03936914			none
dd Smed v4 2337 0 1	1.32115458	0.01387806	NP 690850	COL24A1	8E-59
dd Smed v4 2688 0 1	1.31984536	0.01480726	NP 001091680	CTNNB1	9E-138
dd Smed v4 2928 0 1	1.31541716	0.03368598	NP 597676	TTN	1E-22
dd Smed v4 6958 0 1	1.31517084	0.02957541	NP 776161	AQPEP	9E-78
dd Smed v4 11823 0 1	1.3148143	0.03471913	NP 003459	FZD5	0
dd Smed v4 3527 0 1	1.31098828	0.04003858	XP 005245918		7E-27
dd Smed v4 6524 0 1	1.30340183	0.04057243	XP 005245918		0.00009
dd Smed v4 2197 0 1	1.29689685	0.03203985	NP 690850	COL24A1	6E-61
dd Smed v4 2922 0 1	1.29454162	0.03455608	NP 055601	ARHGEF17	5E-54
dd Smed v4 5635 0 1	1.29039624	0.04849472	NP 002028	FYN	4E-167

**Supplemental Table 1. Anterior pole enriched genes in intact animals.** Genes with significantly higher ( $p_{\text{adj}} < 0.05$ ) expression in anterior pole pieces compared to flanking pieces in intact animals are shown, ranked by their fold-change over control from highest to lowest. Known anterior pole genes are color-coded – *foxD* (blue), *notum* (red), *pitx* (yellow), *fst* (green), and *zic-1* (brown). Also shown are human best BLAST hits and their E-values, along with Dresden transcriptome assembly contig identifiers.

**Supplemental Table 2.** Anterior pole enriched genes in anterior blastema of 72hpa trunks

Contig ID	foldChange	padj	Human accession	Human name	E-value
dd Smed v4 24180 0 1	19.2104175	1.90E-10	NP_848588	NOTUM	8E-73
dd Smed v4 93315 0 1	17.9186861	1.24E-20	NP_005530	INPP5A	2.3
dd Smed v4 43060 0 1	16.2860917	0.00170979	XP_005248824		2E-27
dd Smed v4 16070 0 1	13.0727825	8.82E-10	NP_005089	MSC	6E-12
dd Smed v4 49372 0 1	8.95841348	3.73E-07	XP_005253612		2E-79
dd Smed v4 8201 0 2	8.89927348	5.97E-16	XP_005253612		0
dd Smed v4 39545 0 1	7.72395567	4.00E-16	XP_005245808		9E-37
dd Smed v4 22630 0 1	7.53530779	4.69E-17			none
dd Smed v4 13985 0 1	7.29001044	4.60E-20	NP_003006	SFRP5	2E-37
dd Smed v4 33384 0 1	6.88542826	6.60E-08	NP_001034485	MPEG1	1E-113
dd Smed v4 27668 0 1	6.71063151	2.11E-16	XP_005247264		3E-60
dd Smed v4 23249 0 1	6.22129683	9.22E-11	NP_997188	FOXD	2E-53
dd Smed v4 13188 0 1	6.19594595	1.24E-20	NP_000207	KAL1	1E-21
dd Smed v4 8829 0 1	5.75267461	1.39E-05	NP_002622	PGD	0
dd Smed v4 811 0 1	5.64556804	0.03936867	NP_694949		1.8
dd Smed v4 23400 0 2	5.383817	0.01770941	NP_001171886		6.8
dd Smed v4 35379 0 1	4.98246281	4.67E-14	NP_665804	ISL2	1E-21
dd Smed v4 20026 0 1	4.85114272	5.10E-12	NP_001120963		3.1
dd Smed v4 23030 0 1	4.79826173	2.41E-10	NP_899068		1.8
dd Smed v4 13875 0 1	4.7970656	1.04E-15			none
dd Smed v4 26780 0 1	4.77713424	3.14E-12			none
dd Smed v4 8371 0 1	4.5297811	6.10E-13	NP_002721	PRKACA	2E-168
dd Smed v4 17397 0 1	3.74170611	8.11E-05	NP_835455	PTF1A	4E-26
dd Smed v4 22615 0 1	3.43904371	0.00248363	NP_001171548		8E-11
dd Smed v4 25387 0 1	3.10389403	0.02535133	NP_001664		3E-106
dd Smed v4 12674 0 1	3.02630815	1.65E-09	XP_005272339		1E-21
dd Smed v4 12674 0 3	3.01336957	2.27E-09	XP_005272339		6E-22
dd Smed v4 22585 0 1	2.91837688	3.20E-08	NP_003404	ZIC3	7E-85
dd Smed v4 12674 0 2	2.84959911	1.50E-08	XP_005272339		1E-21
dd Smed v4 28401 0 1	2.8157737	0.01449827			none
dd Smed v4 16571 0 1	2.76772191	3.44E-08	NP_003459	FZD5	0
dd Smed v4 42614 0 2	2.75160348	0.03429768	NP_665802	TRAF6	2.9
dd Smed v4 33456 0 1	2.65087431	6.84E-05	NP_149416	Nkx2-4	3E-26
dd Smed v4 19933 0 1	2.58790847	0.0006014	NP_004113	GHSR	1.4
dd Smed v4 10673 0 1	2.57214062	1.39E-06	XP_005274075		2E-48
dd Smed v4 9910 0 1	2.47624001	6.12E-05	XP_005272444		2E-22
dd Smed v4 9584 0 3	2.43705382	1.17E-05	NP_006341	FST	1E-09
dd Smed v4 30210 0 1	2.31877966	0.0009896	NP_919431		4.7
dd Smed v4 6222 0 1	2.3009088	0.00513488	XP_005269502		0.0002
dd Smed v4 9584 0 2	2.27013247	0.00027233	NP_006341		1E-09

dd Smed v4 18393 0 4	2.26175917	0.00573249	NP 734465		3E-37
dd Smed v4 18393 0 3	2.25821197	0.0054999	NP 734465		3E-37
dd Smed v4 44405 0 1	2.25140824	0.02464183			none
dd Smed v4 13071 0 1	2.24682496	0.00059769	NP 150094	CSMD1	5E-27
dd Smed v4 31236 0 1	2.24101958	0.02124317	NP 003459	FZD5	3E-50
dd Smed v4 15506 0 1	2.23873904	0.00726594	NP 003059	SNAI2	3E-38
dd Smed v4 9584 0 1	2.22006544	0.01520016	NP 006341		1E-09
dd Smed v4 29263 0 1	2.2056746	0.0001583	NP 065907	TSHZ3	0.49
dd Smed v4 13823 0 1	2.1998619	0.0001554	NP 005609		2E-84
dd Smed v4 12943 0 1	2.19478148	0.0010036	XP 005253366		4E-11
dd Smed v4 8804 0 2	2.14794231	0.00018933	NP 006473	DYRK2	0.95
dd Smed v4 18393 0 2	2.12704161	0.01465413	NP 734465		4E-37
dd Smed v4 47123 0 1	2.11159862	0.00696583	XP 005251972		1E-31
dd Smed v4 10732 0 1	2.10451803	0.00047368	NP 000700	BCKDHA	3E-132
dd Smed v4 1312 0 1	2.08080206	0.04144184			none
dd Smed v4 15691 0 1	2.06785537	0.00677505	NP 055289	SMPDL3B	2E-53
dd Smed v4 17154 0 1	2.06360374	0.00352505	XP 005271074		1E-180
dd Smed v4 9120 0 1	2.06045638	0.00248648	NP 001123498	FAM115C	7E-23
dd Smed v4 12111 0 1	2.04690434	0.0395702	NP 003053	SLIT3	0
dd Smed v4 8804 0 1	2.03978761	0.00088081	NP 006473	DYRK2	0.96
dd Smed v4 8804 0 3	2.0266658	0.001511	XP 005254555		2.9
dd Smed v4 12229 0 1	1.95318569	0.00269076	NP 775180		2E-50
dd Smed v4 15531 0 2	1.94127876	0.00707313	NP 001230185		1E-27
dd Smed v4 8729 0 1	1.93763453	0.00526527	XP 005262822		0.003
dd Smed v4 11823 0 1	1.9337992	0.00218544	NP 003459	FZD5	0
dd Smed v4 4311 0 1	1.92850407	0.00839347	NP 076418		2.6
dd Smed v4 9825 0 1	1.92429812	0.00494281			none
dd Smed v4 15531 0 1	1.90988234	0.00439521	NP 009060	ZIC2	6E-79
dd Smed v4 11681 0 1	1.89777614	0.03222184	NP 055916	GLT25D2	6E-98
dd Smed v4 9485 0 1	1.89092128	0.00450234	NP 006746	TALDO1	3E-119
dd Smed v4 7063 0 2	1.86854599	0.00935967	NP 001077075		2E-57
dd Smed v4 10716 0 1	1.8521683	0.0086908	NP 060087	NOTCH1	1E-56
dd Smed v4 13867 0 1	1.82393362	0.02210195	XP 005263345		3.2
dd Smed v4 28209 0 1	1.82090092	0.0293101	NP 000530	RHO	0.0006
dd Smed v4 15423 0 1	1.82074093	0.02912632	NP 005441	NOG	1E-18
dd Smed v4 11070 0 1	1.80805686	0.0138137	NP 003004		4E-24
dd Smed v4 17168 1 1	1.79925792	0.0329622	NP 114072	FZD8	2E-45
dd Smed v4 14635 0 1	1.78837979	0.04173564	NP 001445	FOXJ1	1E-34
dd Smed v4 7063 0 1	1.78216881	0.02304113	NP 001077075		5E-56
dd Smed v4 4267 0 1	1.7741106	0.03204281	NP 000822	GRIK3	3E-146
dd Smed v4 4267 0 9	1.77052086	0.0329622	NP 000822	GRIK3	4E-147
dd Smed v4 12182 0 1	1.76825259	0.03915556	NP 000737	CHRNA7	1E-116

dd Smed v4 9677 0 1	1.75849226	0.02168951	NP_001265548		6E-66
dd Smed v4 2507 0 4	1.75647429	0.02786212	NP_001032394	LPPR5	2E-24
dd Smed v4 13570 0 1	1.7009656	0.0469487	NP_078858	FAT4	4E-58
dd Smed v4 8606 0 1	1.69461589	0.0426178	XP_005271700		2E-61

**Supplemental Table 2. Anterior pole enriched genes in 72hpa blastemas.** Genes with significantly higher ( $p_{\text{adj}} < 0.05$ ) expression in anterior pole pieces compared to flanking pieces in anterior blastemas of 72hpa animals are shown, ranked by their fold-change over control from highest to lowest. Known anterior pole genes are color coded – *foxD* (blue), *notum* (red), *fst* (green), *zic-1* (brown). *pitx* was not on the list. Also shown are human best BLAST hits and their E-values, along with Dresden assembly contig identifiers.

**Supplemental Table 3.** Posterior pole enriched genes from single-cell sequencing and analysis

Contig ID	mle	Z	Human accession	Human name	E-value
dd_Smed_v4_28398_0	9.05128758	7.16081298	NP_005421	WNT1	3.00E-59
dd_Smed_v4_23400_0	8.5279138	7.16081298	NP_001171886		6.8
dd_Smed_v4_16466_0	6.61913887	7.16073803	NP_005240	FOXP1	7.00E-36
dd_Smed_v4_15253_0	7.38880618	7.15736591	NP_005020	PITX3	2.00E-42
dd_Smed_v4_13943_0	7.11172595	7.09043489	NP_059115	ACCN5	7.00E-15
dd_Smed_v4_8860_0	5.32609779	7.01361742	NP_056471	KIF26A	3.00E-41
dd_Smed_v4_6182_0	6.46520541	6.9526941	NP_005771	LHFP	5.00E-16
dd_Smed_v4_16466_1	5.78789818	6.7040162	NP_005240	FOXP1	4.00E-13
dd_Smed_v4_14613_0	6.34205864	6.539963	XP_005266465		6.00E-71
dd_Smed_v4_16650_0	5.91104495	6.44542252			none
dd_Smed_v4_6508_0	5.51081795	6.16651566	NP_056094		6.00E-135
dd_Smed_v4_1230_0	5.07980425	6.14888621	NP_008929	SCGN	5.00E-64
dd_Smed_v4_18843_0	5.38767118	5.90564186	NP_001072	CUBN	7.00E-19
dd_Smed_v4_10673_0	5.94183164	5.86254258	XP_005274075		2.00E-48
dd_Smed_v4_20026_0	5.26452441	5.62205627	NP_001120963		3.1
dd_Smed_v4_15516_0	5.04901756	5.28926772	NP_001186699		3.00E-17
dd_Smed_v4_15362_0	4.77193733	5.26399394	XP_005268509		2.00E-50
dd_Smed_v4_8130_0	4.24856356	4.77200927	XP_005266064		2.00E-12
dd_Smed_v4_13188_0	4.4948571	4.44819458	NP_000207	KAL1	1.00E-21
dd_Smed_v4_13205_0	4.37171033	4.37408858	NP_008819		3.00E-19
dd_Smed_v4_14161_0	4.43328371	4.29039531	NP_940966	DNAH12	2
dd_Smed_v4_11409_0	3.72518979	4.2821464	XP_005254470		3.00E-28
dd_Smed_v4_10911_0	5.81868487	4.26914909	NP_001035880		2.00E-16
dd_Smed_v4_5133_0	4.18699017	4.19750482			none
dd_Smed_v4_21755_0	5.41845787	4.06424792			none
dd_Smed_v4_11827_0	3.72518979	3.85037447	NP_001182325		6.8
dd_Smed_v4_11876_0	3.38653617	3.83539618	NP_000205	JAG1	0
dd_Smed_v4_17402_0	3.81754986	3.80514239	NP_001710	BMP7	7.00E-31
dd_Smed_v4_13823_0	4.21777686	3.79744983	NP_005609		2.00E-84
dd_Smed_v4_8820_0	4.61800387	3.77944944	NP_665804	ISL2	1.00E-44
dd_Smed_v4_10730_0	3.41732286	3.70747439	NP_003719	UNC5C	2.00E-91
dd_Smed_v4_18393_0	3.2633894	3.63023225	NP_734465		3.00E-37
dd_Smed_v4_17288_0	5.60317802	3.55701264	NP_940799	GHSR	4E-09
dd_Smed_v4_16202_0	3.97148332	3.52668391			none
dd_Smed_v4_12432_0	3.90990994	3.51686582	XP_005245278		3.00E-34
dd_Smed_v4_2738_0	3.87912325	3.47466355	NP_001193728		0
dd_Smed_v4_2492_0	3.97148332	3.46423097	XP_005263044		2.00E-54
dd_Smed_v4_7930_0	4.21777686	3.46303789	XP_005266463		4.00E-45
dd_Smed_v4_2511_0	3.90990994	3.24139819	XP_005264622		0.009
dd_Smed_v4_50225_0	3.90990994	3.1748102			none

dd_Smed_v4_10545_0	3.90990994	3.14201629			none
dd_Smed_v4_7392_0	3.01709586	3.13783507	NP_077025	C20orf7	2.00E-26
dd_Smed_v4_9547_0	3.2633894	3.11759697	NP_008954		0
dd_Smed_v4_59018_0	4.4948571	3.10274336	XP_005256266		7.6
dd_Smed_v4_7195_0	2.49372209	3.05348246	NP_005206	DCC	1.00E-21
dd_Smed_v4_3391_0	2.61686886	3.04837432	NP_001104488		0.002
dd_Smed_v4_90059_0	3.04788255	3.03300054	NP_001004297		0.004
dd_Smed_v4_3187_0	3.57125632	3.02748889	NP_114104	TEKT3	2.00E-128
dd_Smed_v4_100368_0	2.58608216	2.99795481	NP_001229597		3.1
dd_Smed_v4_9208_0	3.01709586	2.99142628	XP_005255383		4.00E-131
dd_Smed_v4_8167_0	2.8323757	2.97222176	NP_001161354	ANKRD50	7E-09
dd_Smed_v4_9584_0	3.94069663	2.96333473	NP_006341		1E-09
dd_Smed_v4_68282_0	2.80158901	2.92628752	NP_001073946	ODZ3	0.46
dd_Smed_v4_7482_0	3.57125632	2.91873426	NP_004846	PIGB	2.00E-99
dd_Smed_v4_13603_0	4.34092363	2.8888326			none
dd_Smed_v4_18505_0	3.57125632	2.83792335	NP_002439	MSX1	4.00E-40
dd_Smed_v4_4172_0	2.37057532	2.83116471	NP_057315	NLK	2.00E-135
dd_Smed_v4_15499_0	4.40249702	2.8084847	NP_001158210	CALCR	1.00E-21
dd_Smed_v4_2407_0	3.04788255	2.79493835	NP_001004334	GPR179	0.00000004
dd_Smed_v4_81840_0	2.92473578	2.793424	NP_001392		0.003
dd_Smed_v4_1040_0	2.92473578	2.79108238			none
dd_Smed_v4_6981_0	4.95665748	2.74430179	NP_001244321		5.00E-22
dd_Smed_v4_27499_0	3.57125632	2.74376603	NP_064552	NMUR2	2.00E-45
dd_Smed_v4_11024_0	2.4321487	2.73111521	NP_002002		6.00E-83
dd_Smed_v4_9602_0	2.92473578	2.72584843	XP_005274296		1E-09
dd_Smed_v4_3627_0	3.60204302	2.69193136	NP_057616		7.00E-53
dd_Smed_v4_26059_0	2.98630917	2.65743346	NP_001106272		2
dd_Smed_v4_7345_0	3.81754986	2.62855427	XP_005249734		5E-09
dd_Smed_v4_25503_0	3.01709586	2.58414546			none
dd_Smed_v4_23806_0	3.04788255	2.58128257	NP_003327	UBE2A	7.3
dd_Smed_v4_11533_0	3.47889625	2.55328582	NP_004778	SLIT2	0.0000006
dd_Smed_v4_6306_0	2.67844224	2.53895102	NP_001028198	C19orf6	1.00E-103
dd_Smed_v4_7243_0	3.81754986	2.52279802	NP_689493	SYT11	3.00E-80
dd_Smed_v4_11241_0	3.57125632	2.51974027	NP_078849	C6orf211	2.00E-64
dd_Smed_v4_9658_0	3.38653617	2.51962107	NP_689808	PGBD4	0.00008
dd_Smed_v4_12634_0	2.4321487	2.50292645	NP_005584	MYF5	8.00E-19
dd_Smed_v4_6719_0	3.41732286	2.49533484	NP_002651	PLCG1	8.00E-114
dd_Smed_v4_32635_0	4.18699017	2.45458325			none
dd_Smed_v4_12759_0	3.50968294	2.44878814	NP_055650		3.00E-91
dd_Smed_v4_12423_0	2.70922893	2.42682483	XP_005269823		0.13
dd_Smed_v4_5680_0	2.18585516	2.42588937	NP_003581	CUL3	0
dd_Smed_v4_3754_0	3.81754986	2.42360844	XP_005260560		3.00E-26

dd_Smed_v4_12828_0	2.61686886	2.4191912	NP_064594	SHD	6.00E-16
dd_Smed_v4_5181_0	2.61686886	2.41330568	XP_005265671		3.00E-98
dd_Smed_v4_33278_0	4.4948571	2.40163931			none
dd_Smed_v4_8729_0	3.63282971	2.3940282	XP_005262822		0.003
dd_Smed_v4_37672_0	2.89394909	2.39106589	XP_005264206		0.94
dd_Smed_v4_4381_0	3.10945594	2.39083248	NP_001193599		8.7
dd_Smed_v4_7862_0	3.57125632	2.38630941	NP_277052		2.00E-91
dd_Smed_v4_17743_0	3.94069663	2.38552885	NP_001128522	IGSF9	2.00E-44
dd_Smed_v4_12771_0	3.35574948	2.38517128	XP_005271139		2.00E-92
dd_Smed_v4_13743_0	2.67844224	2.35302051			none
dd_Smed_v4_80809_0	3.10945594	2.35125766	XP_005247656		3.5
dd_Smed_v4_25158_0	4.52564379	2.34716954	NP_009122	WIF1	0.001
dd_Smed_v4_13372_0	2.64765555	2.33973917	NP_001517	HCRTR2	0.000003
dd_Smed_v4_5396_0	2.0319217	2.33374352	NP_001078846	MCC	3.00E-24
dd_Smed_v4_4585_0	2.67844224	2.31912774			none
dd_Smed_v4_52794_0	2.95552247	2.31548622			none
dd_Smed_v4_10295_0	2.18585516	2.31423595	NP_005064	SLC15A1	4.9
dd_Smed_v4_11640_0	3.54046963	2.31325704			none
dd_Smed_v4_11236_0	2.67844224	2.31281982	NP_000515	HTR1A	3.00E-51
dd_Smed_v4_5062_0	1.90877493	2.30582843			none
dd_Smed_v4_21713_0	2.58608216	2.29394765	NP_848545	40971	3.00E-13
dd_Smed_v4_17675_0	2.06270839	2.29345681			none
dd_Smed_v4_3879_0	2.09349509	2.2873832	NP_001153772	PANX2	0.008
dd_Smed_v4_13944_0	3.01709586	2.28453442	NP_001269865		5.00E-13
dd_Smed_v4_15781_0	2.8631624	2.27916112	NP_056501	FAM155B	0.002
dd_Smed_v4_21082_0	2.89394909	2.27848784	NP_000515	HTR1A	2.00E-40
dd_Smed_v4_9830_0	3.81754986	2.27251625			none
dd_Smed_v4_10404_0	3.63282971	2.27091552	NP_006388	RNASEH2A	1.00E-70
dd_Smed_v4_9266_0	2.49372209	2.26513476	XP_005257434		7.00E-88
dd_Smed_v4_4670_0	2.70922893	2.25974649	NP_005264	GNB2	8.00E-101
dd_Smed_v4_6877_0	2.4629354	2.25863451	XP_005263050		0
dd_Smed_v4_817_1	3.87912325	2.2519621	NP_443122	PGLYRP2	2.00E-41
dd_Smed_v4_52590_0	1.97034832	2.25034667			none
dd_Smed_v4_585_0	2.06270839	2.24772157	XP_003960855		5.2
dd_Smed_v4_7847_0	2.4321487	2.24731132	NP_861450		4.00E-17
dd_Smed_v4_7989_0	2.52450878	2.23826976	XP_005257762		9.00E-15
dd_Smed_v4_14230_0	2.92473578	2.22644163			none
dd_Smed_v4_3349_0	2.49372209	2.22396457	XP_005271981		2.00E-53
dd_Smed_v4_11629_0	2.09349509	2.21885031	NP_079187	WLS	5.00E-23
dd_Smed_v4_13377_0	3.38653617	2.21536017	NP_055512	NOS1AP	9.00E-52
dd_Smed_v4_23157_0	2.40136201	2.20631937	NP_001248762		2.00E-13
dd_Smed_v4_11394_0	4.4948571	2.19804343	XP_005251402		0

dd_Smed_v4_29119_0	4.18699017	2.19753504	NP_006047	NMUR1	0.3
dd_Smed_v4_7114_0	2.06270839	2.19060407	XP_005251736		0.92
dd_Smed_v4_10186_0	3.01709586	2.18972804	NP_114091	BBS2	0
dd_Smed_v4_1092_0	2.0319217	2.187676			none
dd_Smed_v4_5758_0	2.24742855	2.18235482	NP_060506	ATG2B	8.00E-28
dd_Smed_v4_11739_0	2.4321487	2.18037384			none
dd_Smed_v4_16503_0	2.92473578	2.17840138			none
dd_Smed_v4_26331_0	3.63282971	2.1782042			none
dd_Smed_v4_38403_0	3.04788255	2.17763311			none
dd_Smed_v4_29966_0	3.54046963	2.17471499	XP_005277406		4.7
dd_Smed_v4_11468_0	3.29417609	2.16890158	XP_005276530		1E-09
dd_Smed_v4_11571_0	2.06270839	2.16879539	XP_005271017		9.00E-84
dd_Smed_v4_13835_0	2.80158901	2.16714053	NP_612201		2.00E-35
dd_Smed_v4_12714_0	1.29304108	2.16507425	NP_758954	FBXO16	2.00E-56
dd_Smed_v4_4302_0	2.95552247	2.15386632	NP_003895	ZNF259	1.00E-106
dd_Smed_v4_2805_0	3.50968294	2.15211166			none
dd_Smed_v4_71655_0	2.30900193	2.1500088	NP_001139728	ZDHHC15	2.3
dd_Smed_v4_1781_0	2.18585516	2.14827657	XP_005256615		0
dd_Smed_v4_49907_0	2.27821524	2.14814216			none
dd_Smed_v4_9546_0	1.90877493	2.14258973	NP_001180263		3.00E-109
dd_Smed_v4_7474_0	2.64765555	2.13477459	NP_004687	SLC16A4	2.00E-15
dd_Smed_v4_9513_0	3.38653617	2.13338605	NP_060712	SLC47A1	1.00E-57
dd_Smed_v4_6180_0	3.38653617	2.12990451	NP_055708		1.00E-19
dd_Smed_v4_38249_0	2.4629354	2.12740021	NP_002146	HSPA6	0.001
dd_Smed_v4_1566_0	3.29417609	2.12704146	NP_001188457		0
dd_Smed_v4_13412_0	2.21664186	2.12227035	NP_002578		2.00E-60
dd_Smed_v4_6736_0	2.24742855	2.11824418	XP_005252032		1.00E-19
dd_Smed_v4_7157_0	2.06270839	2.11315597	NP_066300	LZTS1	2.1
dd_Smed_v4_13085_0	2.27821524	2.1096387	XP_005264558		4.00E-45
dd_Smed_v4_7415_0	2.4629354	2.08165536	XP_005265684		2.00E-89
dd_Smed_v4_10068_0	2.61686886	2.08146866	XP_005246536		2.00E-60
dd_Smed_v4_5187_0	3.07866924	2.08095795	NP_659403	FREM1	3.00E-89
dd_Smed_v4_5823_0	2.80158901	2.0720334	XP_005270594		0.54
dd_Smed_v4_26304_0	2.92473578	2.06947669	NP_954983	NEK5	0.00002
dd_Smed_v4_1173_0	3.20181601	2.06836853			none
dd_Smed_v4_17148_0	3.20181601	2.06750825			none
dd_Smed_v4_7509_0	2.4321487	2.06286282	NP_002065	GNB1	3.00E-37
dd_Smed_v4_26870_0	2.74001563	2.06103463	NP_001070711		3.00E-12
dd_Smed_v4_19912_0	2.8631624	2.06097214	XP_005264764		9.00E-14
dd_Smed_v4_3014_0	2.12428178	2.06014111	NP_002475	NUBP1	1.00E-100
dd_Smed_v4_13817_0	3.6636164	2.05627834	NP_733839		5.00E-52
dd_Smed_v4_3339_0	3.41732286	2.05318556	NP_001243354		8.00E-24

dd Smed v4 835 0	2.55529547	2.04741511	NP_001265128		1.00E-110
dd Smed v4 14730 0	3.60204302	2.04313543	XP_005255711		0
dd Smed v4 39157 0	1.87798824	2.03721468	NP_066549	ART4	9
dd Smed v4 19210 0	3.90990994	2.02772919	NP_004645	USP9Y	1.7
dd Smed v4 10902 0	2.06270839	2.02616879	NP_001111	MFSD10	2.00E-62
dd Smed v4 9941 0	2.4321487	2.02598101	NP_001122101	PAK6	1E-09
dd Smed v4 9272 0	2.37057532	2.02295629	XP_005259609		2.00E-104
dd Smed v4 6075 0	3.20181601	2.02100117	NP_001266279		2.00E-61
dd Smed v4 7015 0	2.49372209	2.01781725	XP_005271090		2.00E-87
dd Smed v4 84769 0	3.01709586	2.01734704			none
dd Smed v4 9010 0	2.67844224	2.01535387	NP_009144	PRAF2	1.00E-15
dd Smed v4 8406 0	2.00113501	2.01220367	NP_000430	PCSK1	4.00E-159
dd Smed v4 2641 0	2.09349509	2.01059142	NP_001779	41159	1.00E-145
dd Smed v4 12850 0	2.27821524	2.01024188	NP_777591	CCDC75	1.00E-36
dd Smed v4 3670 0	4.40249702	1.99942576	NP_775899	DNAH17	0
dd Smed v4 8690 0	2.37057532	1.9981038	NP_071426	LRRC4	6.00E-10
dd Smed v4 17293 0	4.27935025	1.9965563	NP_065210		6.00E-30
dd Smed v4 11432 0	2.27821524	1.9933014	NP_112190	CDT1	0.00000001
dd Smed v4 3375 0	2.40136201	1.99191499	NP_001151		2.00E-16
dd Smed v4 13903 0	2.4321487	1.99168034	XP_005274542		4.00E-23
dd Smed v4 10216 0	1.93956162	1.99048208	NP_003059	SNAI2	5.00E-52
dd Smed v4 9728 0	2.61686886	1.98658445			none
dd Smed v4 7611 0	2.52450878	1.97955316	XP_005269982		1.4
dd Smed v4 11088 0	2.24742855	1.97638153	NP_620305	SON	6.00E-10
dd Smed v4 7700 0	2.09349509	1.97603737	NP_647537		2.00E-31
dd Smed v4 8364 0	2.74001563	1.97466322	XP_005251090		0.1
dd Smed v4 6801 0	2.92473578	1.97436961	NP_006690	MAN1A2	4.00E-175
dd Smed v4 15518 0	2.33978863	1.97165337			none
dd Smed v4 8483 0	2.18585516	1.97048152	NP_201583		0.000001
dd Smed v4 2034 0	2.09349509	1.96632167	XP_005267452		1.00E-68
dd Smed v4 30279 0	3.50968294	1.96515467	NP_001245348		1.00E-16
dd Smed v4 5353 0	2.24742855	1.96182804	NP_003757	BECN1	8.00E-70

**Supplemental Table 3. Posterior pole enriched genes from single-cell sequencing and analysis.** Genes with significantly higher ( $Z > 11.6 = p < 0.05$ ) expression of *wnt1*<sup>+</sup> posterior single-cells compared to *wnt1*<sup>-</sup> muscle cells expressing *collagen* in both uninjured animals and regenerating posterior poles (Fig. S1A) poles. Cells were collected, sorted, and selected for sequencing as described (Fig. S1A). SCDE was used for differential expression analysis. Posterior cell-enriched genes in this table are ranked by their *Z* value from highest to lowest. Known posterior pole genes are color coded – *wnt1* (cyan), *pitx* (yellow), *islet* (magenta). Also shown are human best BLAST hits and their E-values, along with Dresden assembly contig identifiers. mle = maximum likelihood expression.

**Supplemental Table 4. Primers used to clone *nr4A* and its target genes**

Gene	Forward primer	Reverse primer
<i>nr4A</i>	CGCGAGTCAGTCAGCCAT	TGCCGTGGCTGGATGAAG
<i>col21a1</i>	TGGTGACAAATGAATGCTCACT	ACCAGGATCACCTTGGGGA
<i>mmp19</i>	TGCGATAGAATTTTTAGGGGCA	CTTGGGTTGTGCTGGGGT
<i>dd Smed v4 2972 0 1</i>	CAACAACAGAAGAACAACAACC	CAGTATTCGTACGCTCTTTGCA
<i>cal2</i>	TGGATTACTGATCTTCGCTTTTG	TCTTCAGCAGTCATCAAACCTAGA
<i>dd Smed v4 508 0 1</i>	CAGGAAGAAATACTCGTGCATCA	ACCAGTGCACGAAGGCTC
<i>vim</i>	TGCGTTGGAGTAAATAGAAAGCA	TGTTCAAGGGTGATATGCGCT
<i>pcdh1ly</i>	TTCTGCTGACAAAACCTCTCGA	AGTCATGACGCCCGAAG
<i>psap11</i>	TGCGTGACTTCTTCAAAGGA	GTGATCCGGTGCTGGCTT
<i>hspb1</i>	TGTGTAGTCACCTGTCTAGAGT	AGTGAGTTCAATGGATCATGCA
<i>qki</i>	CAATCTTTCACAAATCGTGTCCA	CAACGCAGAGTTCAAACAATGC

**Supplemental Table 4. Primer sequences used to clone *nr4A* and its gene targets.** Forward and reverse primers designed to clone their respective genes from planarian cDNA into pGEM-T Easy Vector. For cloning procedures, see Materials and Methods. Gene names are best human BLAST hits (non-italicized names), contig IDs (beginning with “dd”), or planarian genes with homology verified by phylogenetic analyses (*nr4A* and *vim*)

**Supplemental Table 5.** Nuclear receptor proteins and accession #s used in phylogenetic analysis

gi 74096287 ref NP_001027658.1  nuclear receptor 1 [Ciona intestinalis]
gi 118343705 ref NP_001071673.1  nuclear receptor [Ciona intestinalis]
gi 118343759 ref NP_001071700.1  nuclear receptor [Ciona intestinalis]
gi 118343798 ref NP_001071721.1  nuclear receptor [Ciona intestinalis]
gi 118343826 ref NP_001071735.1  nuclear receptor [Ciona intestinalis]
gi 118343914 ref NP_001071779.1  nuclear receptor [Ciona intestinalis]
gi 118343916 ref NP_001071780.1  nuclear receptor [Ciona intestinalis]
gi 118343962 ref NP_001071801.1  nuclear receptor [Ciona intestinalis]
gi 118343970 ref NP_001071806.1  nuclear receptor [Ciona intestinalis]
gi 118343980 ref NP_001071809.1  nuclear receptor [Ciona intestinalis]
gi 118344048 ref NP_001071847.1  nuclear receptor [Ciona intestinalis]
gi 118344234 ref NP_001071940.1  nuclear receptor [Ciona intestinalis]
gi 118344280 ref NP_001071962.1  nuclear receptor [Ciona intestinalis]
gi 118344390 ref NP_001072021.1  nuclear receptor [Ciona intestinalis]
gi 118344438 ref NP_001072044.1  nuclear receptor [Ciona intestinalis]
gi 147900931 ref NP_001087206.1  nuclear receptor [Ciona intestinalis]
gi 147904386 ref NP_001087213.1  nuclear receptor [Ciona intestinalis]
gi 18859511 ref NP_571415.1  thyroid hormone receptor beta [Danio rerio]
gi 18859543 ref NP_570994.1  vitamin D3 receptor A [Danio rerio]
gi 23308675 ref NP_694491.1  estrogen receptor [Danio rerio]
gi 45387535 ref NP_991109.1  hepatic nuclear factor 4, beta [Danio rerio]
gi 47086127 ref NP_998119.1  estrogen-related receptor gamma [Danio rerio]
gi 50345002 ref NP_001002173.1  nuclear receptor subfamily 4 group A member 1 [Danio rerio]
gi 55925486 ref NP_956886.1  nuclear receptor subfamily 2 group F member 1-B [Danio rerio]
gi 57525699 ref NP_001003608.1  nuclear receptor subfamily 2 group E member 1 [Danio rerio]
gi 62990125 ref NP_571481.2  retinoic acid receptor alpha-A [Danio rerio]
gi 66472508 ref NP_001018458.1  nuclear receptor subfamily 2 group C member 1 [Danio rerio]
gi 118766323 ref NP_571331.2  nuclear receptor subfamily 6 group A member 1-A [Danio rerio]
gi 130497366 ref NP_001076416.1  nuclear receptor subfamily 0 group B member 1 [Danio rerio]
gi 154240734 ref NP_001093873.1  mineralocorticoid receptor [Danio rerio]
gi 164414403 ref NP_001103637.1  nuclear receptor ROR-alpha [Danio rerio]
gi 238550133 ref NP_001154805.1  peroxisome proliferator-activated receptor alpha [Danio rerio]
gi 238859643 ref NP_001155023.1  retinoic acid receptor RXR-alpha-A [Danio rerio]
gi 829569727 ref NP_991292.2  nuclear receptor subfamily 1 group D member 1 [Danio rerio]
gi 922960040 ref NP_001300658.1  nuclear receptor subfamily 5 group A member 2 [Danio rerio]
gi 983616478 ref NP_001017545.2  oxysterols receptor LXR-alpha [Danio rerio]
gi 157236 gb AAA28464.1  DHR39 [Drosophila melanogaster]
gi 157458 gb AAA28542.1  FTZ-F1 [Drosophila melanogaster]
gi 929562 emb CAA61534.1  DHR38 [Drosophila melanogaster]
gi 1036839 gb AAC46927.1  DHR78 [Drosophila melanogaster]
gi 1036841 gb AAC46928.1  DHR96 [Drosophila melanogaster]

gi 10726915 gb AAF51629.2  knirps, isoform A [Drosophila melanogaster]
gi 17136580 ref NP_476781.1  ultraspiracle, isoform A [Drosophila melanogaster]
gi 17864126 ref NP_524596.1  tailless [Drosophila melanogaster]
gi 23171091 gb AAN13541.1  seven up, isoform A [Drosophila melanogaster]
gi 24582907 ref NP_476887.2  hepatocyte nuclear factor 4, isoform A [Drosophila melanogaster]
gi 24585962 ref NP_724456.1  ecdysone receptor, isoform A [Drosophila melanogaster]
gi 24660692 ref NP_729340.1  estrogen-related receptor, isoform A [Drosophila melanogaster]
gi 24666206 ref NP_524133.2  Ecdysone-induced protein 75B, isoform A [Drosophila melanogaster]
gi 24667937 ref NP_524195.2  Ecdysone-induced protein 78C, isoform A [Drosophila melanogaster]
gi 440216341 gb AGB95004.1  Hr4, isoform E [Drosophila melanogaster]
gi 4506755 ref NP_002948.1  retinoic acid receptor RXR-alpha isoform a [Homo sapiens]
gi 4507537 ref NP_003260.1  nuclear receptor subfamily 2 group E member 1 isoform b [Homo sapiens]
gi 5016090 ref NP_000466.2  nuclear receptor subfamily 0 group B member 1 [Homo sapiens]
gi 5032173 ref NP_005645.1  COUP transcription factor 1 [Homo sapiens]
gi 7549811 ref NP_005027.2  peroxisome proliferator-activated receptor alpha [Homo sapiens]
gi 13430848 ref NP_068370.1  nuclear receptor subfamily 1 group D member 1 [Homo sapiens]
gi 14916494 ref NP_000956.2  retinoic acid receptor beta isoform 1 [Homo sapiens]
gi 18860920 ref NP_004442.3  steroid hormone receptor ERR1 isoform 1 [Homo sapiens]
gi 19743903 ref NP_599023.1  nuclear receptor ROR-alpha isoform a [Homo sapiens]
gi 20070193 ref NP_004950.2  steroidogenic factor 1 [Homo sapiens]
gi 20127452 ref NP_003241.2  thyroid hormone receptor alpha isoform 2 [Homo sapiens]
gi 27894344 ref NP_775180.1  nuclear receptor subfamily 4 group A member 1 isoform 1 [Homo sapiens]
gi 53729325 ref NP_201591.2  nuclear receptor subfamily 6 group A member 1 isoform 1 [Homo sapiens]
gi 170295804 ref NP_001116214.1  estrogen receptor isoform 1 [Homo sapiens]
gi 189491739 ref NP_003288.2  nuclear receptor subfamily 2 group C member 1 isoform a [Homo sapiens]
gi 194294517 ref NP_005684.2  oxysterols receptor LXR-alpha isoform 1 [Homo sapiens]
gi 323714265 ref NP_001017536.1  vitamin D3 receptor isoform VDRB1 [Homo sapiens]
gi 324021673 ref NP_001191188.1  glucocorticoid receptor isoform alpha-C1 [Homo sapiens]
gi 385298694 ref NP_001245284.1  hepatocyte nuclear factor 4-alpha isoform HNF4alpha4 [Homo sapiens]
gi 6671531 ref NP_031456.1  nuclear receptor subfamily 0 group B member 1 [Mus musculus]
gi 6679695 ref NP_031982.1  estrogen receptor isoform 1 [Mus musculus]
gi 6754216 ref NP_034574.1  nuclear receptor subfamily 4 group A member 1 [Mus musculus]
gi 6755384 ref NP_035435.1  retinoic acid receptor RXR-alpha isoform 1 [Mus musculus]
gi 7305439 ref NP_038674.1  nuclear receptor ROR-alpha isoform 1 [Mus musculus]
gi 20522231 ref NP_620639.1  steroidogenic factor 1 [Mus musculus]
gi 22726205 ref NP_689415.1  nuclear receptor subfamily 2 group E member 1 [Mus musculus]
gi 30017357 ref NP_835161.1  thyroid hormone receptor alpha isoform 2 [Mus musculus]
gi 31543500 ref NP_035274.2  peroxisome proliferator-activated receptor alpha [Mus musculus]
gi 31543944 ref NP_033530.2  vitamin D3 receptor [Mus musculus]
gi 46575916 ref NP_032287.2  hepatocyte nuclear factor 4-alpha isoform HNF4alpha2 [Mus musculus]
gi 110625908 ref NP_663409.2  nuclear receptor subfamily 1 group D member 1 [Mus musculus]
gi 111185902 ref NP_034281.2  COUP transcription factor 1 [Mus musculus]

gi 112293262 ref NP_031979.2  steroid hormone receptor ERR1 [Mus musculus]
gi 116734873 ref NP_033050.2  retinoic acid receptor alpha isoform 1 [Mus musculus]
gi 121247453 ref NP_032199.3  glucocorticoid receptor [Mus musculus]
gi 171846245 ref NP_035759.3  nuclear receptor subfamily 2 group C member 1 [Mus musculus]
gi 227116316 ref NP_001153020.1  nuclear receptor subfamily 6 group A member 1 isoform 2 [Mus musculus]
gi 295148193 ref NP_001171201.1  oxysterols receptor LXR-alpha [Mus musculus]
gi 156357575 ref XP_001624292.1  predicted protein, partial [Nematostella vectensis]
gi 156359518 ref XP_001624815.1  predicted protein, partial [Nematostella vectensis]
gi 156374224 ref XP_001629708.1  predicted protein [Nematostella vectensis]
gi 156376474 ref XP_001630385.1  predicted protein [Nematostella vectensis]
gi 156376476 ref XP_001630386.1  predicted protein, partial [Nematostella vectensis]
gi 156378253 ref XP_001631058.1  predicted protein [Nematostella vectensis]
gi 156380693 ref XP_001631902.1  predicted protein [Nematostella vectensis]
gi 156387699 ref XP_001634340.1  predicted protein [Nematostella vectensis]
gi 156387775 ref XP_001634378.1  predicted protein [Nematostella vectensis]
gi 156389440 ref XP_001634999.1  predicted protein, partial [Nematostella vectensis]
gi 156389667 ref XP_001635112.1  predicted protein [Nematostella vectensis]
gi 156392347 ref XP_001636010.1  predicted protein [Nematostella vectensis]
gi 156394045 ref XP_001636637.1  predicted protein, partial [Nematostella vectensis]
gi 156399521 ref XP_001638550.1  predicted protein, partial [Nematostella vectensis]

**Supplemental Table 5. Nuclear receptor proteins used in phylogenetic analysis.**

Representative proteins from each of the six subfamilies of the nuclear receptors from *Homo sapiens*, *Mus musculus*, *Danio rerio*, *Nematostella vectensis*, *Ciona intestinalis*, and *Drosophila melanogaster* are shown, along with their names and accession numbers. For more details about phylogenetic analysis see Fig. S2.

## Materials and Methods

### Bulk RNA sequencing

Cut animal fragments were diced with a scalpel, homogenized using Qiagen TissueLyser III, and RNA was extracted using TRIzol according to the manufacturer's protocol. Between 0.5 and 1 $\mu$ g of RNA was used for cDNA sequencing library synthesis using TruSeq RNA library prep kit V2 (Illumina) following the manufacturer's protocol. Libraries were sequenced on Illumina HiSeq for an average sequencing depth of 20-30 million reads per replicate sample.

### Single-cell RNA sequencing and expression analysis

Cut animal fragments were diced with a scalpel, macerated with collagenase treatment, stained with Hoechst (1:25) and propidium iodide (1:5000) and 2C (differentiated, non-dividing) cells were sorted one-cell/well on 96-well plates containing 5 $\mu$ L of Buffer TCL with 1% 2-mercaptoethanol. Single-cell RNA sequencing libraries were prepared via the SmartSeq2 method, as previously described (Picelli et al., 2013; 2014). Briefly, a poly-dT oligo and a template-switching were used for reverse transcription. After cDNA amplification, single cell cDNA libraries were fragmented and tagged using the Nextera XT kit (Illumina). Single-cell cDNA libraries were then qRT-PCR screened for *wnt1* and *collagen* expression with the primers provided in Table S3. Selected libraries were sequenced on Illumina HiSeq for an average of 1-2 million reads per cell. Differential expression analysis of gene expression between pole cells and

non-pole cells was performed using the Single-Cell Differential Expression method, as described (Kharchenko et al., 2014).

### **Gene nomenclature**

Previously published and homology-verified planarian genes are in lowercase italics. Genes not analyzed for homology by phylogenetics but that have strong (E-value < 0.05) human best-BLAST matches are in uppercase italics. Names that begin with “dd\_” are Smedv4.1 Dresden transcriptome assembly contig identifiers for genes that have no human, mouse, or *C. elegans* best BLAST match.

### **Gene cloning**

Primers used to clone *nr4A* and its targets are listed in Table S4. Genes were cloned from cDNA into the pGEM vector (Promega) and transformed into *E. coli* DH10B by heat-shock. Bacteria were plated on agarose plates containing 1:500 carbenicillin, 1:200 Isopropylthio-b-D-galactoside (IPTG), and 1:625 5-bromo-4-chloro-3-indolyl- $\beta$ -D-galactopyranoside (X-gal) for overnight growth. Colonies were screened by colony PCR and gel electrophoresis. Plasmids were extracted from positive (white) colonies and subsequently validated by Sanger-sequencing.

### ***in situ* Hybridizations**

WISH with tetrazolium/5-bromo-4-chloro-3-indolyl phosphate (NBT/BCIP) was performed as described (Pearson et al., 2009). FISH and post-antibody binding washes and tyramide

development was performed as described (King and Newmark, 2013). Briefly, animals were killed in 5% NAC and treated with proteinase K (2 µg/ml). Animals were hybridized with RNA probes at 1:800 dilution overnight at 56 °C. Samples were then washed twice in each of pre-hybridization buffer, 1:1 pre- hybridization-2X SSC, 2X SSC, 0.2X SSC, PBS with Triton-X (PBST). Blocking was performed in 10% Western Blocking Reagent (Roche), 5% Casein and 5% Western Blocking Reagent, or 5% inactivated horse serum and 5% Western Blocking Reagent diluted in PBST solution when anti-DIG, anti-FITC, or anti-DNP antibodies were used. Post-antibody binding washes and tyramide development were performed as described (King and Newmark, 2013). Light images were taken with a Zeiss Discovery Microscope. Fluorescent images were taken with a Zeiss LSM700 Confocal Microscope. Fiji/ImageJ was used for FISH co-localization analyses.

## **RNAi**

dsRNA was transcribed *in vitro* (Promega reagents) from PCR-generated templates with flanking T7 promoters. It was then precipitated in ethanol, annealed after resuspension in water, and mixed with planarian food (liver). Each animal was fed about 2 ul of the liver containing dsRNA twice every week, with about 3 days between each feeding. Animals were then fixed seven days after the last feeding. The total amount of dsRNA per feeding per animal was kept constant as described before. Control RNAi used dsRNA against the *C. elegans unc22* transcript.

## **Immunostainings**

Animals were fixed in 4% formaldehyde solution as for *in situ* hybridization and treated as described (King and Newmark, 2013). The muscle antibody 6G10 was used at 1:100 dilution in PBSTB (0.1% TritonX, 0.1% BSA), and an anti-mouse-Alexa conjugated antibody was used at a 1:500 dilution. The SMEDWI-1 antibody was used at 1:1000 dilution in PBSTx (0.1% TritonX) with 10% horse serum, and an anti-rabbit-HRP antibody was used at 1:300 dilution in PBSTx (0.1% TritonX) with 10% horse serum.

### **Cell quantification and statistics**

All quantification was performed in a condition-blind manner. *collagen*<sup>+</sup> cells were counted in a 150µm wide by 100µm high rectangular area centered around the midline of the tip of the heads and tails in size-matched animals. TUNEL-positive cells were counted within a 550µm x 550µm region centered around the midline of head tips. Double EdU<sup>+</sup> and *collagen*<sup>+</sup> cells were counted within a 640µm x 640µm region centered around the midline of head tips. Unpaired (two-tailed) t-test was performed between conditions using Prism.

### **Phylogenetic analysis**

See Supplemental Figure 2 Legend. Accession numbers for nuclear receptor protein sequences are listed in Table S5.

### **Irradiation and EdU feeding regimen**

Animals were given lethal irradiation dosages of 6000 rads using a Gammcell 40 dual <sup>137</sup>cesium source. F-ara-EdU (Sigma) dissolved in DMSO at 50mg/mL was mixed with liver paste (3:1 liver : planarian water) for a final concentration of 0.5mg/mL. Animals were fed once with EdU and liver mix and fixed 8 days after as in *in situ* hybridization. Development was performed with click reaction, as described (Ji et al., 2017; Salic and Mitchison, 2008).

### **TUNEL Assay**

ApopTag® Red In Situ Apoptosis Detection Kit (Millipore) was used for the TUNEL assay. Animals were fixed as in *in situ* hybridization, incubated overnight at 37 °C in terminal transferase enzyme diluted in reaction buffer, washed in stop/wash buffer, rinsed in PBST (0.3% TritonX), and blocked for 30 min in PBSTx containing 5% heat inactivated horse serum and 5% Roche Western Block Reagent (Roche). Animals were then developed in anti-digoxigenin rhodamine conjugate diluted in block solution overnight at 4 °C in the dark.

## References

- Adell, T., Cebrià, F., Saló, E., Kay, R.R., Thompson, C.R.L., and Strutt, D. (2010). Gradients in planarian regeneration and homeostasis. *Cold Spring Harbor Perspectives in Biology* 2, a000505.
- Adell, T., Saló, E., Boutros, M., and Bartscherer, K. (2009). Smed-Evi/Wntless is required for  $\beta$ -catenin-dependent and -independent processes during planarian regeneration. *Development* 136, 905–910.
- Baker, K.D., Shewchuk, L.M., Kozlova, T., Makishima, M., Hassell, A., Wisely, B., Caravella, J.A., Lambert, M.H., Reinking, J.L., Krause, H., et al. (2003). The *Drosophila* orphan nuclear receptor DHR38 mediates an atypical ecdysteroid signaling pathway. *Cell* 113, 731–742.
- Bertrand, S., Brunet, F.G., Escriva, H., Parmentier, G., Laudet, V., and Robinson-Rechavi, M. (2004). Evolutionary genomics of nuclear receptors: from twenty-five ancestral genes to derived endocrine systems. *Molecular Biology and Evolution* 21, 1923–1937.
- Bridgham, J.T., Eick, G.N., Larroux, C., Deshpande, K., Harms, M.J., Gauthier, M.E.A., Ortlund, E.A., Degnan, B.M., and Thornton, J.W. (2010). Protein evolution by molecular tinkering: diversification of the nuclear receptor superfamily from a ligand-dependent ancestor. *PLoS Biol* 8, e1000497.
- Cebrià, F., Kobayashi, C., Umesono, Y., Nakazawa, M., Mineta, K., Ikeo, K., Gojobori, T., Itoh, M., Taira, M., Sánchez Alvarado, A., et al. (2002). FGFR-related gene *nou-darake* restricts brain tissues to the head region of planarians. *Nature* 419, 620–624.
- Currie, K.W., and Pearson, B.J. (2013). Transcription factors *lhx1/5-1* and *pitx* are required for the maintenance and regeneration of serotonergic neurons in planarians. *Development* 140, 3577–3588.
- Escriva, H., Bertrand, S., and Laudet, V. (2004). The evolution of the nuclear receptor superfamily. *Essays Biochem.* 40, 11–26.
- Forsthoefel, D.J., and Newmark, P.A. (2009). Emerging patterns in planarian regeneration. *Current Opinion in Genetics & Development* 19, 412–420.
- Gaviño, M.A., Wenemoser, D., Wang, I.E., and Reddien, P.W. (2013). Tissue absence initiates regeneration through Follistatin-mediated inhibition of Activin signaling. *Elife* 2, e00247.
- Gurley, K.A., Elliott, S.A., Simakov, O., Schmidt, H.A., Holstein, T.W., and Sánchez Alvarado, A. (2010). Expression of secreted Wnt pathway components reveals unexpected complexity of the planarian amputation response. *Developmental Biology* 347, 24–39.
- Gurley, K.A., Rink, J.C., and Sánchez Alvarado, A. (2008).  $\beta$ -Catenin Defines Head Versus Tail

Identity During Planarian Regeneration and Homeostasis. *Science* 319, 323–327.

Hayashi, T., Motoishi, M., Yazawa, S., Itomi, K., Tanegashima, C., Nishimura, O., Agata, K., and Tarui, H. (2011). A LIM-homeobox gene is required for differentiation of Wnt-expressing cells at the posterior end of the planarian body. *Development (Cambridge, England)* 138, 3679–3688.

Iglesias, M., Gomez-Skarmeta, J.L.J., Saló, E., and Adell, T. (2008). Silencing of *iSmad-βcatenin1/i* generates radial-like hypercephalized planarians. *Development* 135, 1215–1221.

Ji, X., Ji, K., Chittavong, V., Aghoghovbia, R.E., Zhu, M., and Wang, B. (2017). Click and Fluoresce: A Bioorthogonally Activated Smart Probe for Wash-Free Fluorescent Labeling of Biomolecules. *J. Org. Chem.* 82, 1471–1476.

Kharchenko, P.V., Silberstein, L., and Scadden, D.T. (2014). Bayesian approach to single-cell differential expression analysis. *Nat. Methods* 11, 740–742.

King, R.S., and Newmark, P.A. (2013). In situ hybridization protocol for enhanced detection of gene expression in the planarian *iSchmidtea mediterranea/i*. *BMC Developmental Biology* 13, 8.

Lander, R., and Petersen, C. (2016). Wnt, Ptk7, and FGFR1 expression gradients control trunk positional identity in planarian regeneration. *Elife* 5, 1689–1699.

Lemaire, P., and Kodjabachian, L. (1996). The vertebrate organizer: structure and molecules. *Trends in Genetics* 12, 525–531.

Maxwell, M.A., and Muscat, G.E.O. (2006). The NR4A subgroup: immediate early response genes with pleiotropic physiological roles. *Nucl Recept Signal* 4, e002.

März, M., Seebeck, F., and Bartscherer, K. (2013). A Pitx transcription factor controls the establishment and maintenance of the serotonergic lineage in planarians. *Development (Cambridge, England)* 140, 4499–4509.

Molina, M.D., Saló, E., and Cebrià, F. (2007). The BMP pathway is essential for re-specification and maintenance of the dorsoventral axis in regenerating and intact planarians. *Developmental Biology* 311, 79–94.

Oderberg, I.M., Li, D.J., Scimone, M.L., Gaviño, M.A., and Reddien, P.W. (2017). Landmarks in Existing Tissue at Wounds Are Utilized to Generate Pattern in Regenerating Tissue. *Current Biology* 1–24.

Owlarn, S., and Bartscherer, K. (2016). Go ahead, grow a head! A planarian's guide to anterior regeneration. *Regeneration* 3, 139–155.

Paulsen, R.E., Weaver, C.A., Fahrner, T.J., and Milbrandt, J. (1992). Domains regulating transcriptional activity of the inducible orphan receptor NGFI-B. *Journal of Biological Chemistry* 267, 16491–16496.

- Pearson, B.J., Eisenhoffer, G.T., Gurley, K.A., Rink, J.C., Miller, D.E., and Sánchez Alvarado, A. (2009). Formaldehyde-based whole-mount in situ hybridization method for planarians. *Dev. Dyn.* 238, 443–450.
- Petersen, C.P., and Reddien, P.W. (2008). *Smed-βcatenin-1* is required for anteroposterior blastema polarity in planarian regeneration. *Science* 319, 327–330.
- Petersen, C.P., and Reddien, P.W. (2009). A wound-induced Wnt expression program controls planarian regeneration polarity. *Proc. Natl. Acad. Sci. U.S.A.* 106, 17061–17066.
- Petersen, C.P., and Reddien, P.W. (2011). Polarized *notum* activation at wounds inhibits Wnt function to promote planarian head regeneration. *Science* 332, 852–855.
- Picelli, S., Björklund, Å.K., Faridani, O.R., Sagasser, S., Winberg, G., and Sandberg, R. (2013). Smart-seq2 for sensitive full-length transcriptome profiling in single cells. *Nat. Methods* 10, 1096–1098.
- Picelli, S., Faridani, O.R., Björklund, Å.K., Winberg, G., Sagasser, S., and Sandberg, R. (2014). Full-length RNA-seq from single cells using Smart-seq2. *Nat Protoc* 9, 171–181.
- Reddien, P.W., Bermange, A.L., Murfitt, K.J., Jennings, J.R., Sánchez Alvarado, A., and Alvarado, A.S. (2005). Identification of genes needed for regeneration, stem cell function, and tissue homeostasis by systematic gene perturbation in planaria. *Developmental Cell* 8, 635–649.
- Reddien, P.W. (2011). Constitutive gene expression and the specification of tissue identity in adult planarian biology. *Trends in Genetics* 27, 277–285.
- Roberts-Galbraith, R.H.R., and Newmark, P.A.P. (2013). Follistatin antagonizes Activin signaling and acts with Notum to direct planarian head regeneration. *Proc Natl Acad Sci U S A* 110, 1363–1368.
- Ross, K.G., Omuro, K.C., Taylor, M.R., Munday, R.K., Hubert, A., King, R.S., and Zayas, R.M. (2015). Novel monoclonal antibodies to study tissue regeneration in planarians. *BMC Developmental Biology* 15, 2.
- Rugarli, E.I. (1999). Kallmann syndrome and the link between olfactory and reproductive development. *Am. J. Hum. Genet.* 65, 943–948.
- Rugarli, E.I., Lutz, B., Kuratani, S.C., Wawersik, S., Borsani, G., Ballabio, A., and Eichele, G. (1993). Expression pattern of the Kallmann syndrome gene in the olfactory system suggests a role in neuronal targeting. *Nature Genetics* 4, 19–26.
- Safe, S., Jin, U.-H., Morpurgo, B., Abudayyeh, A., Singh, M., and Tjalkens, R.B. (2016). Nuclear receptor 4A (NR4A) family - orphans no more. *J. Steroid Biochem. Mol. Biol.* 157, 48–60.
- Salic, A., and Mitchison, T.J. (2008). A chemical method for fast and sensitive detection of DNA synthesis in vivo. *Proc. Natl. Acad. Sci. U.S.A.* 105, 2415–2420.

- Scimone, M.L., Cote, L.E., Rogers, T., and Reddien, P.W. (2016). Two FGFR1-Wnt circuits organize the planarian anteroposterior axis. *Elife* 5, 905.
- Scimone, M.L., Lapan, S.W., and Reddien, P.W. (2014). A *forkhead* Transcription Factor Is Wound-Induced at the Planarian Midline and Required for Anterior Pole Regeneration. *PLoS Genet* 10, e1003999.
- Sekiya, T., Kashiwagi, I., Yoshida, R., Fukaya, T., Morita, R., Kimura, A., Ichinose, H., Metzger, D., Chambon, P., and Yoshimura, A. (2013). Nr4a receptors are essential for thymic regulatory T cell development and immune homeostasis. *Nat Immunol* 14, 230–237.
- Spemann, H., and Mangold, H. (1924). Über Induktion von Embryonalanlagen durch Implantation artfremder Organisatoren. *Archiv Fur Entwicklungsmechanik Der Organismen* 100, 599–638.
- Vásquez-Doorman, C., and Petersen, C.P. (2014). *zic-1* Expression in Planarian Neoblasts after Injury Controls Anterior Pole Regeneration. *PLoS Genet* 10, e1004452.
- Vogg, M.C., Owlarn, S., Pérez Rico, Y.A., Xie, J., Suzuki, Y., Gentile, L., Wu, W., and Bartscherer, K. (2014). Stem cell-dependent formation of a functional anterior regeneration pole in planarians requires *Zic* and *Forkhead* transcription factors. *Developmental Biology* 390, 136–148.
- Vogg, M.C., Wenger, Y., and Galliot, B. (2016). How Somatic Adult Tissues Develop Organizer Activity. *Current Topics in Developmental Biology* 116, 391–414.
- Wagner, D.E., Wang, I.E., and Reddien, P.W. (2011). Clonogenic Neoblasts Are Pluripotent Adult Stem Cells That Underlie Planarian Regeneration. *Science* 332, 811–816.
- Wenemoser, D., Lapan, S.W., Wilkinson, A.W., Bell, G.W., and Reddien, P.W. (2012). A molecular wound response program associated with regeneration initiation in planarians. *Genes & Development* 26, 988–1002.
- Wenemoser, D., and Reddien, P.W. (2010). Planarian regeneration involves distinct stem cell responses to wounds and tissue absence. *Developmental Biology* 344, 979–991.
- Witchley, J.N., Mayer, M., Wagner, D.E., Owen, J.H., and Reddien, P.W. (2013). Muscle Cells Provide Instructions for Planarian Regeneration. *Cell Reports* 4, 1–9.
- Wurtzel, O., Cote, L.E., Poirier, A., Satija, R., Regev, A., and Reddien, P.W. (2015). A Generic and Cell-Type-Specific Wound Response Precedes Regeneration in Planarians. *Developmental Cell* 35, 632–645.
- Wurtzel, O., Oderberg, I.M., and Reddien, P.W. (2017). Planarian Epidermal Stem Cells Respond to Positional Cues to Promote Cell-Type Diversity. *Developmental Cell* 40, 491–504.e495.



**CHAPTER 4**

**Conclusions and Future Directions**



## **The Organizing Activity of the Planarian Poles**

Transplantation experiments have long been used to study the inductive properties of tissues, and their remarkable outcomes have led to a better understanding of the molecular mechanisms of patterning. In both developmental and regenerative systems, transplantation of signaling centers enabled the characterization of organizers and morphogenic fields, tools and strategies employed by a variety of metazoans to establish and maintain pattern (Beddington, 1994; Oppenheimer, 1936; Shih and Fraser, 1996; Spemann and Mangold, 1924; Waddington, 1933; 1932).

Several transplantation studies in planarians, dating back to the work by Felix Santos (Santos, 1931), have advanced our knowledge of patterning mechanisms of this powerful regenerative organism. It has long been shown that planarian transplantations involving the juxtaposition of tissues with disparate positional identities (e.g. head grafts in tail regions) trigger outgrowths that regenerate the missing positional identities in between (Chandebois, 1985; Kato et al., 1999; Okada and Sugino, 1937; Sal and Bagu, 1985). This phenomenon, termed intercalary regeneration, has also been observed in other organisms such as cockroaches and amphibians, in which mismatching limb segment transplantations were performed (Maden, 1980; Stocum, 1975). Furthermore, in planarians, irradiation of either the donor or host tissue prior to transplantation resulted in similar regenerative outcomes as non-irradiated controls (Kato et al., 2001). Altogether, these transplantation experiments suggest that 1) differentiated tissues contain inductive information and 2) regeneration after transplantation proceeds until continuity of positional identity between the graft and the host is restored.

Our anterior pole transplantations helped us refine our understanding of these

phenomena. We specifically sought to test the inductive capacity of anterior-pole enriched head tip fragments. Our results showing the emergence of properly patterned head outgrowths from irradiated transplants are to date the most direct experimental evidence for the organizing activity of the anterior pole. We demonstrated by irradiating the donors that differentiated cells from the head tip are capable of inducing new AP and ML axes. In addition, by using flank fragments as control grafts we showed that the inductive potential of a tissue varied with even minor deviations in its axial location. Whether the induction of a fully patterned head is solely attributable to anterior pole cells is uncertain, but improperly patterned outgrowths from head tip flank transplants strongly suggest that cells along the midline of the head tip, chief among them anterior pole cells, are responsible. Definitive experiments showing the specific requirement of anterior pole cells in inducing patterned heads involve transplanting head tips from uninjured donors that have undergone long-term *foxD* RNAi to genetically ablate the anterior pole. Failure of these pole-lacking grafts to induce fully patterned heads will provide convincing evidence of the organizing activity of pole cells.

Notably, pole-containing grafts successfully induced the formation of a new midline, even when they were transplanted in regions lateral to the existing midline. However, we cannot rule out the possibility that *slit*-expressing midline cells from pole-containing grafts were responsible for the outcome. Moreover, the *slit*-expressing cells and not the anterior pole cells could have been responsible for the induction of the fully patterned heads. Ruling out the contributions of *slit*-expressing cells may require transplanting head tip grafts from uninjured animals subjected to long-term *slit* RNAi.

The outcome of the head tip transplants complicates our understanding of intercalary regeneration. Under this model, grafts from the anterior-most regions of the animal, when

juxtaposed to posterior host tissue, would trigger the regeneration of all the AP axial identities in between. Yet we did not observe in any of our fully patterned head outgrowths evidence of emerging pharynges. It is possible that trunk identities and improperly formed pharynges were present, so staining the outgrowths with pharynx and trunk markers could resolve this ambiguity. Additionally, the intercalary model predicts that the pole-containing and flank grafts from the head tip (due to their axial positions anterior to the eyes) would both trigger the formation of eyes in similar frequencies when transplanted to the posterior regions of the host. Yet pole-containing fragments generated head outgrowths with eyes at significantly higher frequencies than flank fragments. Although the outgrowths from the flank pieces could have developed eyes at later times, the disparate outcomes from grafts at similar AP axial levels suggest that regenerative mechanism may not be as simple as just intercalation.

## Planarian Pole Transcriptome and Function

Given the organizing properties of the planarian poles, we sought to better understand the biology of pole cells from their transcriptional activity. Organizers during embryogenesis and regeneration are characterized by the production of secreted signaling factors that mediate their inductive properties (Lemaire and Kodjabachian, 1996; Vogg et al., 2016). While we know of a few secreted factors produced by the planarian poles (e.g. *notum*, *fst*, *wnt1*, *wnt11-2*), it is unclear whether they represent the full complement of pole signals and the extent to which these and other unknown pole factors mediate AP and ML midline patterning. Furthermore, our analysis of the dynamics of anterior pole formation revealed that pole progenitors are specialized broadly along the midline of the DV axis and coalesce at the anterior midpoint of the DV axis as post-mitotic progenitors. This, together with BrdU labeling and analysis of anterior pole cells at different time points during regeneration, provided indirect evidence of directed pole cell migration. Migration implies the existence of cell surface receptors that interact with extracellular signals and matrix to mediate cell movement.

Using bulk and single-cell RNA sequencing of the planarian anterior and posterior poles during regeneration and homeostasis, we have generated the most comprehensive list yet of pole-enriched genes. One of these genes, *kallmann1*, is expressed specifically in both poles and encode an extracellular matrix protein implicated in neuronal migration and axonal branching in humans and *C. elegans*, respectively (Hardelin, 2001) (Rugarli et al., 1993) (Bülow et al., 2002) (Rugarli et al., 2002). Other genes, like *musculin* and *islet2*, represent new pole transcription factors. Finally, a large subset of the new anterior and posterior pole genes encode cell surface

receptors, including ephrin receptors, which participate in short-distance cell-cell signaling affecting cellular motility and/or morphology (Kullander and Klein, 2002). Although RNAi of most of the new pole genes did not produce the dramatic pole and patterning disturbances we observed in *nr4A* RNAi, more detailed pole migration or neuronal branching analyses, for example, may uncover important roles for these genes in pole biology.

Compared to the anterior pole, the posterior pole is less well studied and more enigmatic. During regeneration, *wnt1*-expressing cells at the posterior pole are organized in a cluster in the blastema (Petersen and Reddien, 2009). In uninjured animals, the *wnt1* domain is linear at the tail tip (Gurley et al., 2010; Petersen and Reddien, 2011; 2009). It is unclear whether the same *wnt1*-expressing cells in the blastema reorganize to form the linear domain in fully regenerated tails or whether these domains comprise different sets of cells with different roles during regeneration and homeostasis. To explore this question, it will be informative to compare the single-cell transcriptomes of the posterior pole from regenerating and uninjured animals and analyze for differences in the transcriptional profiles between these two pole cell populations.

In our single-cell RNA sequencing of the posterior pole, we chose to use *wnt1* expression to identify pole cells for transcriptome analysis. Although *pitx*, *islet*, and *wnt11-2* also have expression domains at the posterior pole, we focused on *wnt1* because its expression is the most restricted to the posterior pole. This restricted expression may have resulted in the exclusion of some posterior pole cells, for example tail tip cells expressing *wnt11-2*, from our analysis. Improvements to our current posterior pole transcriptome could be made using the other posterior pole genes in the selection criteria to expand the number of posterior pole cells analyzed. Recent advances in high-throughput genome-wide expression profiling of single cells (Macosko et al., 2015; Zilionis et al., 2017) will facilitate such an effort, as they enable us to

collect unprecedented amounts of data at feasible costs.

Whereas the requirement for anterior and posterior poles in patterning during regeneration has been widely demonstrated, pole function during homeostasis is less clear. While RNAi of *notum* in uninjured animals resulted in anterior ectopic eye formation and decreased brain size, these patterning anomalies have been likely attributed to *notum* expression in neural cells in the anterior commissure of the brain rather than at the anterior pole (Hill and Petersen, 2015). RNAi of *foxD* and *zic-1* in uninjured animals resulted in the loss of *notum* and *fst* expression specifically at the anterior pole, but no overt patterning defects during tissue turnover have been reported (Scimone et al., 2014; Vásquez-Doorman and Petersen, 2014; Vogg et al., 2014). RNAi of *fst* during homeostasis also failed to yield a patterning phenotype (Gaviño et al., 2013). Finally, *pitx* is mainly required for the maintenance of serotonergic marker expression, and homeostatic patterning defects for *pitx* and *islet* have not been studied (Currie and Pearson, 2013; Hayashi et al., 2011; März et al., 2013). It is possible that the poles are required specifically during regeneration to establish new AP and ML identities in the blastema. Once anterior and posterior identities are formed, the expression of other head and tail mRGs may make the poles dispensable for the maintenance of patterning. Testing this hypothesis requires detailed mRG expression analysis after long-term RNAi of anterior and posterior pole genes in uninjured animals.

## The Role of *nr4A* in Patterning

During homeostasis, we found that the locations of the anterior and posterior poles at the ends of the planarian AP axis is maintained by the activity of *nr4A*. Similarly, the transcription factor *pbx* is required for the formation and maintenance of both poles during regeneration and homeostasis, and *pbx* RNAi results in head and tail patterning defects (Chen et al., 2013). However, while in *pbx* RNAi the expression of anterior and posterior markers is reduced at the head and tail tips, in *nr4A* RNAi the anterior and posterior identities are all preserved but shifted towards the midbody.

Detailed studies of the sequence of changes in *nr4A* RNAi has provided us an unprecedented look at patterning in action. Two phases of *nr4A* phenotype progression could be detected, an early PCG shift and a late differentiated tissue shift. The former is marked by the early shift of anterior and posterior pole cells away from the head and tail tips, respectively, along with similar shifts in other head and tail PCGs. This is followed by the posteriorization of differentiated tissues in the head and the anteriorization of differentiated tissues in the tail. Although causation cannot be inferred from the sequence of events, PCG changes occurring before differentiated tissue changes is consistent with the model in which instructive cues provided by the muscle affect the identities of surrounding tissues (Reddien, 2011; Witchley et al., 2013). Given the organizing activity of the anterior pole cells, the posterior shift of the anterior pole might in theory cause a cascade of signaling events leading to similar shifts in other PCGs and eventually in the ectopic specification of differentiated tissue. Testing this hypothesis requires RNAi of *foxD* in uninjured animals to ablate the anterior pole followed by simultaneous

*nr4A* RNAi. Suppression of the *nr4A* RNAi phenotype by pole ablation would demonstrate the anterior pole shift's causative role in the phenotype.

What then causes the initial shift in pole cells? Because the change in the anterior pole preceded changes in muscle fibers at the head tip, it is unlikely that disruptions in the integrity of muscle fibers was responsible. Furthermore, newly specified anterior pole cells were observed in ectopically posterior locations, suggesting that the mislocalization of new pole cells at least partially underlies the phenotype. Given that decreased expression of genes encoding ECM components like collagen and metalloproteinase is the earliest transcriptional change in *nr4A* RNAi in both the head and the tail, defects in ECM could be responsible for the mistargeting of differentiating pole cells. From our studies of anterior pole formation, we know that pole cells are specified from neoblasts in a broad midline region posterior to the point at which differentiated pole cells accumulate. Disrupting muscle cell's ability to produce ECM components may impede the migration of new anterior pole cells to their final destination at the apex of the head. Similar defects would be observed in posterior pole localization at the tail tip. Because anterior pole cell function remains intact, as evidenced by the continued expression of *foxD* and *notum* of ectopic pole cells, a head tip identity is specified at a more posterior location, resulting in the posterior shift of head PCGs and specialized cells. If this is true, then inhibiting *nr4A* transcriptional targets during homeostasis may phenocopy the effects of *nr4A* RNAi. Genes like *col4a1* and *mmp19* would be prioritized in the RNAi screen, as they both decrease in their expression early in *nr4A* RNAi. *mmp19*, especially, is a promising candidate because its enriched expression in the head and tail, which is decreased in *nr4A* RNAi, may explain the head- and tail-specificity of the *nr4A* RNAi phenotype.

## Summary

From surgical manipulations to single-cell transcriptional analysis, we have attempted to gain a better understanding of the mechanisms of patterning using the planarian poles as a case study. In the process, we provided strong evidence of the inductive properties of the anterior pole, demonstrated its role in integrating pattern from preexisting tissue to organize new tissue, expanded the repertoire of known pole-enriched genes, and characterized a novel function of a gene in head and tail patterning. All of these efforts have been aimed to provide insights into how positional identity is established and maintained, a critical process during regeneration and tissue turnover. Aided by advancements in our ever-expanding experimental toolkit, we have come a long way in understanding the cellular and molecular processes underlying regeneration. Continuing investigations into the mechanisms governing tissue patterning promise to unravel one of nature's most fascinating mysteries – how cellular activity translates into the production and reproduction of diverse body forms.

## References

- Beddington, R.S. (1994). Induction of a second neural axis by the mouse node. *Development (Cambridge, England)* *120*, 613–620.
- Bülow, H.E., Berry, K.L., Topper, L.H., Peles, E., and Hobert, O. (2002). Heparan sulfate proteoglycan-dependent induction of axon branching and axon misrouting by the Kallmann syndrome gene *kal-1*. *Proc Natl Acad Sci U S A* *99*, 6346–6351.
- Chandebois, R. (1985). Intercalary regeneration and level interactions in the fresh-water planarian *Dugesia lugubris*. *Roux's Archives Biology* *53*, 390–396.
- Chen, C.C.G., Wang, I.E., and Reddien, P.W. (2013). *pbx* is required for pole and eye regeneration in planarians. *Development* *140*, 719–729.
- Currie, K.W., and Pearson, B.J. (2013). Transcription factors *lhx1/5-1* and *pitx* are required for the maintenance and regeneration of serotonergic neurons in planarians. *Development* *140*, 3577–3588.
- Gaviño, M.A., Wenemoser, D., Wang, I.E., and Reddien, P.W. (2013). Tissue absence initiates regeneration through Follistatin-mediated inhibition of Activin signaling. *Elife* *2*, e00247.
- Gurley, K.A., Elliott, S.A., Simakov, O., Schmidt, H.A., Holstein, T.W., and Sánchez Alvarado, A. (2010). Expression of secreted Wnt pathway components reveals unexpected complexity of the planarian amputation response. *Developmental Biology* *347*, 24–39.
- Hardelin, J.P. (2001). Kallmann syndrome: towards molecular pathogenesis. *Mol. Cell. Endocrinol.* *179*, 75–81.
- Hayashi, T., Motoishi, M., Yazawa, S., Itomi, K., Tanegashima, C., Nishimura, O., Agata, K., and Tarui, H. (2011). A LIM-homeobox gene is required for differentiation of Wnt-expressing cells at the posterior end of the planarian body. *Development (Cambridge, England)* *138*, 3679–3688.
- Hill, E.M., and Petersen, C.P. (2015). Wnt/Notum spatial feedback inhibition controls neoblast differentiation to regulate reversible growth of the planarian brain. *Development (Cambridge, England)* *142*, 4217–4229.
- Kato, K., Orii, H., Watanabe, K., and Agata, K. (1999). The role of dorsoventral interaction in the onset of planarian regeneration. *Development* *126*, 1031–1040.
- Kato, K., Orii, H., Watanabe, K., and Agata, K. (2001). Dorsal and ventral positional cues required for the onset of planarian regeneration may reside in differentiated cells.
- Kullander, K., and Klein, R. (2002). Mechanisms and functions of Eph and ephrin signalling.

Nat. Rev. Mol. Cell Biol. 3, 475–486.

Lemaire, P., and Kodjabachian, L. (1996). The vertebrate organizer: structure and molecules. *Trends in Genetics* 12, 525–531.

Macosko, E.Z., Basu, A., Satija, R., Nemesh, J., Shekhar, K., Goldman, M., Tirosh, I., Bialas, A.R., Kamitaki, N., Martersteck, E.M., et al. (2015). Highly Parallel Genome-wide Expression Profiling of Individual Cells Using Nanoliter Droplets. *Cell* 161, 1202–1214.

Maden, M. (1980). Intercalary regeneration in the amphibian limb and the rule of distal transformation. *J Embryol Exp Morphol* 56, 201–209.

März, M., Seebeck, F., and Bartscherer, K. (2013). A Pitx transcription factor controls the establishment and maintenance of the serotonergic lineage in planarians. *Development (Cambridge, England)* 140, 4499–4509.

Okada, Y., and Sugino, H. (1937). Transplantation experiments in Planaria. 1–67.

Oppenheimer, J.M. (1936). Structures Developed in Amphibians by Implantation of Living Fish Organizer. *Proceedings of the Society for Experimental Biology and Medicine. Society for Experimental Biology and Medicine (New York, N.Y.)* 34, 461–463.

Petersen, C.P., and Reddien, P.W. (2011). Polarized *notum* Activation at Wounds Inhibits Wnt Function to Promote Planarian Head Regeneration. *Science* 332, 852–855.

Petersen, C.P., and Reddien, P.W. (2009). A wound-induced Wnt expression program controls planarian regeneration polarity. *Proc. Natl. Acad. Sci. U.S.A.* 106, 17061–17066.

Reddien, P.W. (2011). Constitutive gene expression and the specification of tissue identity in adult planarian biology. *Trends in Genetics* 27, 277–285.

Rugarli, E.I., Lutz, B., Kuratani, S.C., Wawersik, S., Borsani, G., Ballabio, A., and Eichele, G. (1993). Expression pattern of the Kallmann syndrome gene in the olfactory system suggests a role in neuronal targeting. *Nature Genetics* 4, 19–26.

Rugarli, E.I., Di Schiavi, E., Hilliard, M.A., Arbucci, S., Ghezzi, C., Faccioli, A., Coppola, G., Ballabio, A., and Bazzicalupo, P. (2002). The Kallmann syndrome gene homolog in *C. elegans* is involved in epidermal morphogenesis and neurite branching. *Development (Cambridge, England)* 129, 1283–1294.

Sal, E., and Bagu, J. (1985). Proximal and distal transformation during intercalary regeneration in the planarian *Dugesia(S)mediterranea*. *Wilhelm Roux' Archiv* 194, 364–368.

Santos, F.V. (1931). Studies on transplantation in planaria. *Physiological Zoology* 4, 111–164.

Scimone, M.L., Lapan, S.W., and Reddien, P.W. (2014). A *forkhead* Transcription Factor Is Wound-Induced at the Planarian Midline and Required for Anterior Pole Regeneration. *PLoS Genet* 10, e1003999.

- Shih, J., and Fraser, S.E. (1996). Characterizing the zebrafish organizer: microsurgical analysis at the early-shield stage. *Development (Cambridge, England)* *122*, 1313–1322.
- Spemann, H., and Mangold, H. (1924). Über Induktion von Embryonalanlagen durch Implantation artfremder Organisatoren. *Archiv Fur Entwicklungsmechanik Der Organismen* *100*, 599–638.
- Stocum, D.L. (1975). Regulation after proximal or distal transposition of limb regeneration blastemas and determination of the proximal boundary of the regenerate. *Developmental ...* *45*, 112–136.
- Vásquez-Doorman, C., and Petersen, C.P. (2014). *zic-1* Expression in Planarian Neoblasts after Injury Controls Anterior Pole Regeneration. *PLoS Genet* *10*, e1004452.
- Vogg, M.C., Owlarn, S., Pérez Rico, Y.A., Xie, J., Suzuki, Y., Gentile, L., Wu, W., and Bartscherer, K. (2014). Stem cell-dependent formation of a functional anterior regeneration pole in planarians requires Zic and Forkhead transcription factors. *Developmental Biology* *390*, 136–148.
- Vogg, M.C., Wenger, Y., and Galliot, B. (2016). How Somatic Adult Tissues Develop Organizer Activity. *Current Topics in Developmental Biology* *116*, 391–414.
- Waddington, C.H. (1933). Induction by the Primitive Streak and its Derivatives in the Chick. *Journal of Experimental Biology* *10*, 38–46.
- Waddington, C.H. (1932). Experiments on the development of chick and duck embryos, cultivated in vitro. *Philosophical Transactions of the Royal Society of London. Series B, Biological Sciences* *221*, 179–230.
- Witchley, J.N., Mayer, M., Wagner, D.E., Owen, J.H., and Reddien, P.W. (2013). Muscle Cells Provide Instructions for Planarian Regeneration. *Cell Reports* *4*, 1–9.
- Zilionis, R., Nainys, J., Veres, A., Savova, V., Zemmour, D., Klein, A.M., and Mazutis, L. (2017). Single-cell barcoding and sequencing using droplet microfluidics. *Nat Protoc* *12*, 44–73.

